IONOSPHERIC RANGE-RATE CORRECTIONS IN SATELLITE-TO-SATELLITE TRACKING

IONOSPHERIC RANGE-RATE EFFECTS IN SATELLITE-TO-SATELLITE TRACKING

Prepared by:

J. R. Lipofsky
R. B. Bent
S. K. Llewellyn
P. E. Schmid *

Atlantic Science Corporation
P.O. Box 3201
Indialantic, Florida 32903

Prepared for:

*National Aeronautics and Space Administration
Goddard Space Flight Center
Greenbelt, Maryland 20771

Contract Number: NAS5-23899

November 1977

TABLE OF CONTENTS

LIST OF FIGURES

List of Figures

continued .....

List of Figures

continued .....

1.0 INTRODUCTION

Several previous studies have been made to determine ionospheric refraction corrections to range-rate observations in the tracking of low orbiting spacecraft by a high altitude satellite acting in a relay capacity to the ground tracking stations. A good ionospheric correction model based on the NASA 3-dimensional worldwide ionospheric model was developed by Atlantic Science Corporation for the Gravsat/Geopause configuration satisfying the required tracking accuracies to the order of 0.02 meters in range and 0.003 cm/sec in range-rate. From many orbits simulated for severe refraction conditions, the maximum ionospheric corrections to range and range-rate to be expected along the satellite-to-satellite link were determined as shown in Table 1 [1]. The same model was also used to compute corrections to actual tracking data for the ATS-6 to Apollo/Soyuz geometrical configuration in conjunction with the geodynamic satellite experiments. The results showed the ionospheric effects to be of significant magnitude compared with the gravitational effects. Hence, adequate removal of ionospheric effects by modeling proved necessary, and updating the range-rate corrections with actual ionospheric measurements was performed in this study.

It became apparent in analyzing these data that the variations in the ionospheric refractions were not easily interpreted and causes were difficult to attribute in the complex orbit configurations with changing ionospheric conditions. In order to understand the characteristics of the refraction errors and to estimate residual errors that might remain due to short term ionospheric variations even after removing ionospheric effects by use of a prediction model, a study of the problem under simple well known conditions was necessary and is presented here. With the NASA 3-dimensional worldwide model the investigation was expanded to examine how the various parameters of solar flux, season and diurnal variation effect the range-rate corrections. Actual and simulated orbits of Apollo, Geos and Nimbus tracked by ATS-6 were used in this study.

Table 1. Maximum ionospheric refraction corrections expected along satellite link with low satellite at 307 km as in the Gravsat/Geopause configuration.

Refraction Type	Maximum refraction corrections obtained for selected orbits		Corrections possible under extreme refraction conditions based on a median f_0F2 value of 16 MHz	
	ΔR (m)	$\lvert\Delta\dot{R}\rvert$ (mm/sec)	ΔR (m)	$\lvert\Delta\dot{R}\rvert$ (mm/sec)
Ionospheric				
at 13.472 GHz	1.17	9.21	2.64	17.31
normalized to 1 GHz	212.35	1671.57	479.15	3142.12

2.0 SIMPLE MODEL INVESTIGATIONS

2.1 Conditions Investigated

The two major causes of the sudden and sometimes large variations apparent in the ionospheric range and range-rate corrections along the satellite arc are the geometric effects of the raypath and the curved ionosphere, and the localized perturbations in electron density along the satellite-to-satellite line of sight. The raypath may follow along the region of maximum electron density for a considerable distance, it may pierce the ionosphere at two separated locations, pass through it once, or only partially, or remain above it, allowing for a great range in the magnitude of the effect. Conditions possible for a low altitude satellite like Apollo-Soyuz are illustrated in Figure 1. Significant gradients in the electron density, as occur in the equatorial anomaly, result in very large perturbations.

Ionospheric tracking errors are greatly effected by the following parameters, whose influences are investigated: satellite height, height of maximum electron density, electron density variations, and localized ionospheric perturbations and gradients. Changes in these parameters can produce large variations in the magnitude of errors as well as time shifts of the peak errors along the satellite arc.

The orbits were generated for three low orbiting spacecraft at different heights, to resemble the Apollo-Soyuz arcs at 200 km, the Geos arcs at 850 km, and the Nimbus arcs at 1100 km above the earth's surface. The high altitude satellite was stationary at a height of 35,785 km like ATS-6. To allow a clear understanding of the geometric effects the orbits were chosen coplanar, and each arc was started where the high and low satellites were aligned with the earth's center, as shown in Figure 2. In each case the arcs terminated when the low satellite disappeared from the view of the high tracking satellite in the geometric sense being blocked by the earth. Low satellite positions underneath the earth's horizon that might still be visible from the high satellite, due to refractive effects on

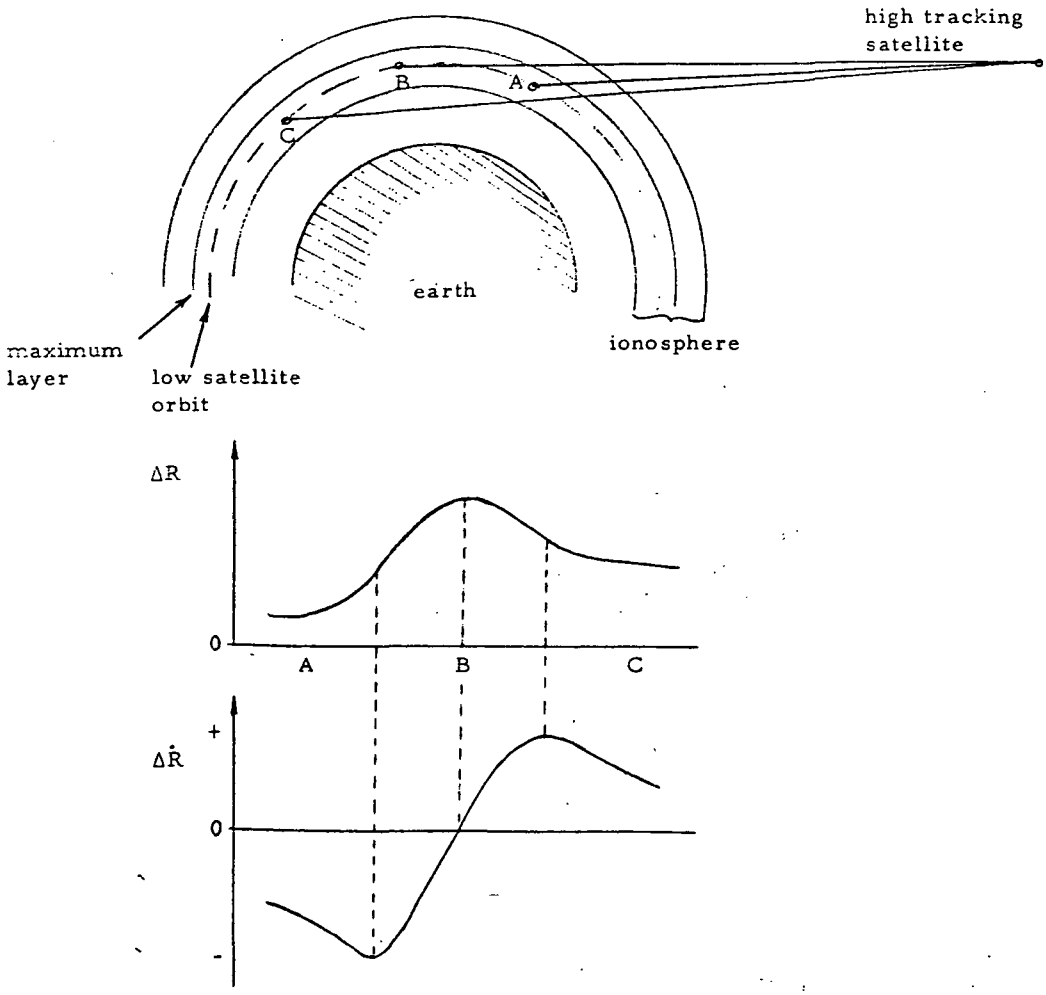

Figure 1. Satellite to satellite ionosphere range corrections reach peak at B and are greater at C than at A; range-rate corrections will pan through zero at B.

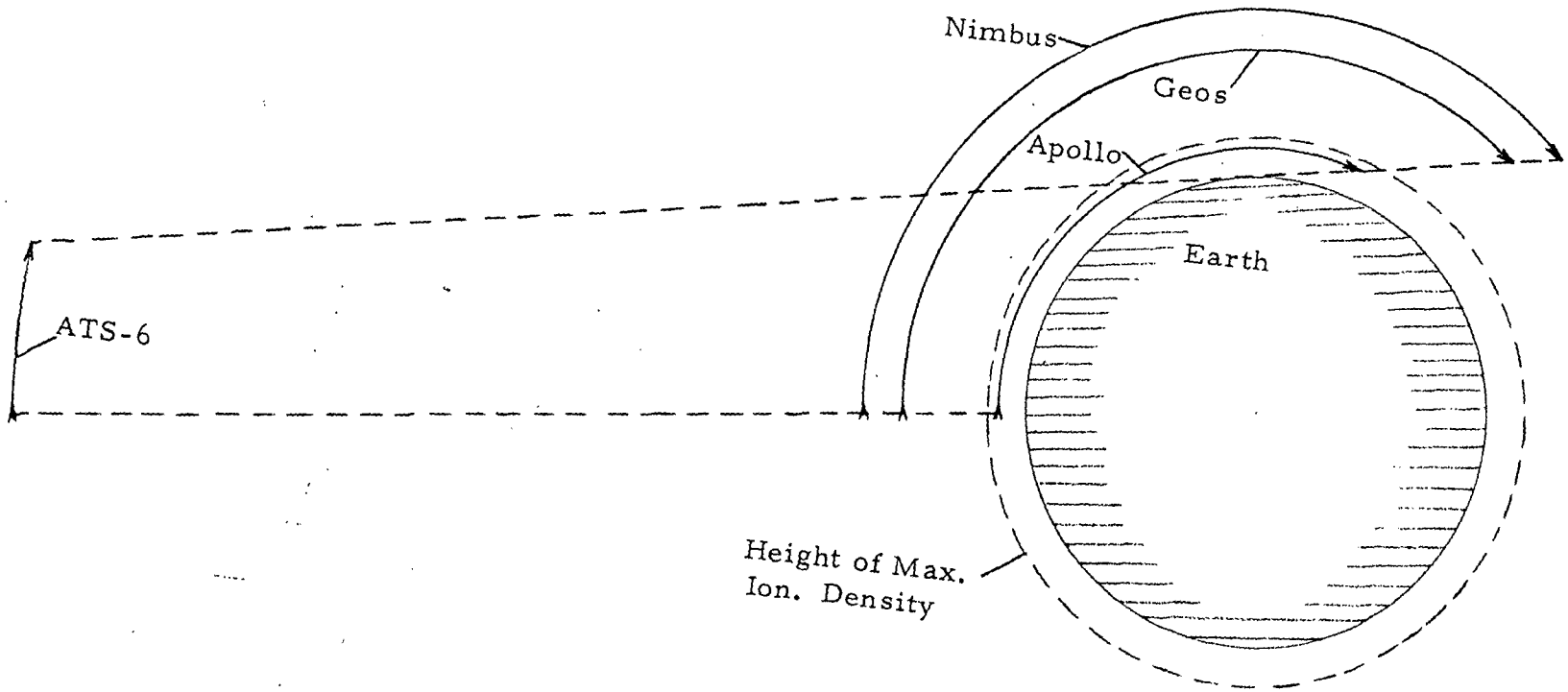

Figure 2 . Orbit configurations used for investigating geometric and perturbation contributions to the ionospheric refraction along the satellite-to-satellite link (not to scale).

the raypath through the earth's atmosphere, were not considered.

To first investigate the purely geometric effects, the ionosphere was considered uniform all over the globe with a density versus height profile as in the Bent Ionospheric Model with five exponentially decaying topside layers, a parabolic layer just above the densest region, and a bi-parabolic bottomside layer. The critical frequency f_0F2 and the height at the maximum electron density h_m were chosen for different cases, while all other variables were held fixed, to evaluate the effect of ionospheric variations on tracking observations. Values of f_0F2 were chosen as 5, 10 and 15 MHz, and h_m was considered at 25 km steps during the Apollo-Soyuz orbits and at 50 km increments for Geos and Nimbus arcs.

To investigate how severe ionospheric gradients influence the range-rate corrections, perturbations in density were superimposed on the worldwide uniform ionosphere at selected locations. The perturbations were chosen from gradients that are characteristic for severe equatorial anomalies or sunrise effects as they actually occur, with an increase or decrease in f_0F2 of 5 MHz tapering off over a radius of about 1400 km (=755 nautical miles) from the perturbation center. More severe ionospheric disturbances as are possible during geomagnetic storms were modeled by a drop of 10 MHz in f_0F2 at the perturbation center recovering to normal over 1400 km.

The decline of the perturbations with distance from the center was chosen to best represent actual ionospheric variations. This was accomplished by correlating with a study on updating ionospheric predictions with data observed at various distances [2]. Most improvement in the accuracy of corrections was achieved through updating, when the distance weighting function resembled the decay of ionospheric variations. Hence the best weighting function from the update procedure, $e^{-(d/D)^2}$ with D=400 nautical miles as shown in Figure 3, was used to model the spacial decay of the perturbation over the distance d.

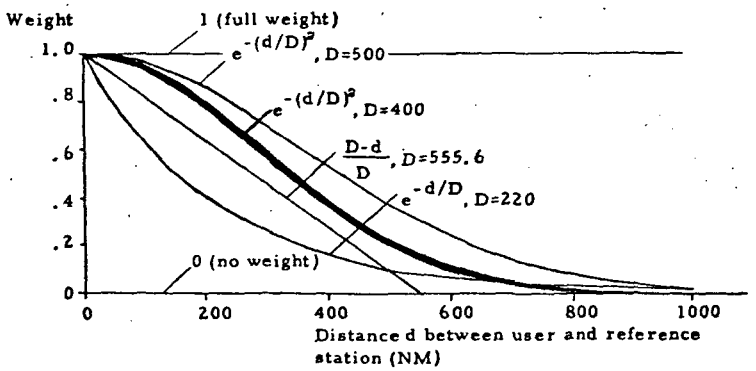

User Station	Reference Station	User-Ref. Distance d (NM)	Diurnal Mean of RMS Group Delay Residuals (nsec) ⟵ Linear Weight ⟶ =0 (no updt)	=1 (full updt)	$=\frac{(D-d)}{D}$ D=555.5	← Exponential Weight → $=e^{-d/D}$ D=220	$=e^{-(d/D)^2}$ D=400	$=e^{-(d/D)^2}$ D=500(NM)
Wash.	Ft. Mon.	170.4	4.05	1.42	1.72	2.37	1.47	1.41
Ft. Mon.	Otto.	305.0	3.97	3.41	2.76	3.13	2.71	2.77
Wash.	Otto.	410.0	4.69	4.50	3.44	3.62	3.38	3.41

best weight for test cases

Fig. 3 Methods of Distance Weighting in the Update Procedure of the Ionospheric Model

To summarize the results of the study on update weights, the size of the area over which ionospheric values showed similar deviations from normal was determined by performing many comparisons with three or more stations. When applying the same percent change to the ionosphere at an evaluation site as was found at an update station, the results achieved with data from nearby stations were excellent. However, where large distances were involved and when the ionospheric disturbances were not consistent over such distances, it had been observed that the basic predictions could be more accurate than the updated values. For this reason, a distance weight had been introduced in conjunction with the update. The possibilities considered included as weights both linear and exponential functions of the distance. Figure 3 shows the various weights along with the test results obtained from them. The best weighting function minimizing the residuals of measured minus updated data is an exponential bell-shaped curve with a decay constant of D=400 nautical miles, that gives almost full effect to the update from stations nearby and little effect to update over large distances.

The range-rate corrections are computed as one-way corrections along the satellite-to-satellite link and are to be subtracted from the tracking observations. They are computed by range differencing based on two consecutive range corrections 10 seconds apart; such a presentation best resembles typical range-rate tracking observations. The results are all normalized to 1GHz for easy conversion to any particular frequency of interest; the range-rate correction at frequency f in GHz is,

$$\Delta \dot{R}_f = \Delta \dot{R}_{1\,GHz} / f^2 \quad .$$

2.2 Effects of Satellite Geometry and Ionospheric Characteristics

A simple ionosphere uniform all over the globe was used with selected characteristics of f_0F2 and h_m, and ionospheric corrections to range-rate data were computed for ATS-6 tracking the simulated Apollo, Geos and Nimbus orbits as depicted in Figure 2. The corrections along the arc from the point underneath the high satellite to the point of disappearance are shown in Figure 4 for all three low orbiting spacecraft. The results are clearly explained by the geometric configuration of the raypath through the curved ionosphere as illustrated in Figure 1 with corresponding range and range-rate corrections. At the zero crossing of the range-rate, the range correction reaches its maximum with the satellite-to-satellite beam penetrating the ionospheres at a large slant angle and remaining in the vicinity of h_m over a long distance. The conditions are not as severe a bit earlier or later, the distances along the ray passing through the segments of maximum electron density are shorter, and the range correction smaller. At the inversion points along the range correction curve the range-rate correction reaches its maximum or minimum.

Only during the last few minutes of visibility of the satellite arcs are the corrections of significant value for high satellites, and orders of magnitude greater than the effects of ground to satellite tracking for low satellites. In actual tracking data the initial period after appearance above the horizon also has to be considered, which however was not presented here, because the ionosphere was chosen as uniform, and the corrections during the first half of the arc would be the identical mirror image of the one's shown for the second half. The lower the satellite orbit is, the shorter is its arc visible from ATS-6 and the longer is the time period over which ionospheric corrections are important: for Apollo-Soyuz at 200 km the last 13 minutes of its arc have to be considered for corrections, for Geos at 850 km the last 7.5 minutes and for Nimbus at 1100 the last 5.5 minutes. Figure 5 shows a linear correlation between this time interval and the satellite altitude.

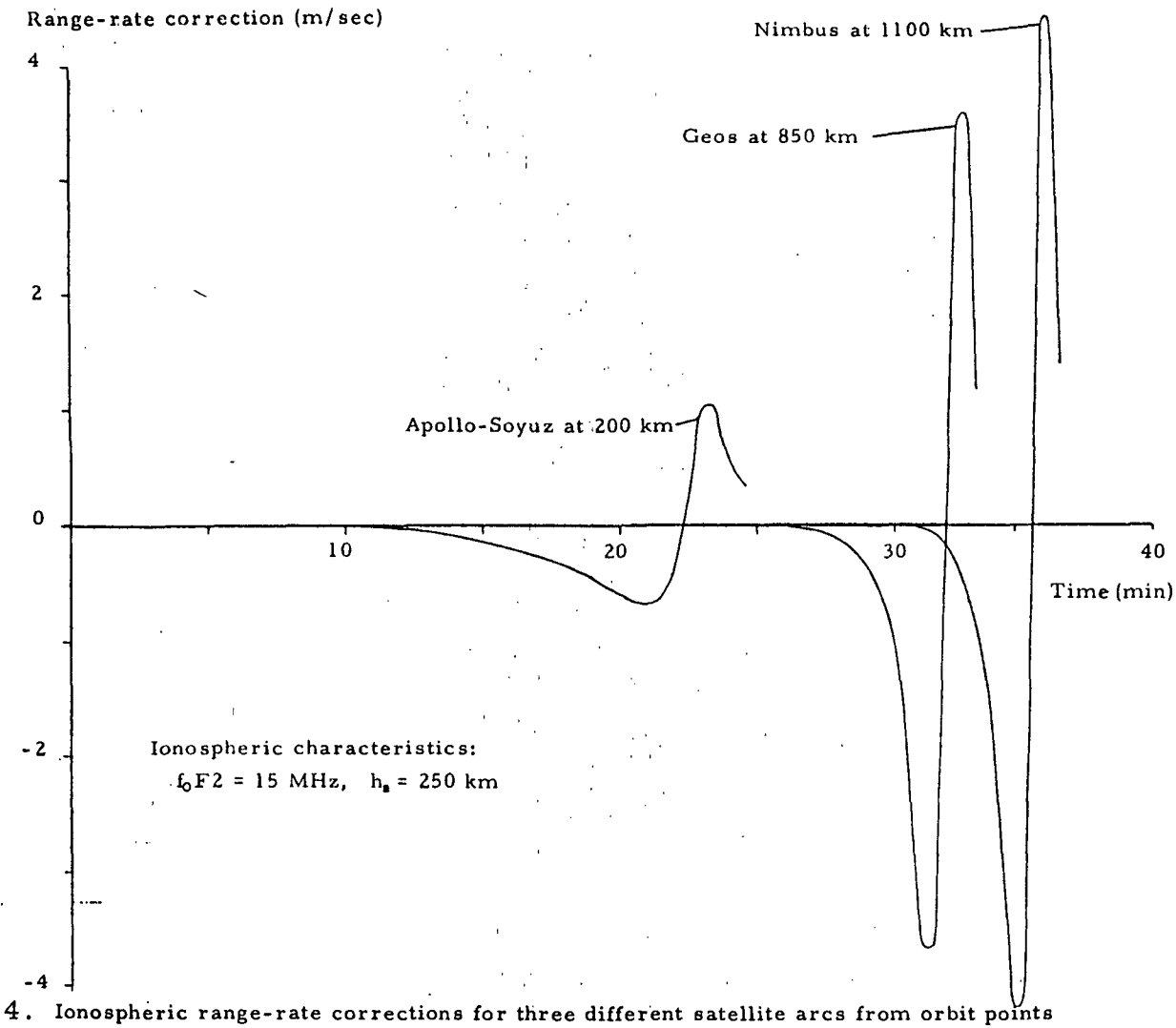

Figure 4. Ionospheric range-rate corrections for three different satellite arcs from orbit points underneath the high satellite to the points of disappearance computed at one minute intervals.

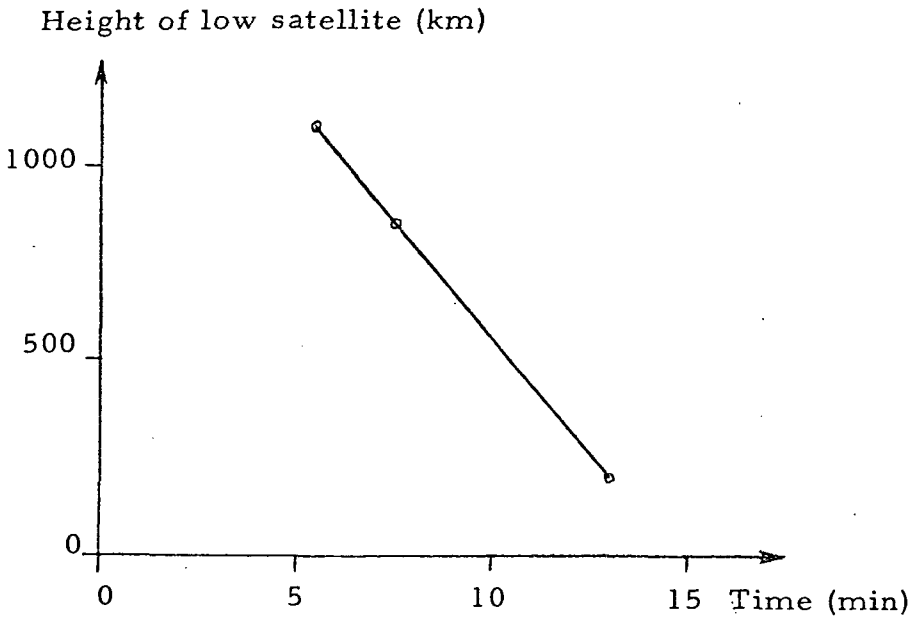

Figure 5. Time intervals at end of arc for satellite at different heights, during which ionospheric corrections several orders of magnitude greater than in ground to satellite tracking have to be considered for tracking data from ATS-6.

The range-rate corrections in Figure 4 were computed at one minute intervals based on two consecutive range corrections ten seconds apart. To gain a better time resolution and to not miss peaks in the data occurring between even minutes, range-rate corrections were computed at ten second intervals and only the last six to ten minutes of each arc are plotted, showing all significant variations in the corrections. Figure 6 is a repeat of Figure 4 on an expanded time scale. The data are lined up from the end of the arcs for convenience, and higher values in the peaks of the Apollo and Geos corrections are observed due to increased accuracy through better time resolution. The range-rate correction curves have steeper slopes and larger maxima the further out the satellite is. At h_m =250 km and f_0F2 = 15 MHz, the maximum correction for Apollo is about 1.2 m/sec, for Geos 4.2 m/sec and for Nimbus 4.4 m/sec, all at normalized frequencies of 1GHz.

The effect of changes in the height of the maximum electron density was investigated for the three low satellite orbits by recomputing the corrections for the simple ionospheres at different heights, setting h_m to values between 225 and 350 km. Variations in the height of the ionosphere, which often changes by $\pm$ 50 km per day, cause interference in the satellite-to-satellite path. Over the whole globe h_m ranges between 200 and 450 km resulting in diverse geometric effects on the raypath at different geographic locations.

Figure 7 is the result of the first attempt of computing the range-rate corrections along the Apollo-Soyuz arc for the selected ionospheric height conditions. A problem unique to the low satellite configuration shows up in the irregular deviations and oscillations along the correction curve. Such irregularities are not caused by the uniform ionosphere, but by the satellite-to-satellite correction model, which was thoroughly tested with the Gravsat (300 km)/Geopause configuration for which the problem did not show up. As seen in Figure 7, instabilities in the corrections occur only at the high values of h_m for Apollo at 200 km; in similar graphs for Geos and Nimbus the problem was not apparent. In the model, a stepsize of 3° in earth central angle was used to sample the electron densities below h_m along

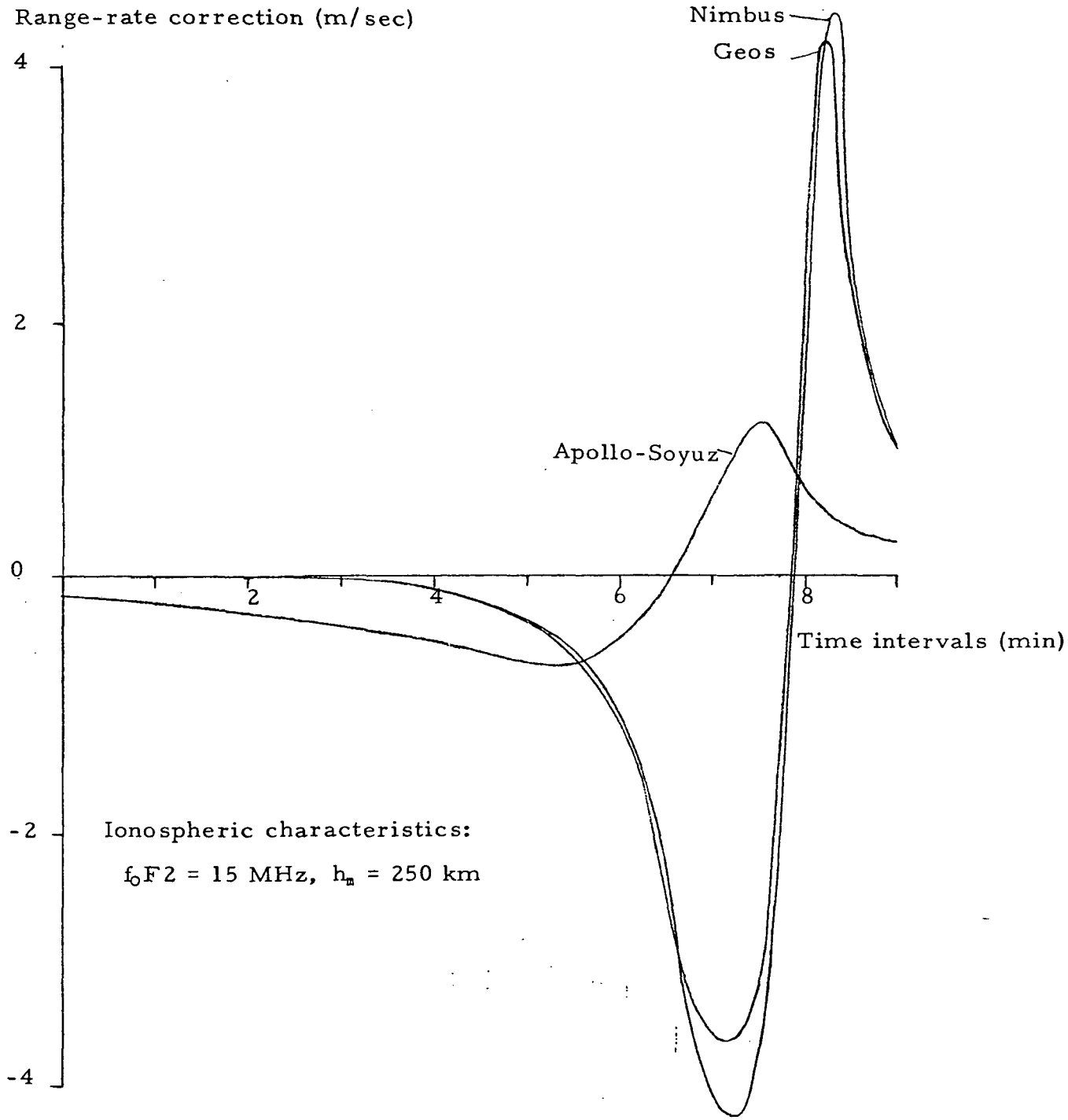

Figure 6. Range-rate corrections during last few minutes of various height satellite arcs computed at ten second intervals. Expanded time scale shows peak values more accurate than in Figure 4.

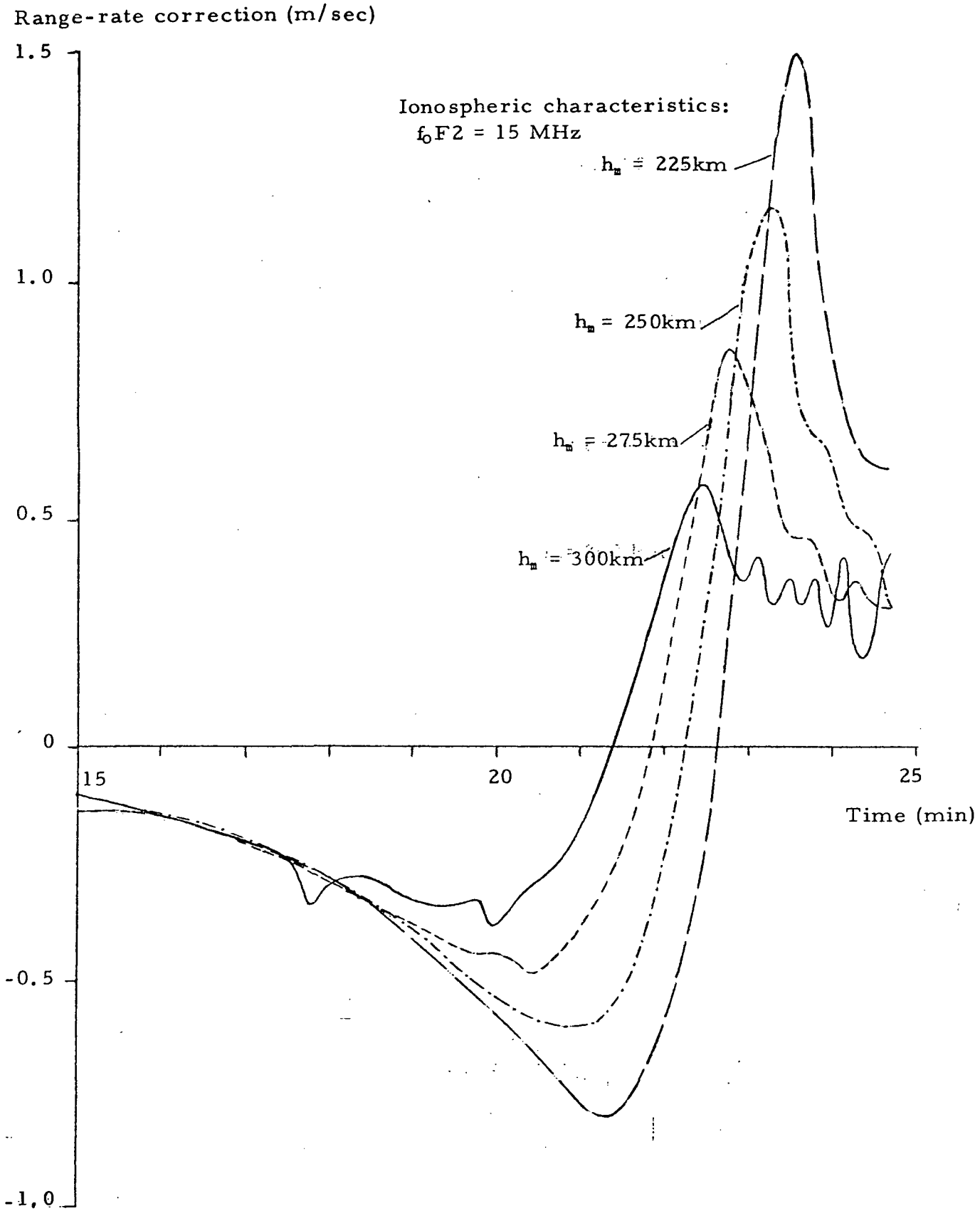

Figure 7. Range-rate corrections for the last ten minutes of Apollo-Soyuz arc show irregular oscillations, not induced by the uniform ionosphere, but by the model. A central angle step size of 3° was used to sample the density below h_m along the high to low satellite line. Figure 8 shows that using a 1° step size in the model removes the irregularities.

the high to low satellite line. This stepsize was too crude under the special circumstances of the low Apollo arc in combination with certain values of h_m. It was reduced to a 1° stepsize which clearly removed the irregularities as shown in Figure 8. This finding suggests to review the previously calculated corrections to the actual Apollo-Soyuz data for small oscillations that might be model induced.

The effect of changes in height on the corrections along the Apollo arc is very significant. A time shift of the peak value along the arc is experienced. A shift of 1.3 minutes in the occurrence of the peak exists between values of h_m at 225 and 300 km, and of 0.9 minutes for a 50 km height difference with h_m at 250 and 300 km. In addition, large changes in the maximum range-rate values are apparent; the lower the ionosphere, the larger the peak values are. Range-rate corrections vary from about 1.5 to 0.6 m/sec for h_m between 225 and 300 km, showing an increase of about 0.3 m/sec in the peak value for each 25 km drop in h_m.

The tests were repeated for the Geos and the Nimbus satellites with the height of the maximum electron density at 250, 300 and 350 km. The results are shown in Figures 9 and 10. A time shift of the maximum and minimum corrections is again clearly evident, and is of similar order for both satellites, about 0.35 minutes for a 50 km change in h_m and 0.7 minutes for a 100 km change. Even though some small variation exists in the size of the peak values, there is no definite trend, and it can probably be attributed to the chance of selecting the ten second points along the arc along slightly denser ionospheric paths. The large amplitude changes connected with different h_m in Figure 7 are therefore typical for the Apollo satellite at 200 km altitude, which always remains below h_m.

Effects of changes in electron density on the range-rate corrections along the satellite arcs were examined by choosing f_0F2 at 5, 10 and 15 MHz for the uniform ionosphere. Such variations in f_0F2 can be caused by localized ionospheric perturbations, diurnal variations, day-to-day changes, seasonal effects and solar cycle patterns. The results are shown in Figures 11, 12 and

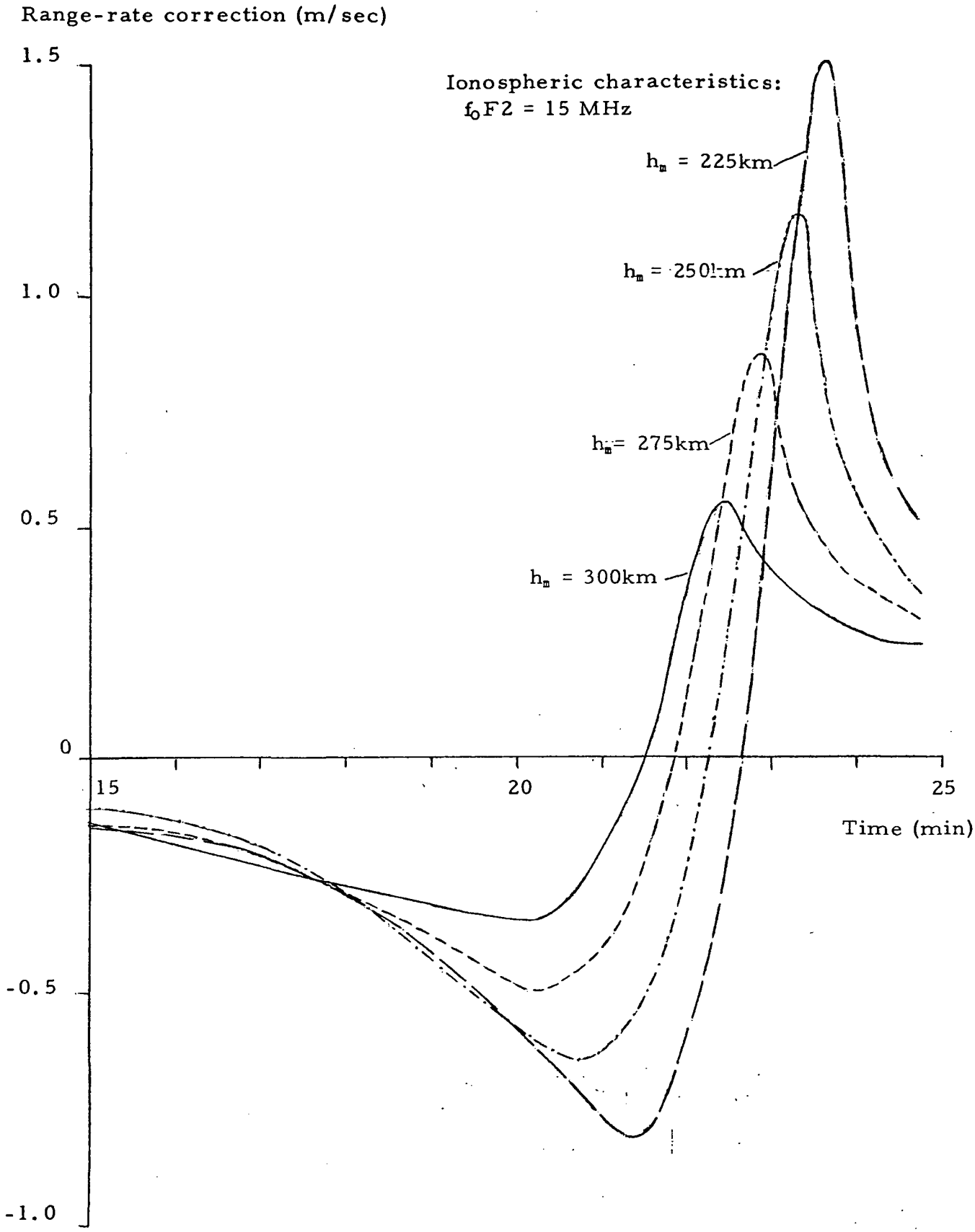

Figure 8. Range-rate corrections during last ten minutes of Apollo-Soyuz arc using uniform ionosphere at several different heights. The effect of h_m is obvious in great amplitude variations as well as in a definite time shift of the peak corrections along the arc. A central angle step size of 1° was used in the model to eliminate model induced irregularities.

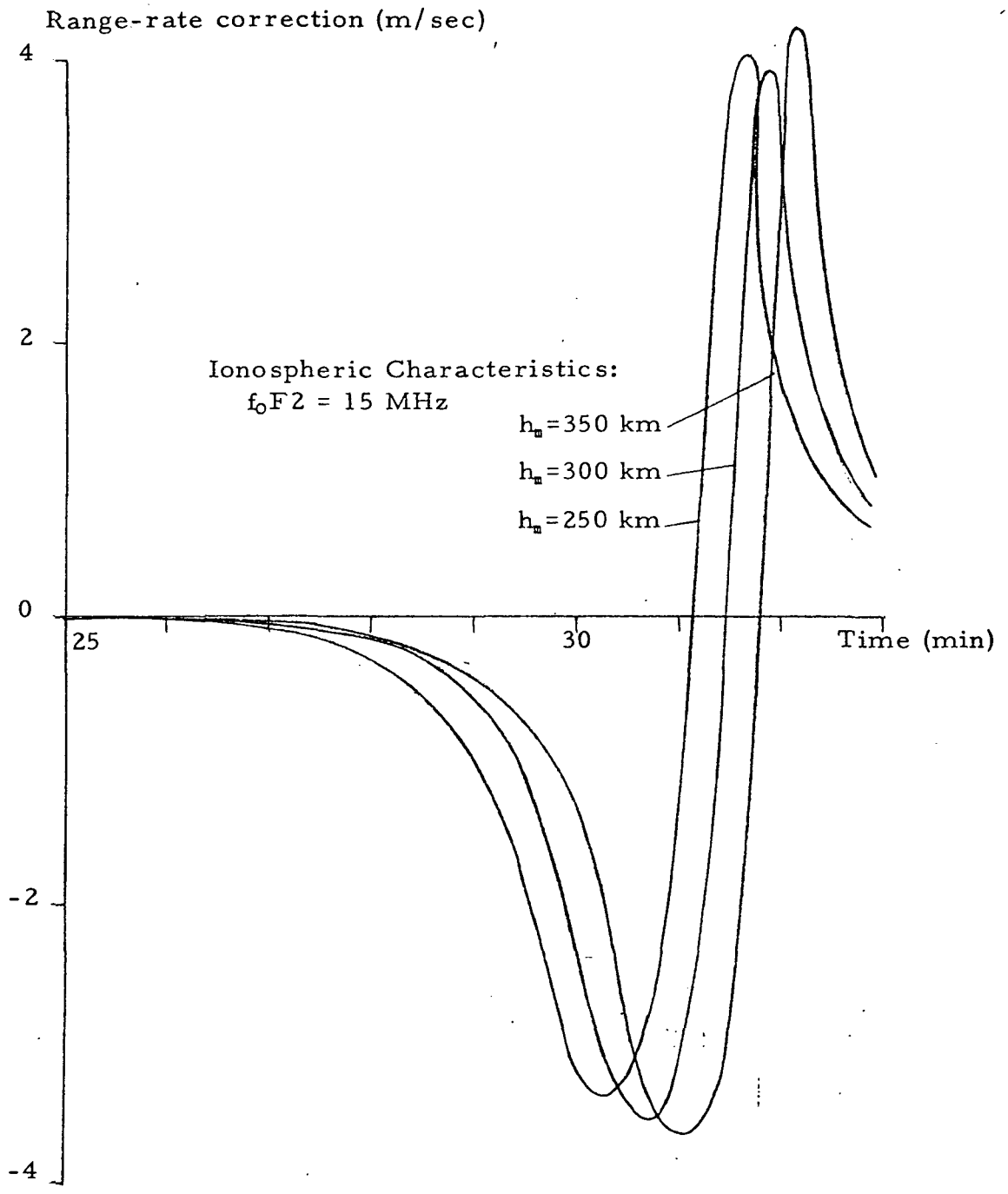

Figure 9. Range-rate corrections during last few minutes of Geos arc using uniform ionosphere at different heights. The effect of h_m is evident in a time shift of the peak corrections along the arc.

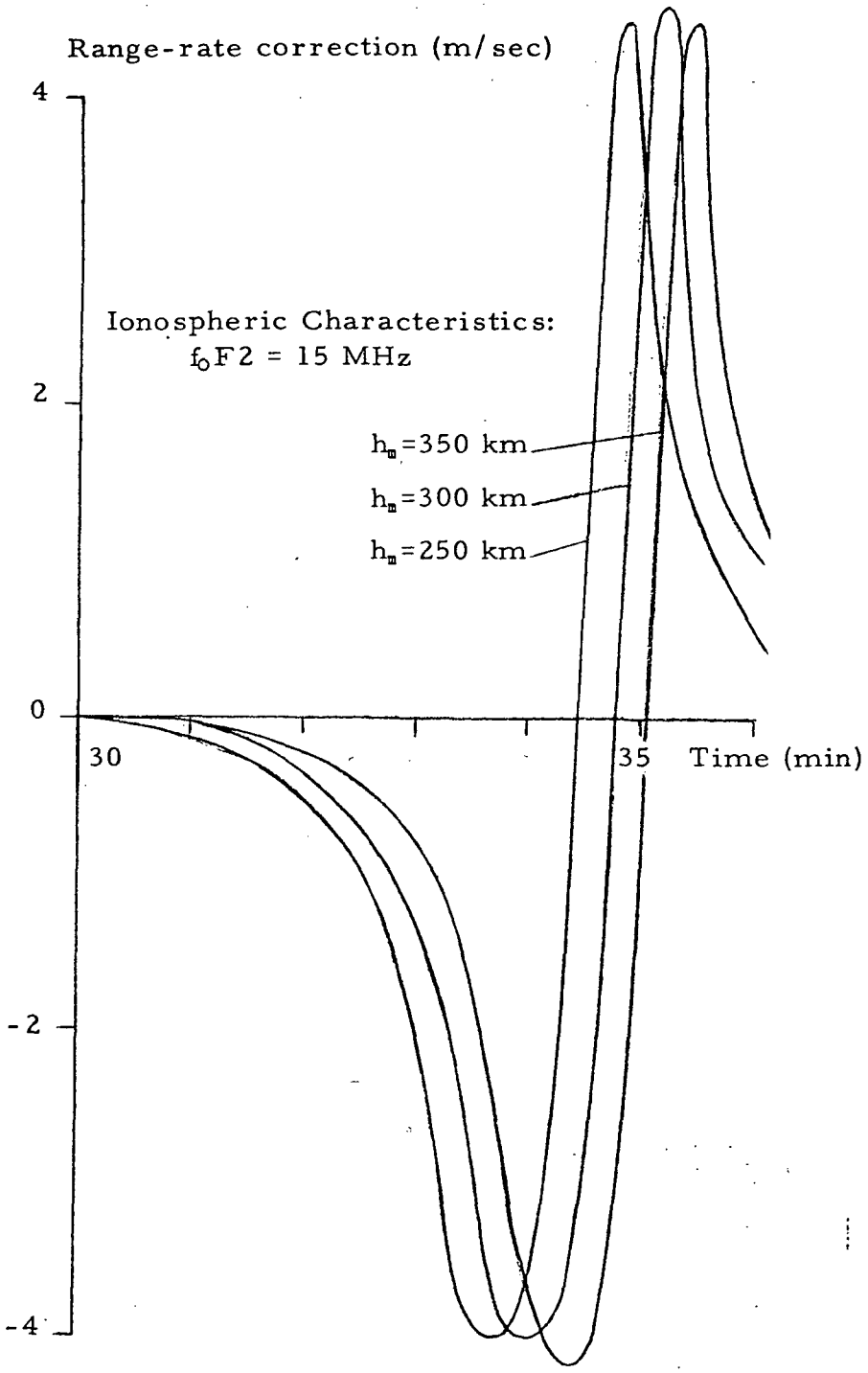

Figure 10. Range-rate corrections during last few minutes of Nimbus arc using uniform ionosphere at different heights. The effect of h_m is evident in a time shift of the peak corrections.

13 for Apollo, Geos and Nimbus respectively. In all instances a considerable increase in the absolute values of the range-rate corrections was achieved when increasing f_0F2. The peak values for each satellite are approximately in the same ratios as the squares of the f_0F2s. It is also seen when comparing the figures for the three satellites that for each set of ionospheric characteristics the peak range-rate corrections are larger and the slopes steeper, the higher the satellite is, as was already evident in Figure 6 for another set of conditions. For h_m = 300 km and f_0F2 = 15 MHz for example, peak values of about 0.6 m/sec exist for Apollo, 3.9 m/sec for Geos and 4.7 m/sec for Nimbus. A time shift of the peak corrections along the satellite arc, as was associated with changes in h_m, is not apparent for changes in f_0F2.

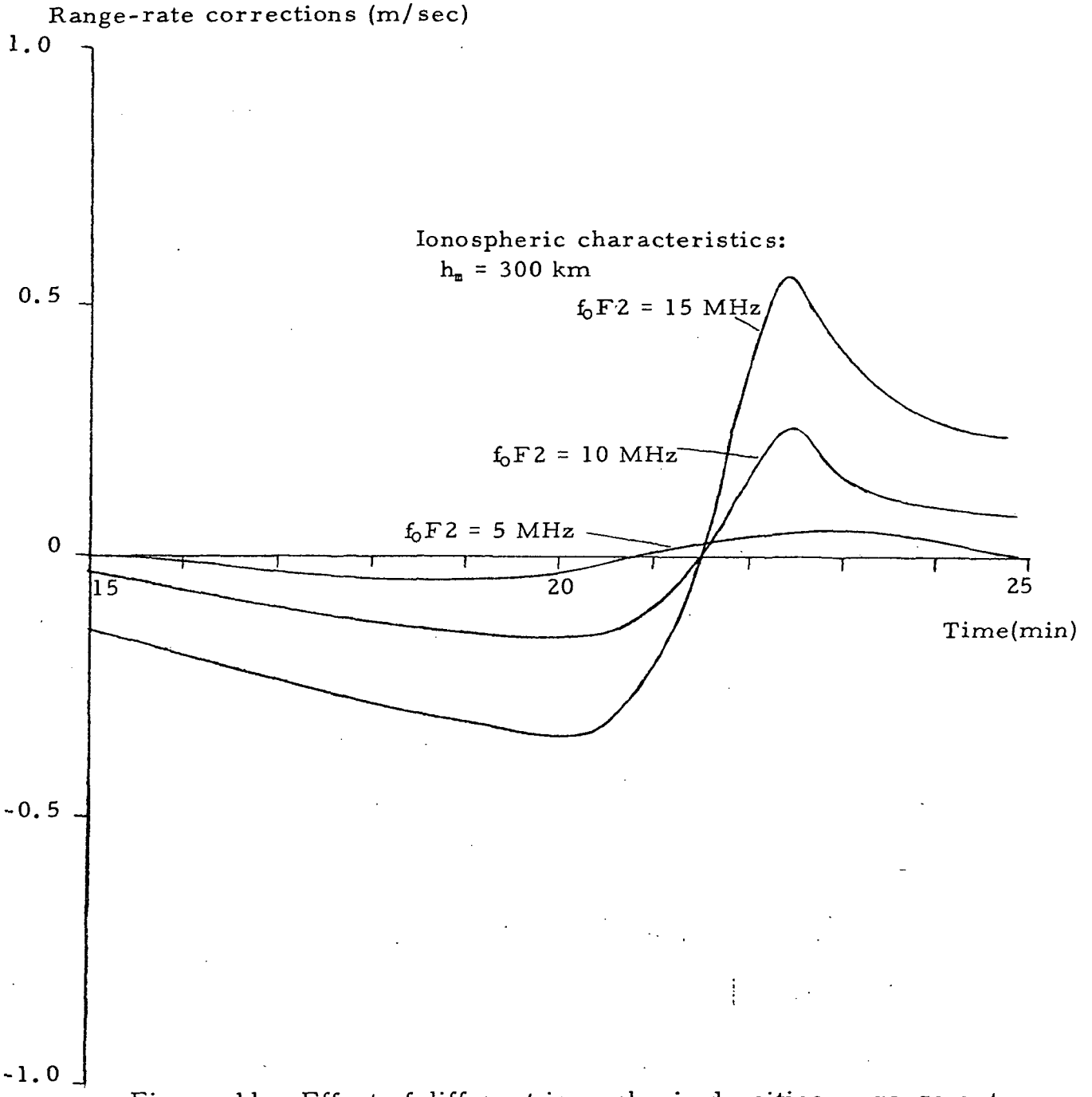

Figure 11. Effect of different ionospheric densities on range-rate corrections during last ten minutes of Apollo-Soyuz arc. The vàrious f_0F2 produce significant variations in amplitude.

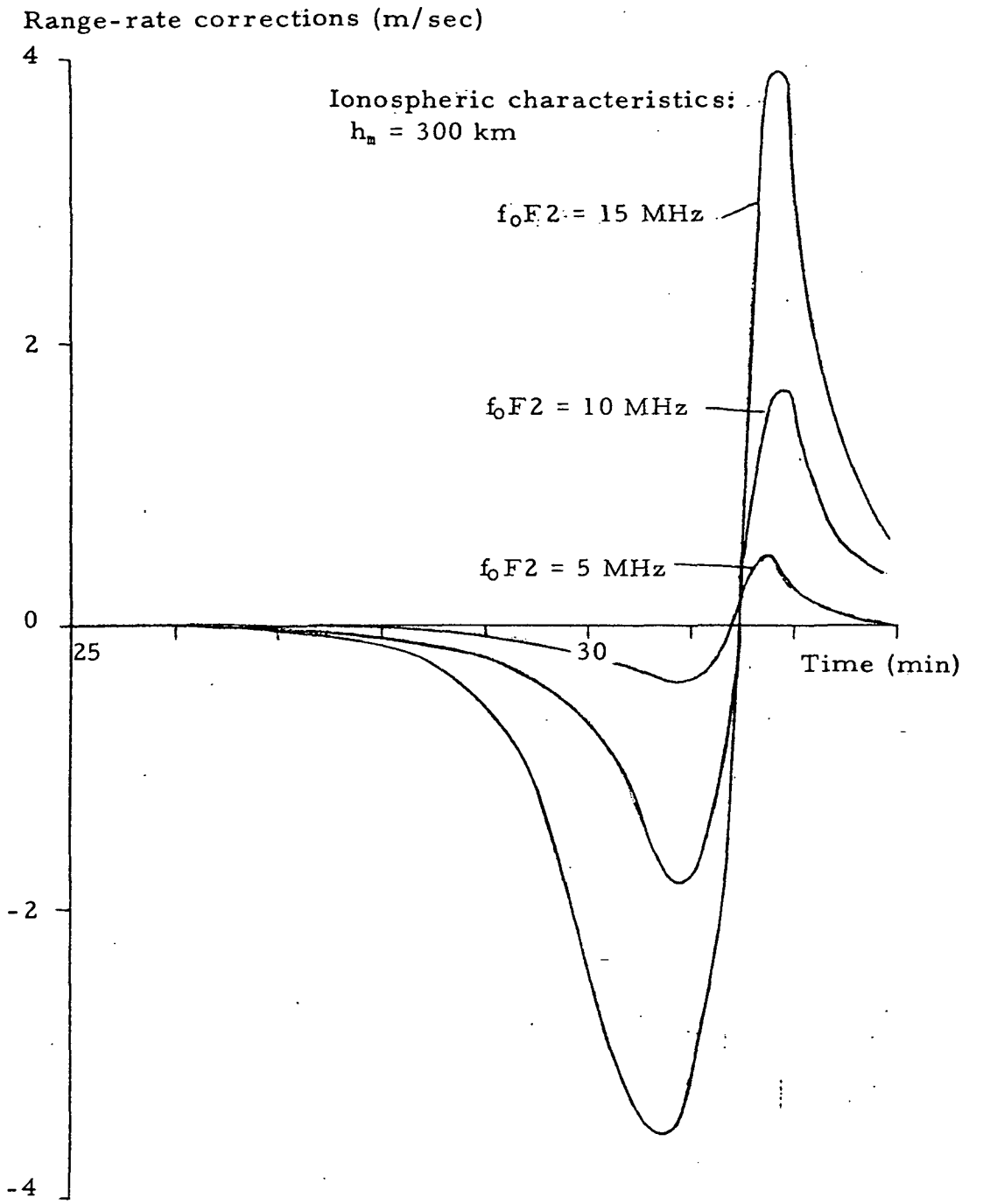

Figure 12. Effect of different ionospheric densities on range-rate corrections during last few minutes of Geos arc. The various f_oF2 produce significant variations in amplitude.

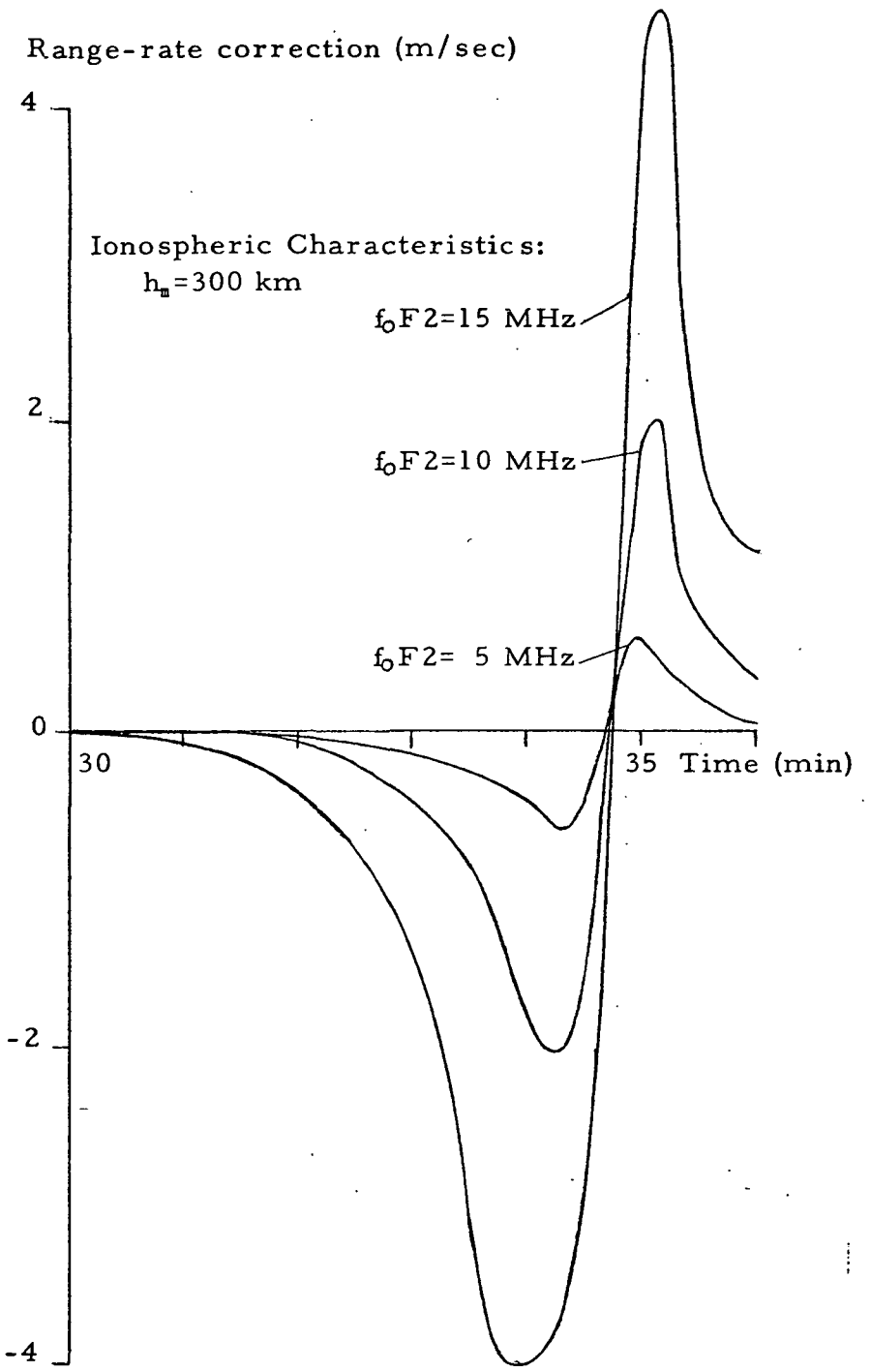

Figure 13. Effect of different ionospheric densities on range-rate corrections during last few minutes of Nimbus arc. The various f_oF2 produce significant changes in amplitude.

2.3 Effects of Ionospheric Perturbations

The influence of steep ionospheric gradients on the satellite-to-satellite range-rate corrections along the spacecraft arc needed to be investigated. Such large gradients are observed in regions of the equatorial anomaly and the sunrise region, and during the irregular occurrences of ionospheric disturbances. They were simulated by injecting into the previously uniform ionosphere variations in electron density, which have maximum effect at the perturbation center and gradually decrease with increasing distance from the center. The distance weighting function is shown in Figure 3. The perturbation centers were selected at different geographic locations, so that at times the satellite arc would pass through the center causing a maximum change from the unperturbed range corrections. It was also arranged at times that the satellite arc would pass some distance from the center, where the slope of the weighting function is the steepest, resulting in a fast changing density as the satellite travels along its arc, and hence in great variation in range-rate corrections.

The effects of perturbations were examined on both the simulated Apollo-Soyuz arc at 200 km and the Geos arc at 850 km. In Figure 14 the range-rate corrections using a uniform ionosphere with a maximum density of $f_0F2 = 15$ MHz at height $h_m = 300$ km are compared with the result when a local perturbation is superimposed at 75° or at 80° latitude along or close to the low satellite arc. The results from Apollo and Geos are plotted on the same scales for easy correlation, showing the Geos corrections to be of much larger amplitude, but the effects of the perturbations on the Apollo arc to be of greater relative severity persisting over a longer period of time. For both satellites the perturbations can cause drastic changes in the amplitudes of the peak range-rate corrections along the arc, and in the case of the Apollo-Soyuz arc the range-rate corrections even experience a change in sign as is evident when injecting an ionospheric perturbation at 80° latitude. A shift in the peak amplitudes along the arc is possible for both satellites, as well as the occurrence of additional maxima and minima. On the whole,

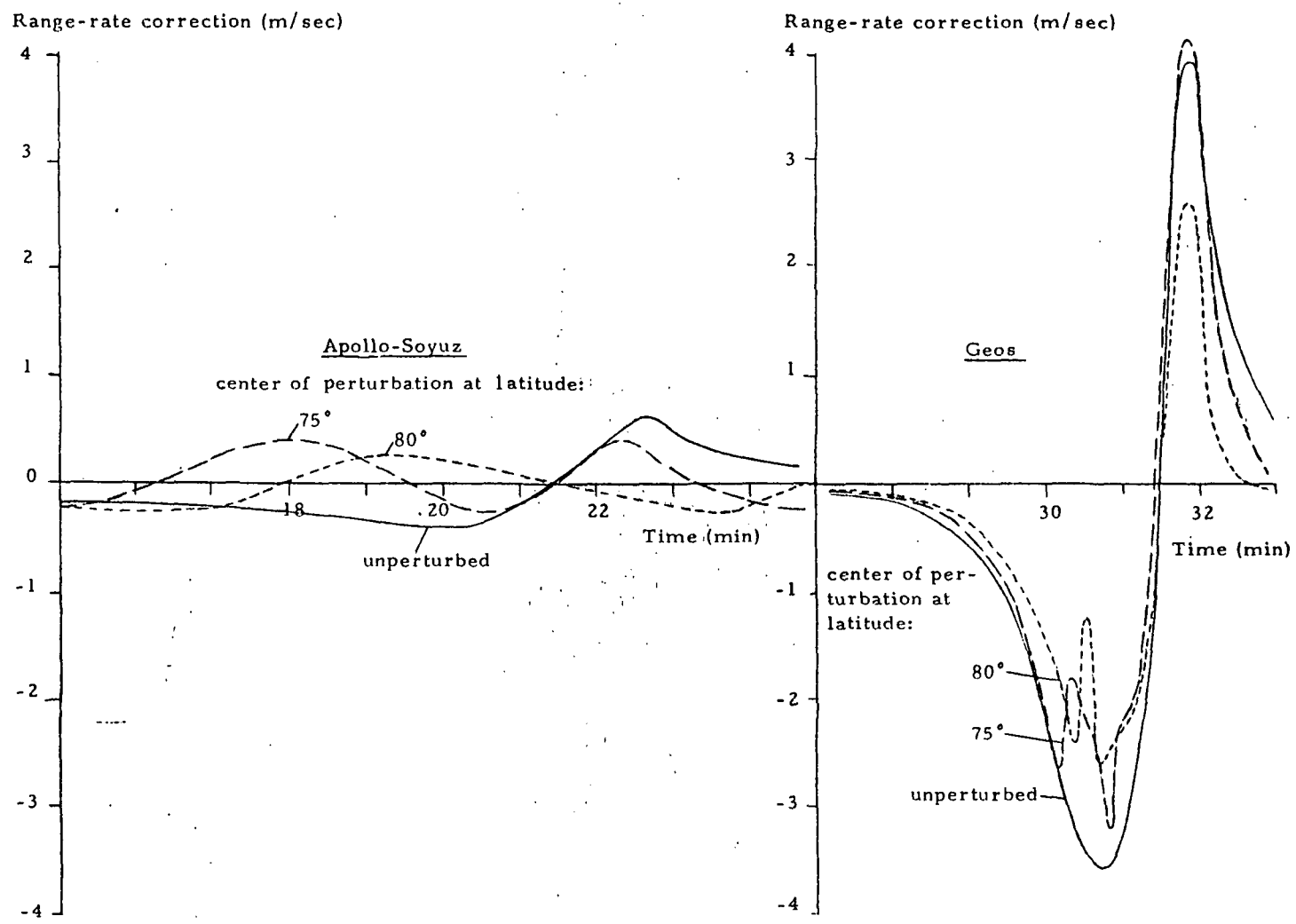

Figure 14. Effect of ionospheric perturbations on range-rate corrections along Apollo-Soyuz and Geos arcs on same scales. Ionospheric characteristics h_m = 300 km, f_0F2 = 15 MHz are perturbed to f_0F2 = 5 MHz at 75° and 80° latitude along satellite path, and results are compared with unperturbed data.

the ionospheric gradients can greatly modify the smooth predictable correction curves from the geometric effects.

Figure 15 illustrates how the amplitude of the perturbation applied at a fixed geographic location modifies the correction curves of the purely geometric effects along the Apollo-Soyuz arc. A drop of 5 MHz at the perturbation center of 75° latitude causes a final peak amplitude to be modified from the unperturbed value and introduces an additional maximum several minutes earlier. A drop of 10 MHz lowers the final peak even more and causes a much larger early maximum with a single oscillation right at the peak. The peaks for the cases of the 5 and 10 MHz drops coincide in time. An increase of 5 MHz at the center produces a quite different pattern however, creating significantly larger absolute values for maxima and minima as well as a shift in peaks.

Shifting the center of perturbation to different latitudes along or close to the Apollo-Soyuz arc mainly manifests itself in a large time shift of the additional extremum of roughly 1.5 minutes for each 5°latitude shift, as shown in Figure 16. This spike is a maximum in Figure 16a for a drop of 10 MHz at the perturbation center, and a minimum in Figure 16b for an increase of 5 MHz. Much variation is evident in the final peak of the range-rate corrections from 0.6 m/sec, which is larger than the unperturbed peak, to the negative value of -0.05 m/sec. The center of the 70° latitude perturbation is located at the piece point of the satellite-to-satellite beam with the densest portion of the ionosphere at 17.9 minutes into the arc, as illustrated in Figure 17. For the 75° latitude perturbation this situation occurs 19.8 and 22.7 minutes into the arc, and the 80° perturbation always remains 4°or more away from this piercepoint so that the section of the distance weighting function with maximum slope effects the corrections along the satellite line of sight.

While the Apollo-Soyuz corrections were relatively small for the ionosphere at h_m = 300 km in Figure 16, they more than double for the case of a low height of maximum electron density, h_m = 225 km, as demonstrated

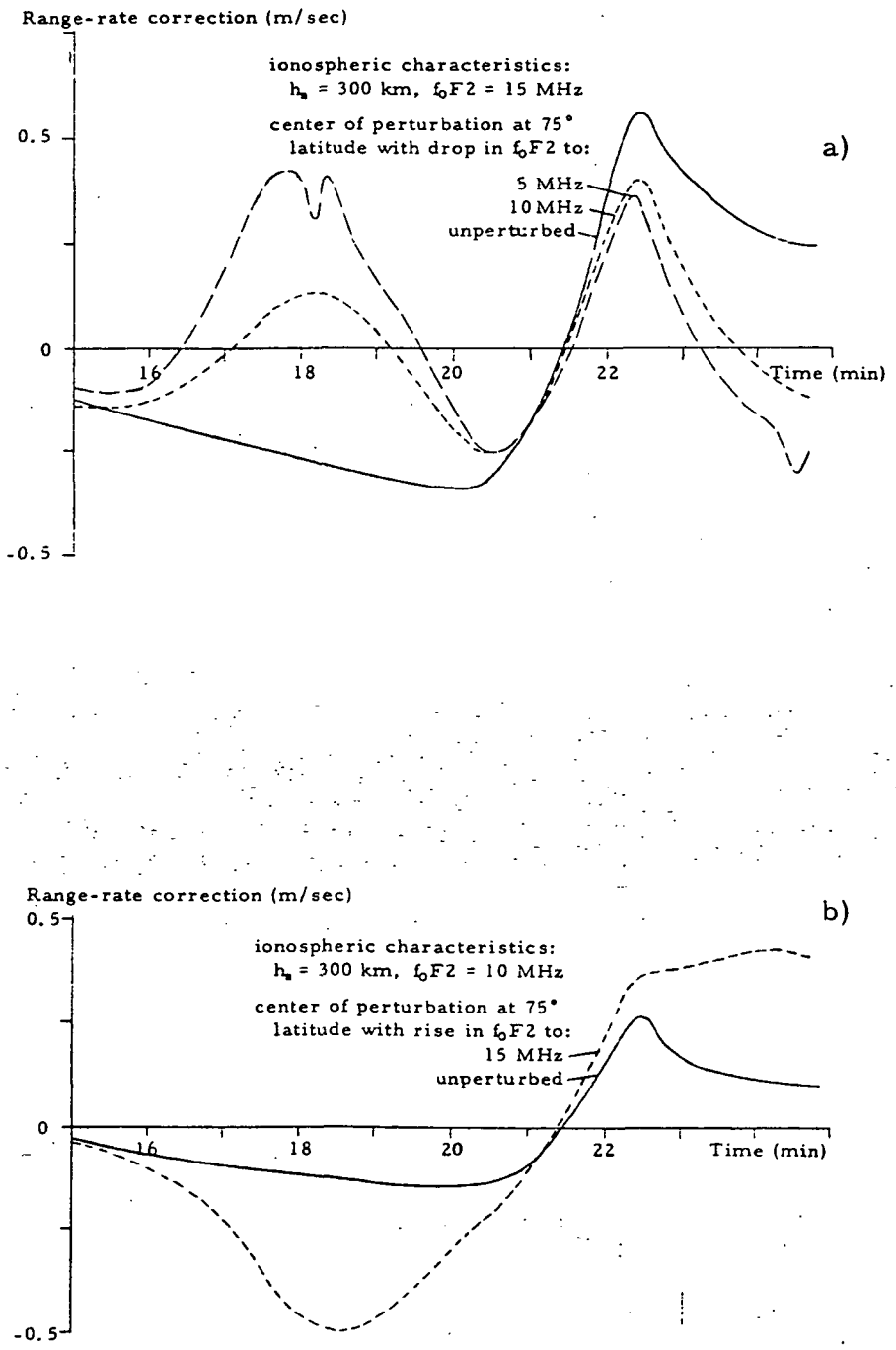

Figure 15. Effect of ionospheric perturbations of different magnitude on range-rate corrections along the Apollo-Soyuz arc. In a) the result of a 5 and 10 MHz drop in f_0F2 below the uniform 15 MHz is shown, and in b) the result of a 5 MHz rise above the uniform 10 MHz.

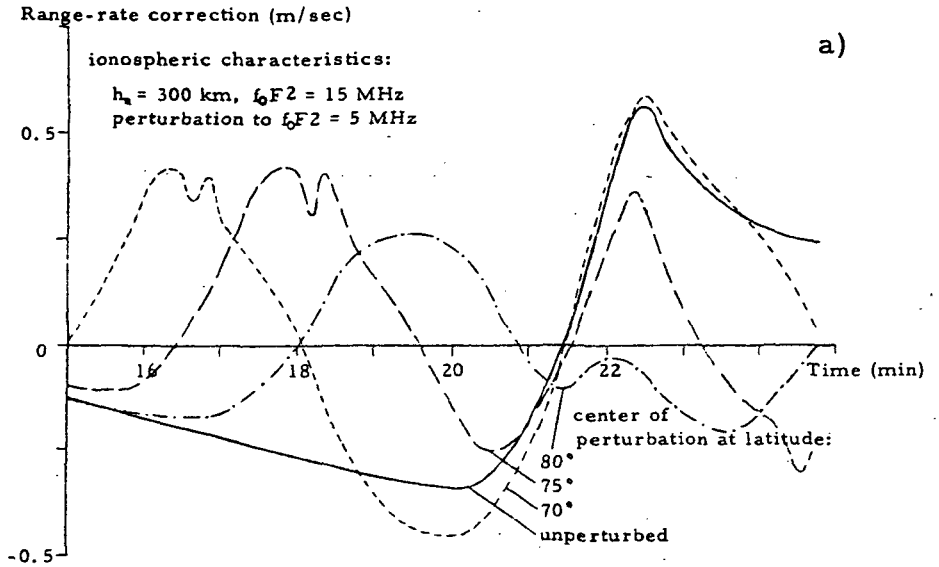

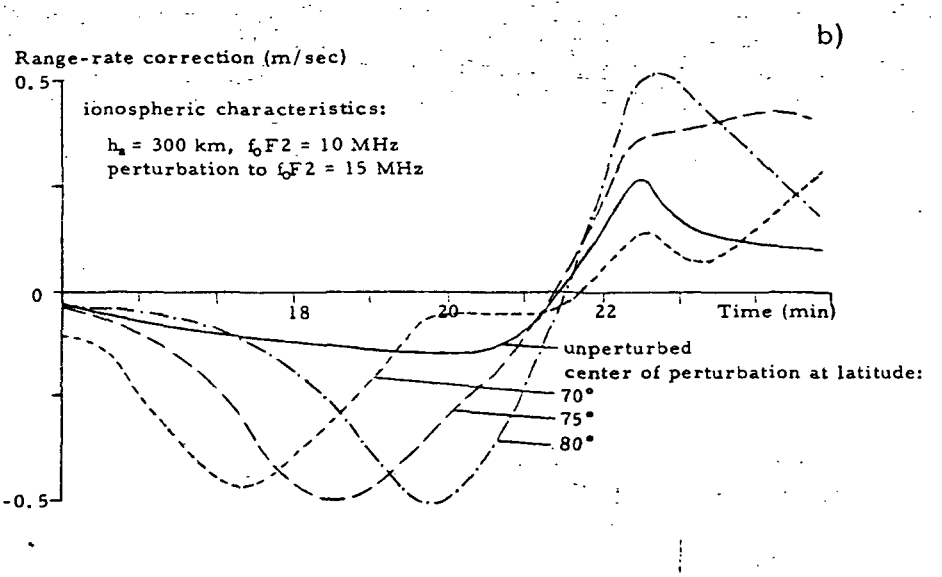

Figure 16. The effect of the location of the ionospheric perturbation center on the range-rate corrections along the Apollo-Soyuz arc is demonstrated for h_m = 300 km. The perturbation is characterized by a drop at the center of 10 MHz in a) and 5 MHz in b).

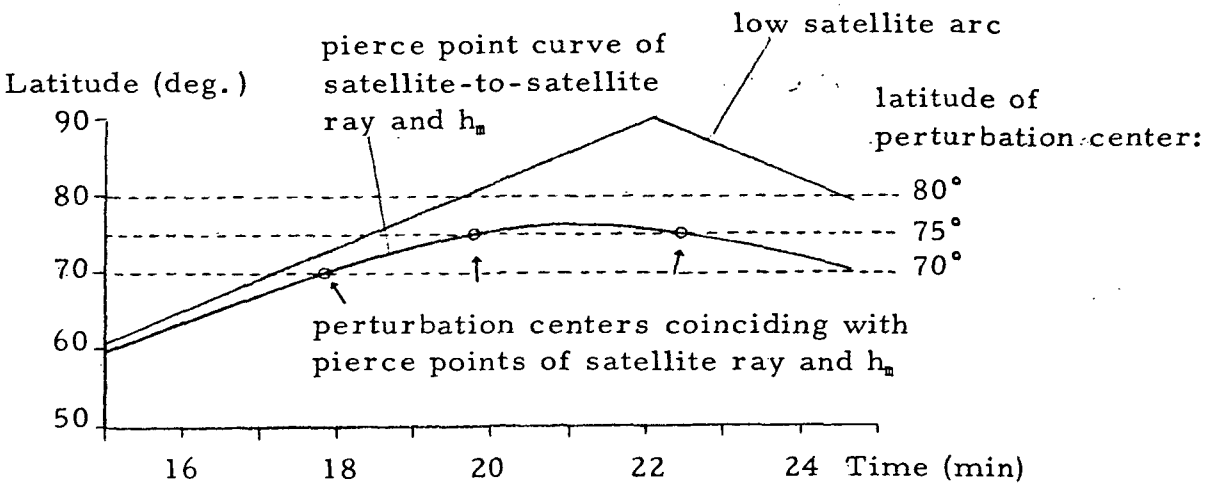

Figure 17. Illustration of placement of perturbation centers in space and time along Apollo-Soyuz type arc. The low satellite is at 200 km altitude in polar orbit, and is tracked by a satellite at 36,000 km altitude also in polar orbit.

in Figure 18. The perturbation centers at 62°, 75° and 81° latitude were selected to coincide with the intersection point of the satellite connecting ray and the height h_m at 15 minutes, at 18.5 as well as 24.2 minutes and at 21.5 minutes along the arc respectively. Hence, perturbation centers where chosen at times when the unperturbed range-rate correction were at an extreme at 21.5 minutes, but also at times when the corrections were low at 15 and 18.5 minutes, or changing most rapidly at 24.2 minutes. The perturbation at 81° latitude causes the final peak of the geometric effect to diminish to a very small amplitude and introduces a double spiked maximum some 4.5 minutes earlier. With the center at 75° latitude the final peak is reduced by a smaller amount and a double spiked earlier peak occurs 6 minutes before the final one. The 62° latitude perturbation creates a final peak greater than that of the pure geometric effect and has an even earlier additional peak, which is off the scale to the left.

The results in Figures 16a and 18 both for a drop from 15 to 5 MHz at the perturbation center, but for the different ionospheric heights show quite similar patterns: modification of the geometry caused final peak amplitude, and introduction of an additional maximum. The earlier the perturbation center appears along the arc, shown in Figure 17, the earlier does the extra peak occur.

The large additional peaks caused by the perturbations in the simulated Apollo-Soyuz range-rate correction data were found as large as 500 mm/sec at 1 GHz and f_0F2 = 15 MHz. Converting to the tracking frequency of 2.2 GHz used in the actual Apollo-Soyuz experiments for which ionospheric corrections had been computed in an earlier contract, and converting to a critical frequency of 7 MHz more typical for the July 1975 data, the amplitudes of extra peaks would be of the order of 22 mm/sec. Such correction maxima occur 6 to 12 minutes before the end of the arc in Figure 18, and therefore correlate very closely in location and in size to the Indian Ocean gravitational anomalies that had been found in the range-rate tracking data, and hence these effects can be explained by perturbations in the ionosphere.

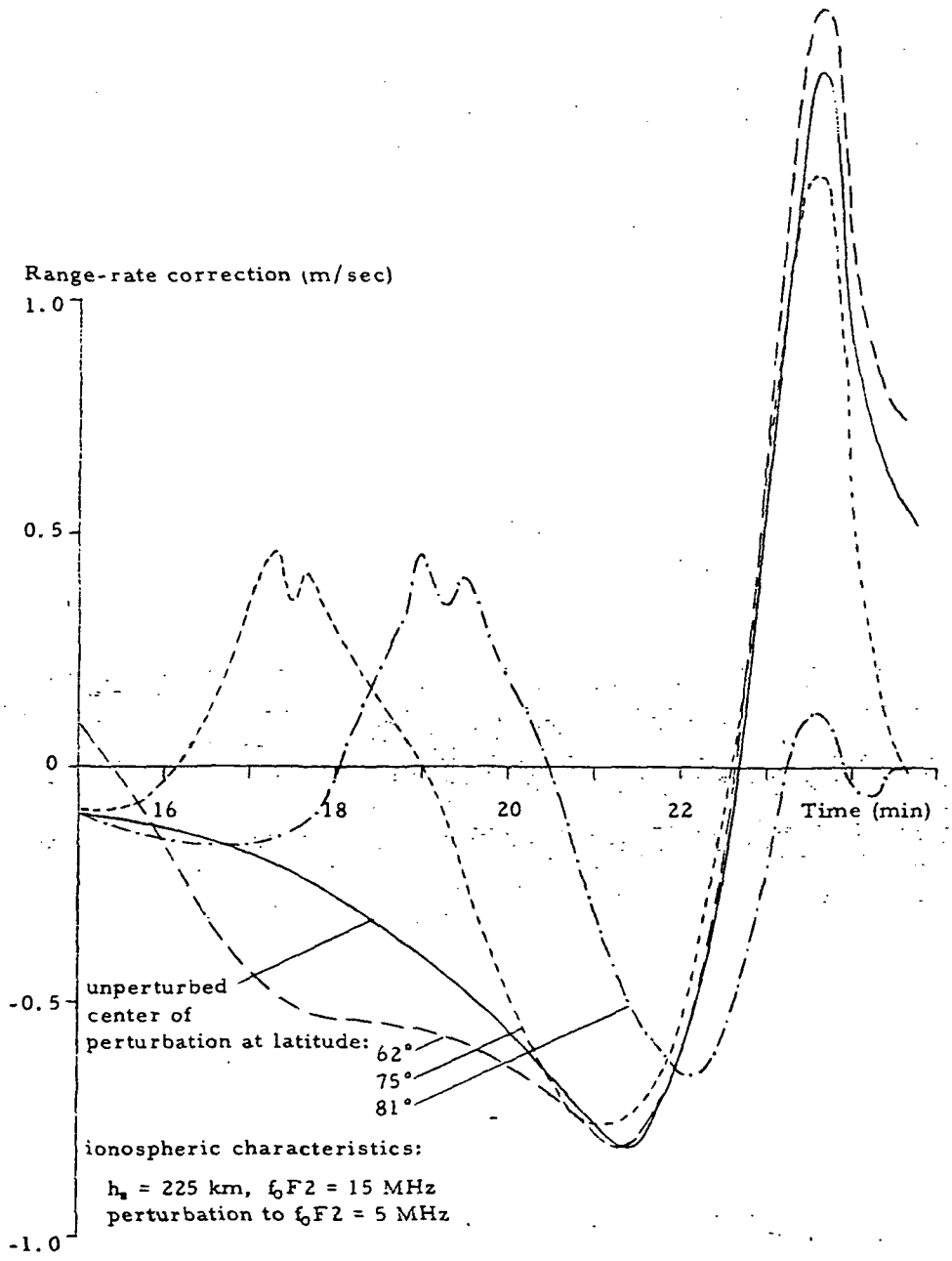

Figure 18. The effect of the location of the perturbation center on the range-rate corrections along the Apollo-Soyuz arc is demonstrated for a low ionosphere with h_m = 225 km.

Figures 19 and 20 illustrate the effects of steep ionospheric gradients on the range-rate corrections along the higher Geos satellite arc. Figure 19 shows how the size of the electron density perturbation effects the corrections for several choices of locating the disturbance center. The unperturbed curve due purely to the geometric effect through a uniform ionosphere with f_0F2 = 15 MHz can be compared with the cases, where a decrease of 5 MHz and of 10 MHz occurs at the perturbation center. The perturbation can cause lower or higher peak corrections, a shift in the peak of about one half minute, as well as the occurrence of double peaks in place of the geometry caused single peak. In all cases the deviations from the smooth unperturbed curve are more severe, the greater the amplitude of the disturbance is.

The effects of locating the perturbation center at different latitudes close to the Geos arc are investigated in Figure 20. Figure 21 illustrates the positions of the perturbation centers in latitude and in time along the low satellite arc, and with respect to the low satellite latitude and the satellite-to-satellite beam intersection points with the height of maximum electron density of the ionosphere. Cases for different size drop or rise in f_0F2 at the center are given in Figure 20a-d. The position of the center of disturbance matters greatly and can modify the smooth unperturbed curve in quite different manners. The extreme values due to geometric effects can be increased or decreased significantly, the peaks may shift in time along the arc, and additional oscillations of large amplitude may be introduced into the range-rate correction curve as visible in Figure 20c, up to 4.5 minutes before the end of the arc. The variations in the curves are difficult to predict and interpret, and do not show a pattern as regular as in the Apollo-Soyuz case.

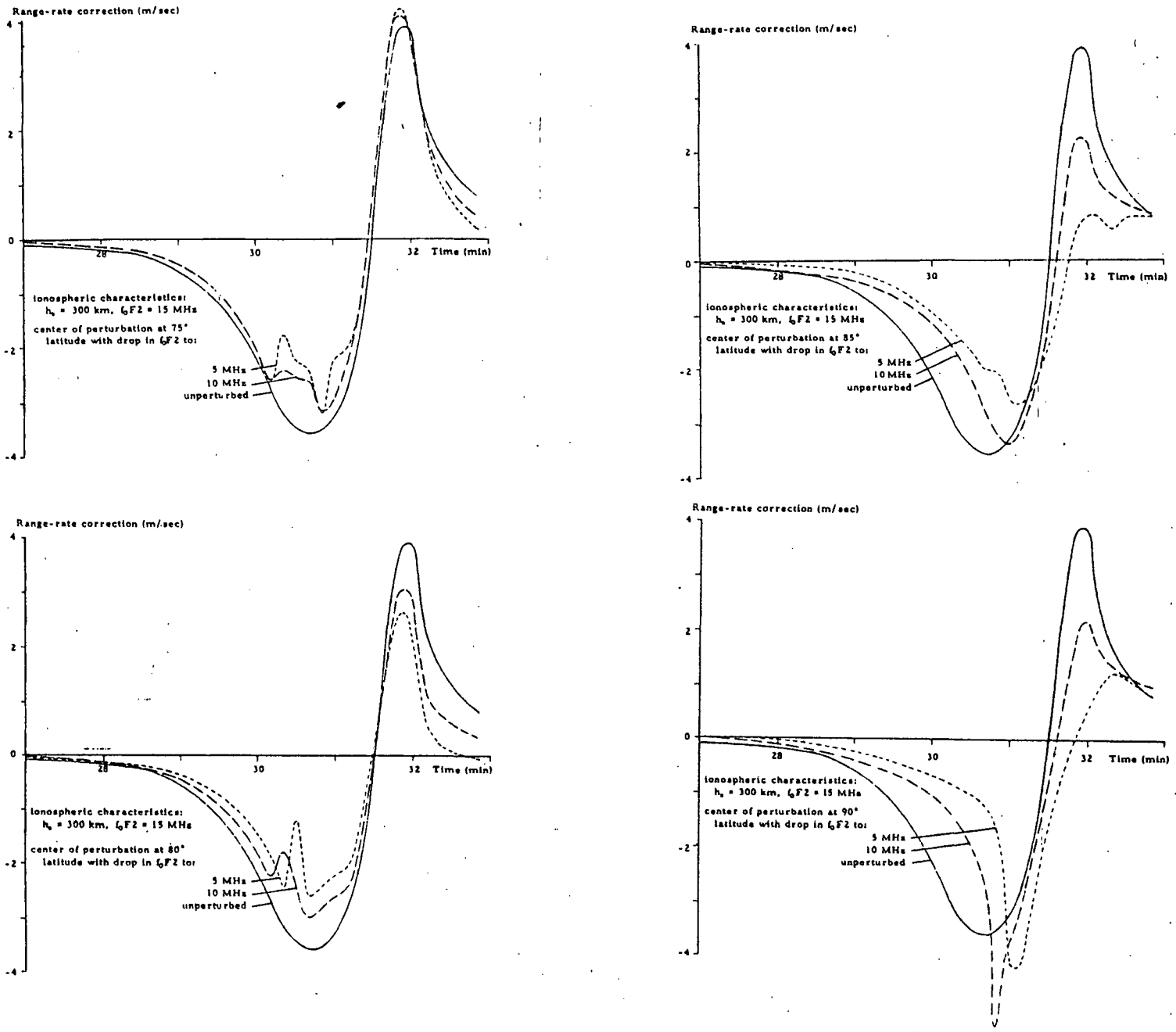

Figure 19. Effect of ionospheric perturbations of different magnitude on range-rate corrections along the Geos arc. The results of a 5 and 10 MHz drop at the perturbation center, which is located at different latitudes, are compared with the results of the uniform 15 MHz ionosphere.

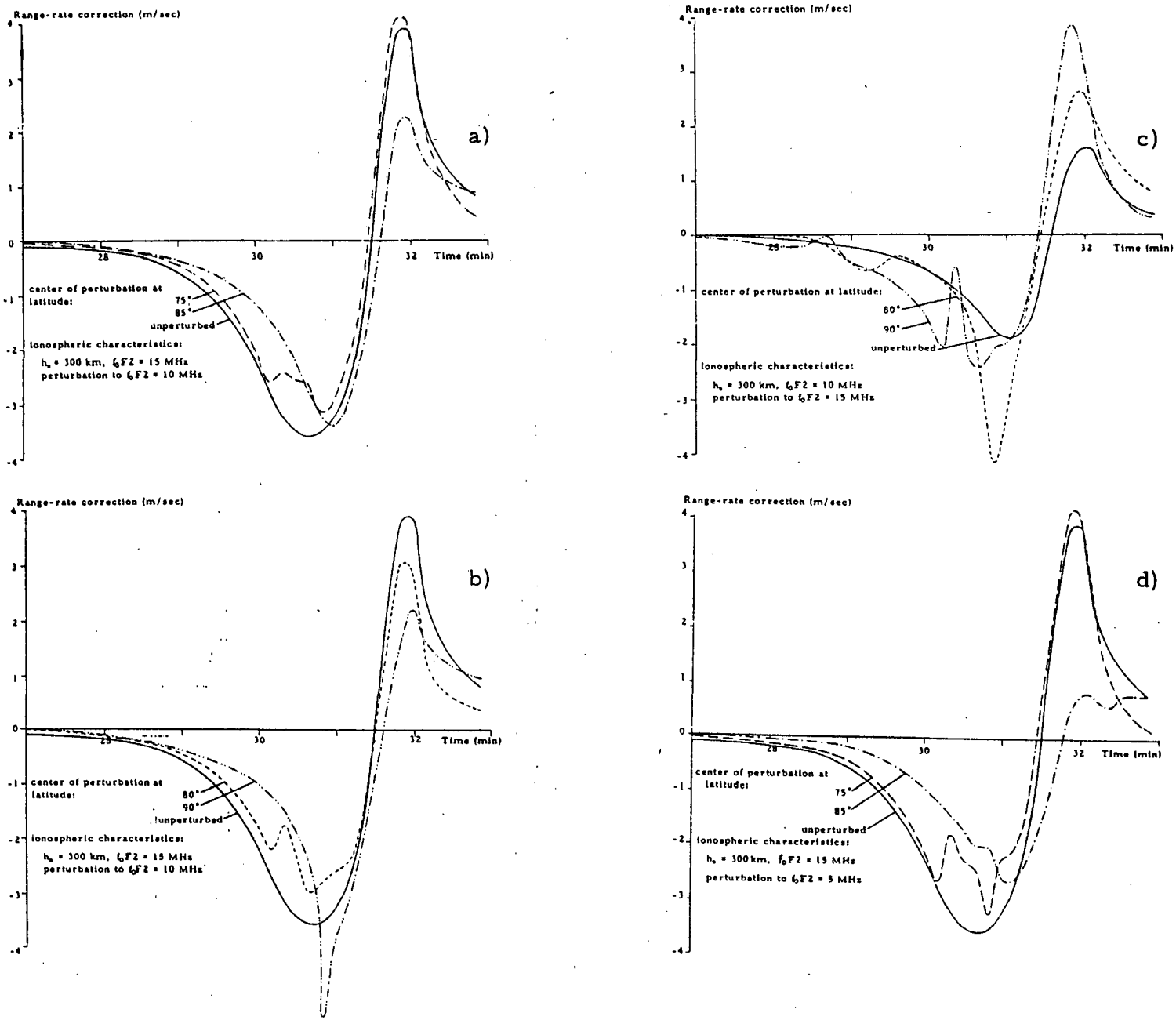

Figure 20. Effect of the location of the ionospheric perturbation center on the range-rate corrections along the Geos arc. The results of a 5 MHz drop at different latitudes is shown in a)b), of a 5 MHz rise in c) and a 10 MHz drop in d).

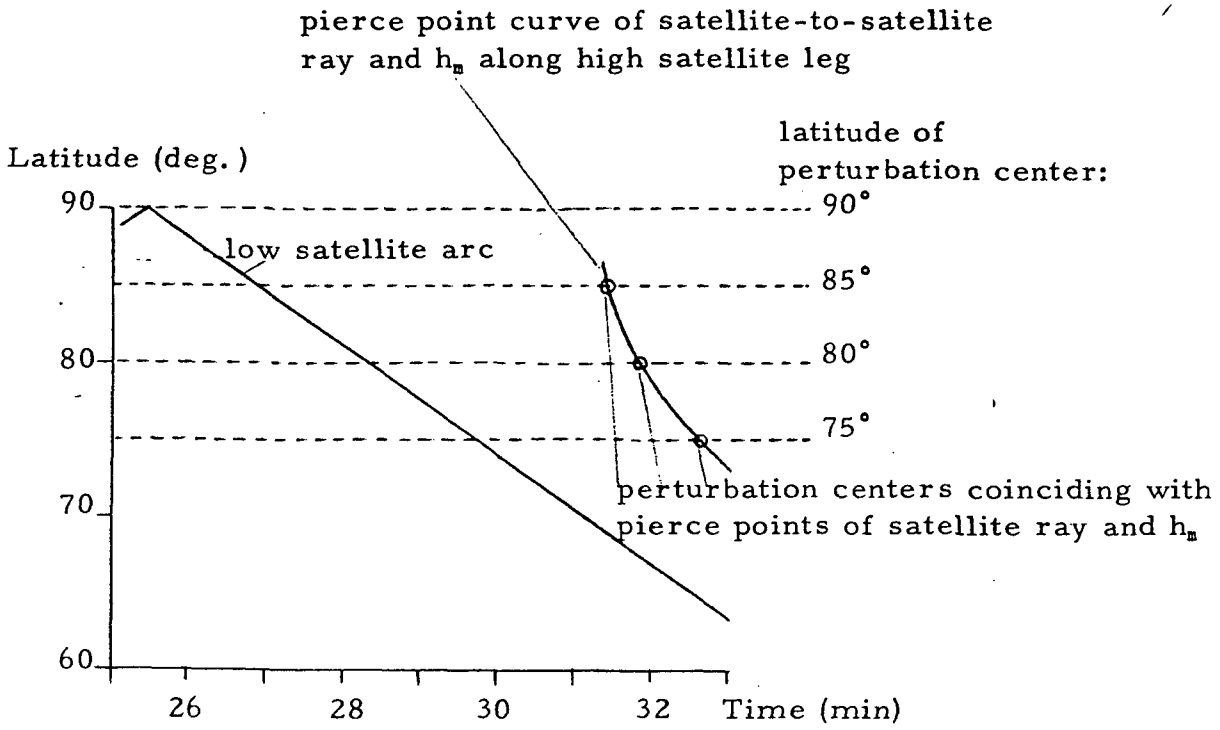

Figure 21. Illustration of perturbation centers in space and time along Geos type arc. The low satellite is at 850 km altitude, and is tracked by a satellite at 36,000 km altitude, both in polar orbit. Initially the satellite-to-satellite ray remains completely above h_m, and only after 31.4 minutes into the arc does it pierce h_m.

2.4 Simple Model Results

In satellite-to-satellite tracking the effects of ionospheric refraction are difficult to predict because of complex orbit configurations with changing ionospheric conditions. Evaluating the effects of a simple uniform ionosphere on coplanar satellite orbits at various altitudes clarified the size and duration of refraction errors incurred purely by the geometry of the slanted raypath through the curved ionosphere. Modification of the ionospheric characteristics of the maximum electron density and the corresponding height illustrated the variations that refraction errors will undergo for changing conditions. The height of the ionosphere often changes by $\pm$ 50 km per day, and differences of 5 to 10 MHz in critical frequency can easily be caused by localized perturbations, diurnal variations, day-to-day changes, by seasonal effects and solar cycle patterns. To further investigate the effects of local perturbations, steep ionospheric gradients were injected into the otherwise uniform ionosphere, as they are observed in the equatorial anomaly region, the sunrise region and during irregular occurring ionospheric disturbances.

The following are the results of major importance of this study:

1) The ionospheric range-rate corrections due to the geometric effect along the satellite arc are illustrated in Figure 4 for different altitude satellites. The lower the satellite orbit is, the shorter is its arc visible from the high tracking satellite, and the longer is the time period over which ionospheric corrections are orders of magnitude larger than in ground-to-satellite tracking; for Apollo-Soyuz at 200 km the last 13 minutes of its arc show such large corrections, for Geos at 850 km the last 7.5 minutes, and for Nimbus at 1100 km the last 5.5 minutes considering coplanar orbits. However, if low and high satellites are moving at right angles to each other and are close to the point of disappearance, then such large effects can be observed for extended periods of time, see Section 3.

2) Range-rate correction curves as a function of time along the arc have steeper slopes and larger positive and negative peaks the higher the satellite altitude is. At h_m = 250 km, f_0F2 = 15 MHz and a tracking frequency of 2.2 GHz the maximum corrections are

25 cm/sec, 87 cm/sec, 91 cm/sec for Apollo, Geos and Nimbus respectively. At a lower value of f_0F2 = 8 MHz the corrections would still be about 7 cm/sec, 24 cm/sec and 26 cm/sec for the three satellites respectively.

3) Changes in the height of the ionosphere which are typically $\pm$ 25 km, produce very significant effects on the range-rate corrections, as shown in Figures 8, 9 and 10. Time shifts of the peak values along the arc are experienced; for a 50 km shift in h_m they are of the order of 0.9 minutes for Apollo and 0.35 minutes for Geos and Nimbus. Such time changes are significant when attempting to derive localized gravitational effects. In addition, for the Apollo spacecraft which always remains below h_m, large changes in the maximum correction values are apparent. Increases of about 62 cm/sec in the peak value occur for each 25 km drop in h_m at f_0F2 = 15 MHz and a tracking frequency of 2.2 GHz. Such changes in peak values are, however, not apparent from the higher satellite data from Geos and Nimbus.

4) Changes in electron density effect the amplitude of the range-rate corrections such that the peak correction values for each satellite are approximately in the same ratios as the squares of the f_0F2s. Time shifts of the peak corrections along the satellite arc are not associated with changes in f_0F2. See Figures 11, 12 and 13.

5) Ionospheric perturbations with associated steep gradients in electron density can greatly modify the smooth range-rate correction curves as predictable from geometric effects in satellite-to-satellite tracking. The peak values may experience drastic increases or decreases in amplitude as well as shifts in time, and additional maxima and minima can occur along the arc. As shown in Figure 14, the effects of the perturbations on the Geos corrections are of larger amplitude, but the effects on the Apollo arc are of greater relative severity persisting over a longer period of time.

6) For different size disturbances under otherwise fixed conditions the range-rate corrections show similar patterns. However, the greater the amplitude of the electron density perturbation and the steeper the slopes of the gradients are, the more severe are the deviations from the smooth unperturbed correction curve. See Figures 15 and 19.

7) Shifting the location of the perturbation center to different latitudes close to the Apollo-Soyuz arc manifested itself mainly in a large time shift, of the order of minutes, of the additional single or double peak extremum. The earlier the perturbation center appears along the arc, the earlier does the extra peak occur, see Figures 16 and 18. An amplitude variation of the final unperturbed positive peak is also experienced from a slight increase to a drop to negative values depending on the location of the disturbance. Shifting the perturbation center has similar effects on the Geos tracking data, see Figure 20, but the pattern does not appear as regular as in the Apollo case.

8) When converting to the appropriate tracking frequencies and f_0F2, and considering the effects of shifts in amplitude and location of typical ionospheric disturbances, the perturbations cause variations in range-rate corrections that are closely correlated in location and size to the Indian Ocean gravitational anomalies that were extracted from the Apollo-Soyuz tracking data.

3.0 INVESTIGATION OF EFFECTS DUE TO IONOSPHERIC VARIATIONS USING THE BENT MODEL

In this section the effects of actual variations and gradients in the ionosphere on satellite-to-satellite range-rate corrections are investigated. These gradients occur along the arc of a low satellite being tracked by a high satellite. For this purpose the 3-dimensional worldwide Bent ionospheric prediction model was used to show the effects of steep spacial gradients as well as of short and long term temporal gradients, such as diurnal variations, day-to-day deviations from the monthly mean, seasonal and solar cycle variations.

3.1 Simulated Orbits

To capture the ionospheric variations, the orbit configuration was chosen quite different from the coplanar orbits used for the simple model investigations in Section 2. The satellite orbits were simulated perpendicular to each other, the stationary high satellite in an equatorial orbit, and the low satellites at various heights in polar orbits both prograde and retrograde. The angular separation between the satellites was chosen in the proximity of the disappearance points, and under such circumstances significant range-rate corrections exist along most of the orbit. Tracking frequencies of 1GHz were used in the simulations and conversions to any other frequency are simply done using the conversion formula in Section 2.2. The range-rate corrections are presented as the one-way values.

In Figures 22-24 several of the orbit configurations are shown. The low satellites in prograde orbits disappear from the sight of the high satellite for a portion of their orbits in Figure 22 and become visible again as they cross the equator. Three such cases were considered for low altitude satellites at 200, 300 and 850 km and the high tracking satellite at 35, 785 km. The graphs show two of the orbits superimposed on a world map of the ionospheric characteristic of $f_x F2$. Where the $f_x F2$ equal value lines are concentrated, large ionospheric gradients exist, and it is indicated where the ionospheric pierce point curve crosses these gradients. The intersection of

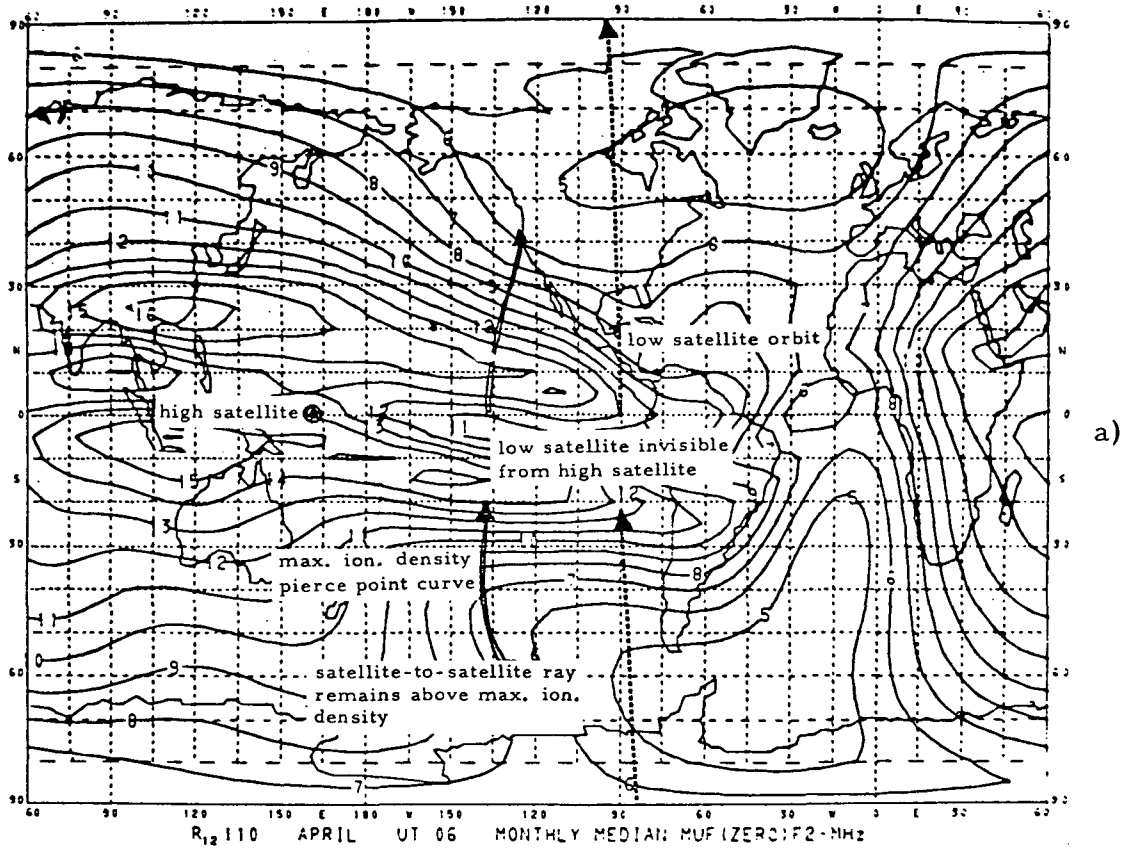

a)

a) low satellite altitude = 850 km

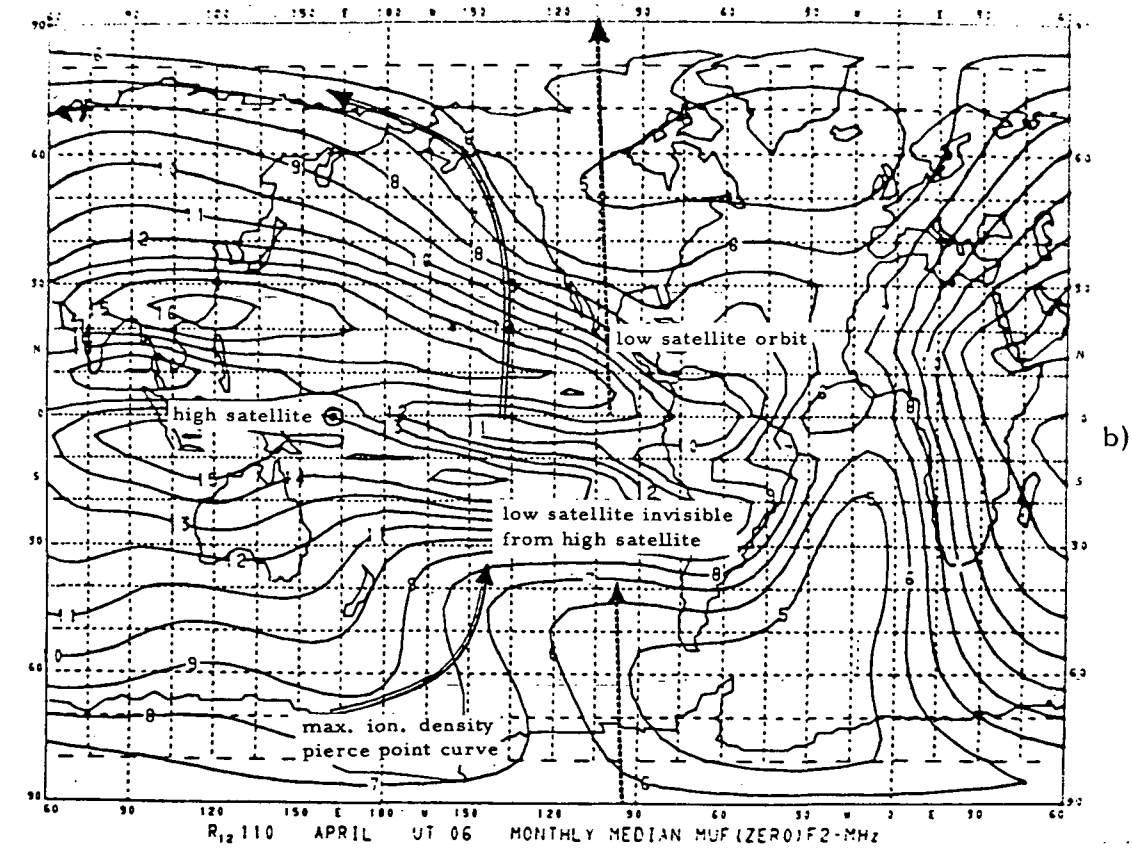

b)

b) low satellite altitude = 300 km

Figure 22. Ground traces of high satellite position, low satellite orbit and maximum electron density pierce point curve superimposed on world map of fxF2.

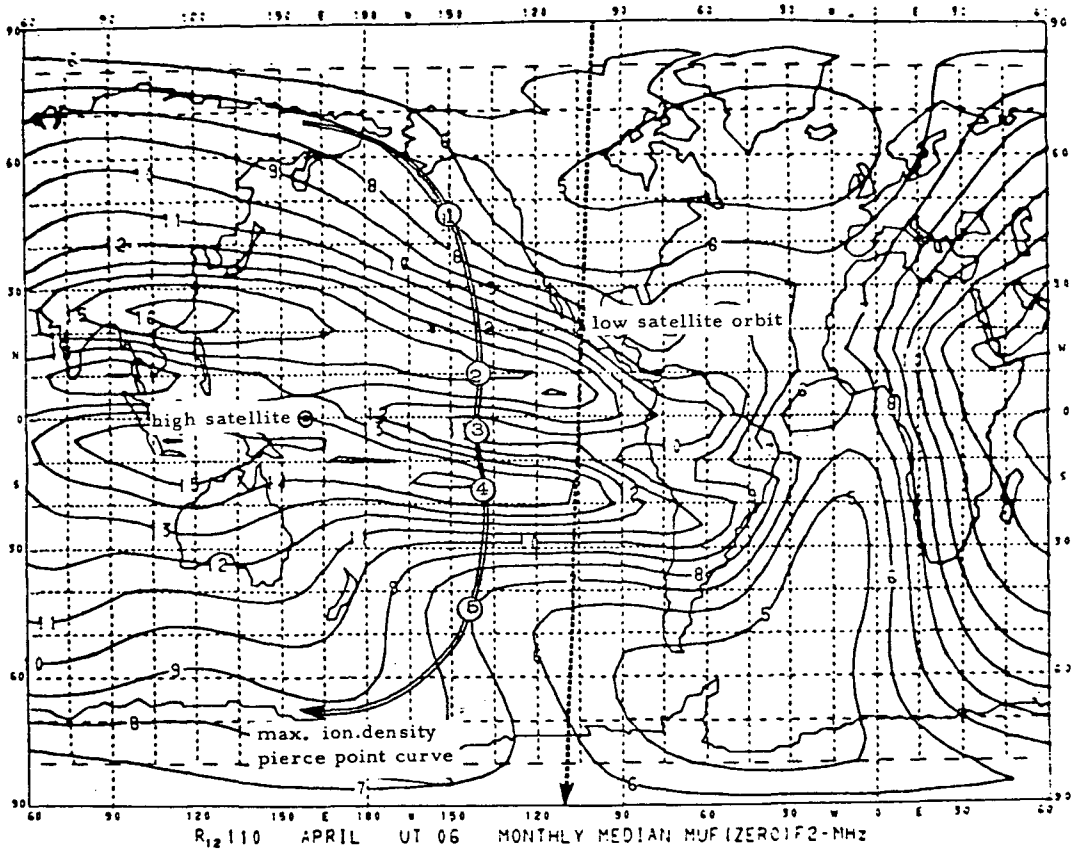

Figure 23. Low satellite orbit at 300 km superimposed on world map of f_xF2.

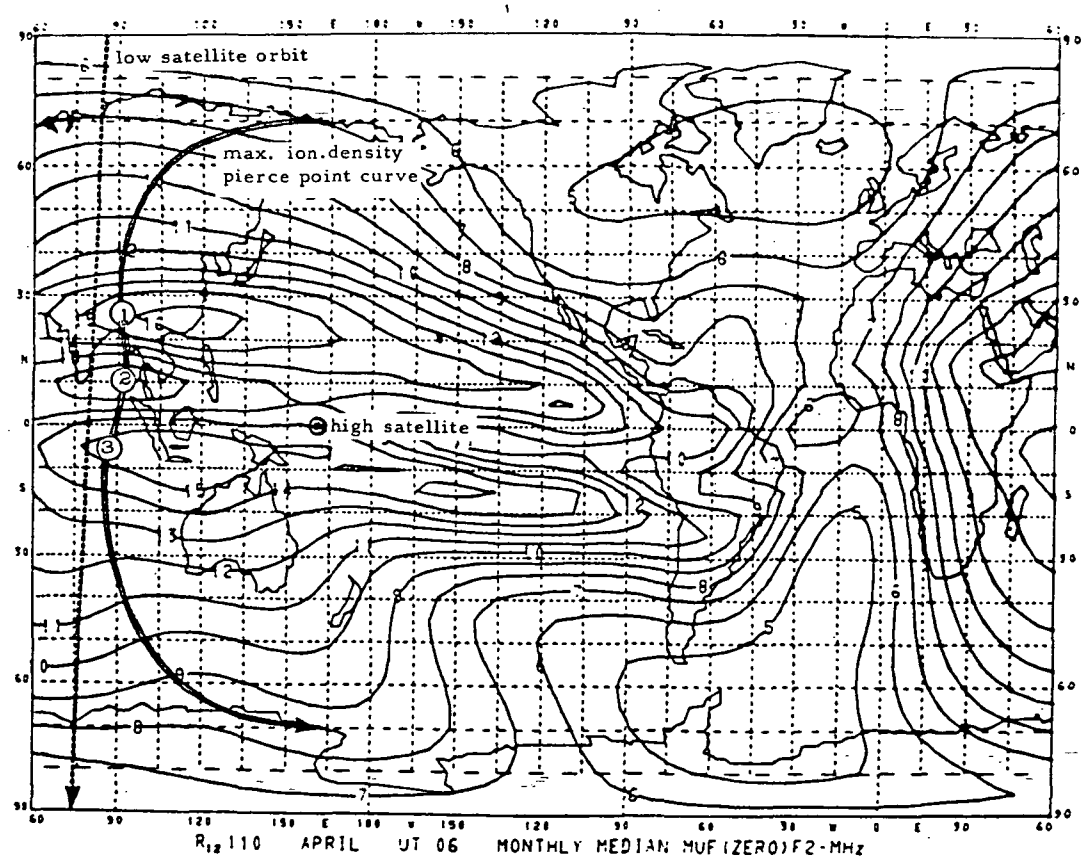

Figure 24. Low satellite orbit at 300 km superimposed on world map of f_xF2.

the satellite-to-satellite line of sight with the region of maximum electron density establishes the ionospheric pierce point. When two distinct intersection points exist, as is the case for satellites altitudes above the height of maximum density, only the pierce points along the high satellite leg are traced. For the 850 km orbit the second pierce point, which is closer to the low satellite, can be as much as 38 degrees separated from the first.

In Figure 23 the satellite separation is reduced by a few degrees so that the low satellite remains visible from the high altitude spacecraft throughout the simulated half-orbit. The low polar orbit passing east of the high satellite was chosen retrograde to provide better geometric conditions, keeping the satellite distance fairly constant over the equatorial anomaly region, assisted by the slight longitude shift due to the earth rotation. The ionospheric pierce point curve shows that the satellite line of sight, as it moves along the orbit, penetrates the ionosphere in the equatorial anomaly region where the density, as well as the gradients, are most severe.

Figure 24 shows another retrograde polar orbit, this time crossing the equatorial anomaly west of the high satellite over some very dense regions. The angular separation between the satellites is less than in the previous case, and at the equator crossing the satellite line of sight is practically perpendicular to the radius vector of the low orbit. Figure 25 illustrates the angular relationships between low and high satellites for all four of the displayed orbits.

3.2 Spacial Gradients

To examine the effect of the low satellite altitude on the range-rate corrections along the arc, the geometric conditions were fixed, such as the high satellite position and the ionospheric pierce point location at the equator crossing and with that also the satellite line of sight, see Figure 25, and only the height of the orbit was varied. The range-rate corrections for the orbits depicted in Figures 22 and 23 and for two additional orbits are correlated in Figure 26.

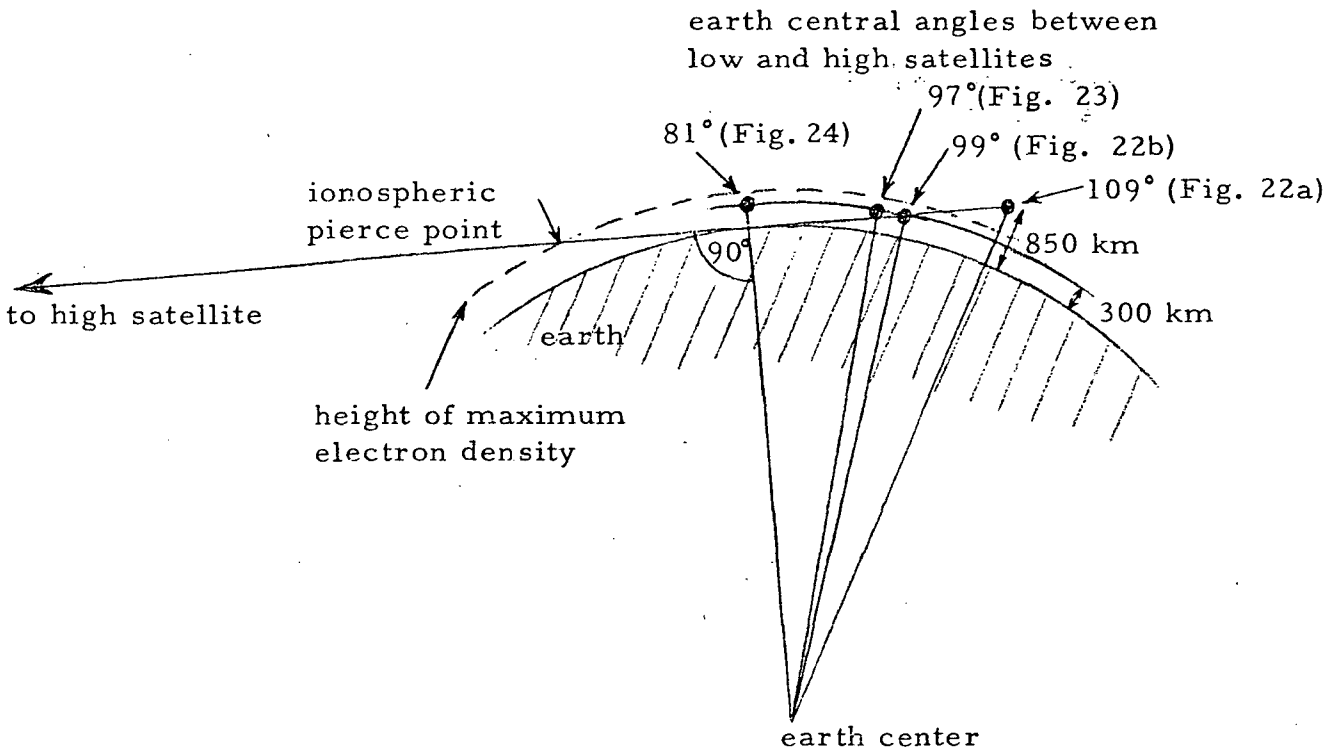

Figure 25 . Diagram of equator crossings of four low satellite orbits showing angular separation from high satellite.

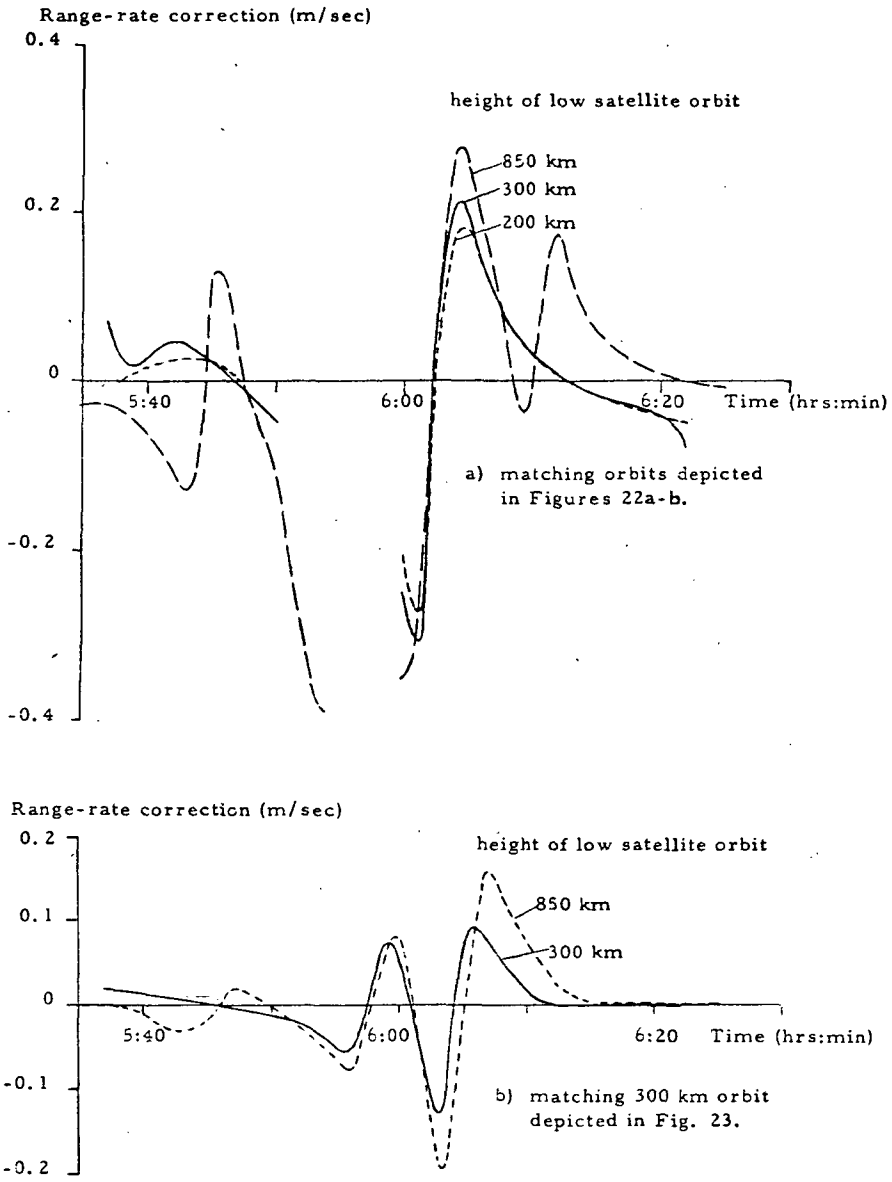

Figure 26. Effect of satellite height on range-rate corrections in April 1968. All three are polar orbits. In a) the orbits are prograde and constructed such that the low satellite just becomes visible from the high equatorial satellite as it crosses zero latitude at 6 UT. In b) the orbits are retrograde and the satellite line of sight remains just above the horizon.

In Figure 26a there is an invisible portion for all satellite orbits, but at 6 UT they become visible again as they cross the equator and the 200, 300 and 850 km satellites all lie along the same line of sight from the high satellite. The very large deviations to both sides of the invisible region are caused by the changing geometric conditions of the satellite raypath through the curved ionosphere as it disappears, which is illustrated in Figure 1. The higher the low satellite orbit is, the larger are the range-rate corrections caused by this effect. The reason for this is that for a low satellite at a relatively high altitude the tracking raypath remains above most of the ionosphere over large segments of its orbit and penetrates significant electron density layers only at the beginning and end of each arc. The higher the satellite is, the faster it passes from the region where the satellite line pierces the ionosphere to the point of invisibility. This faster rate of change produces larger amplitudes in the range-rate corrections.

Superimposed on these geometric effects in Figure 26a are the ionospheric gradient effects, because the ionospheric density and height along the line of sight changes as the low satellite travels along its orbit.

The geometric effects are minimized in Figure 26b by decreasing the high to low satellite separation angle by about 3 degrees at the equator crossing and maintaining visibility throughout the half-orbits. The difference between the range-rate corrections along the 300 and 850 km orbits are now mainly due to the gradients in ionospheric density and height. Again the higher altitude orbit displays the larger amplitude refractive effects, but they are only about half as large as those caused by the geometric conditions in Figure 26a.

To better understand how the variations in the refraction corrections along the satellite path are caused by the ionospheric conditions, the two orbits in Figures 23 and 24, the ionospheric densities depicted in the $f_x F2$ world maps, the ionospheric heights and the satellite angular separation shown in Figure 27 were examined in detail and were correlated to the range-rate corrections also shown in Figure 27. The circled numbers along the time scale of Figure 27 tie up with the ones along the ionospheric pierce point

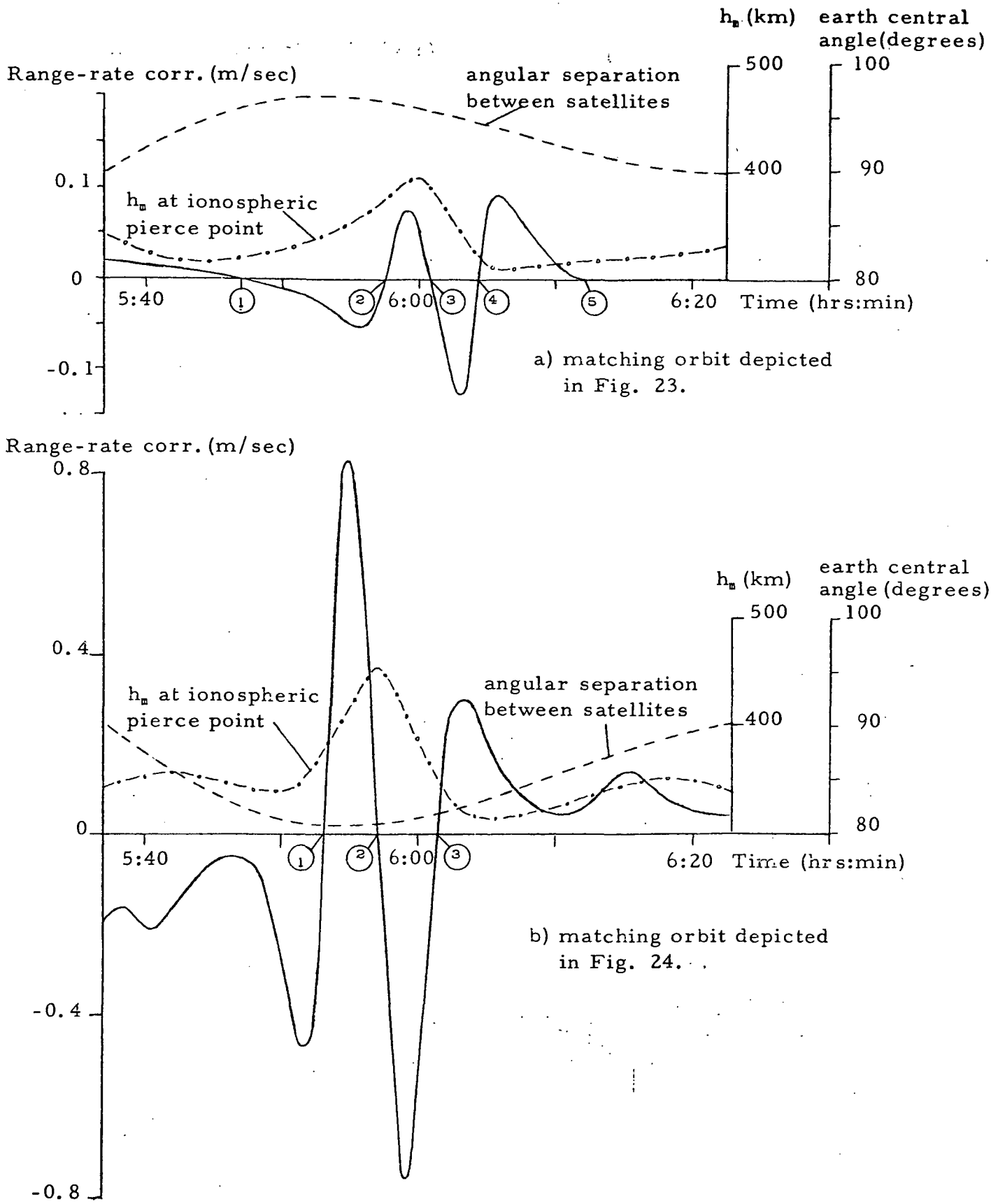

Figure 27. Variations in ionospheric range-rate corrections along 300 km low satellite arcs in April 1968 around 6 UT are caused by ionospheric gradients of equatorial anomaly. Curves of the height of maximum electron density at the ionospheric pierce point and of the separation angle between the satellites are superimposed.

curve on the orbit graphs in Figures 23 and 24. From the curve giving the angular separation between the satellites it is apparent that while this separation varies somewhat at the beginning and end of the arc, it is fairly constant over the central region of the equatorial anomaly where most of the large range-rate deviations occur. Hence, in the region of interest the corrections are mostly due to ionospheric gradients, because the geometric configuration remains nearly fixed. Between points 2 and 4 of Figure 27a, the angular separation between the satellites varies by only 2 degrees and in Figure 27b between points 1 and 3 only by 1 degree.

The marked zero crossings of the range-rate corrections (Figure 27) correspond very clearly to the maxima or minima of f_xF2 shown on the world maps (Figures 23, 24). This is to be expected since extrema in f_xF2 cause extrema in electron density and range corrections, hence zero crossings in range-rate corrections, see Figure 1. The range-rate corrections give a very clear picture of the gradients encountered as the satellite connecting beam sweeps the equatorial anomaly.

As is indicated by the equatorial dip in the ionospheric pierce point curve, (Figures 23, 24) not just the electron density but also the height at the maximum undergoes steep gradients in the anomaly region. In Figure 27 it is shown that the height of the pierce point has a definite maximum at the magnetic equator around which the equatorial anomaly is centered, and its values vary between 314 and 456 km over the arc. The smaller variations in the range-rate corrections toward the ends of the arc in Figure 27b might be influenced by the ionospheric height changes.

It should be noted that different vertical scales are employed in Figure 27. Maximum absolute amplitudes in b) are about seven times as large as in a). The major reason for this lies in the satellite configurations shown in Figure 25. The satellite with range-rate results in a) remains barely above the horizon when crossing the equator, 97° away from the high satellite, and the line of sight pierces the ionosphere at a slanted angle. The satellite with results in b), however, is closer to the high satellite separated by 81° at the equator.

The 300 km satellite used in both these examples is below the height of maximum density which varies in b) between 350 and 456 km in the equatorial region, and the line of sight between the satellites pierces the ionosphere at extremely slanted angles, remaining in the vicinity of the maximum electron density over very long distances, hence the very large refraction effects. In addition, slightly steeper gradients exist in ionospheric height and density for b) than exist for a) which also contributes to the larger range-rate corrections in b). The maximum pierce point of f_0F2 in b) was 14.2 MHz, in a) 12.9 MHz.

In using the April 1968 data, the spacial gradient investigations were performed for average solar maximum conditions; the smoothed sunspot number was 107. It should be recognized, however, that during a more severe solar cycle the range-rate corrections could be significantly larger than the 0.8 m/sec in Figure 27. During the maximum cycle recorded in 1958, the smoothed sunspot number went as high as 201 in March.

3.3 Temporal Gradients

The effects of short and long term ionospheric temporal gradients on satellite-to-satellite range-rate corrections was investigated by comparing the corrections along the orbits, which were obtained for ionospheric situations where all conditions, except the one tested parameter, were held constant.

3.3.1 Diurnal effect

The diurnal effect on range-rate corrections was examined by computing corrections for satellites crossing the equator at 6 hours and at 14 hours universal time to provide information with high and low gradients, and the results show large differences in amplitude. In Figure 28a the ionospheric pierce point occurs at longitude 222° or 21 hours local time. At this time very rapid changes in electron density are encountered as the satellite connecting ray sweeps across the equatorial anomaly while following the low satellite orbit. The steep gradients are apparent along the pierce point curve in Figure 22b, and the resulting range-rate corrections are large.

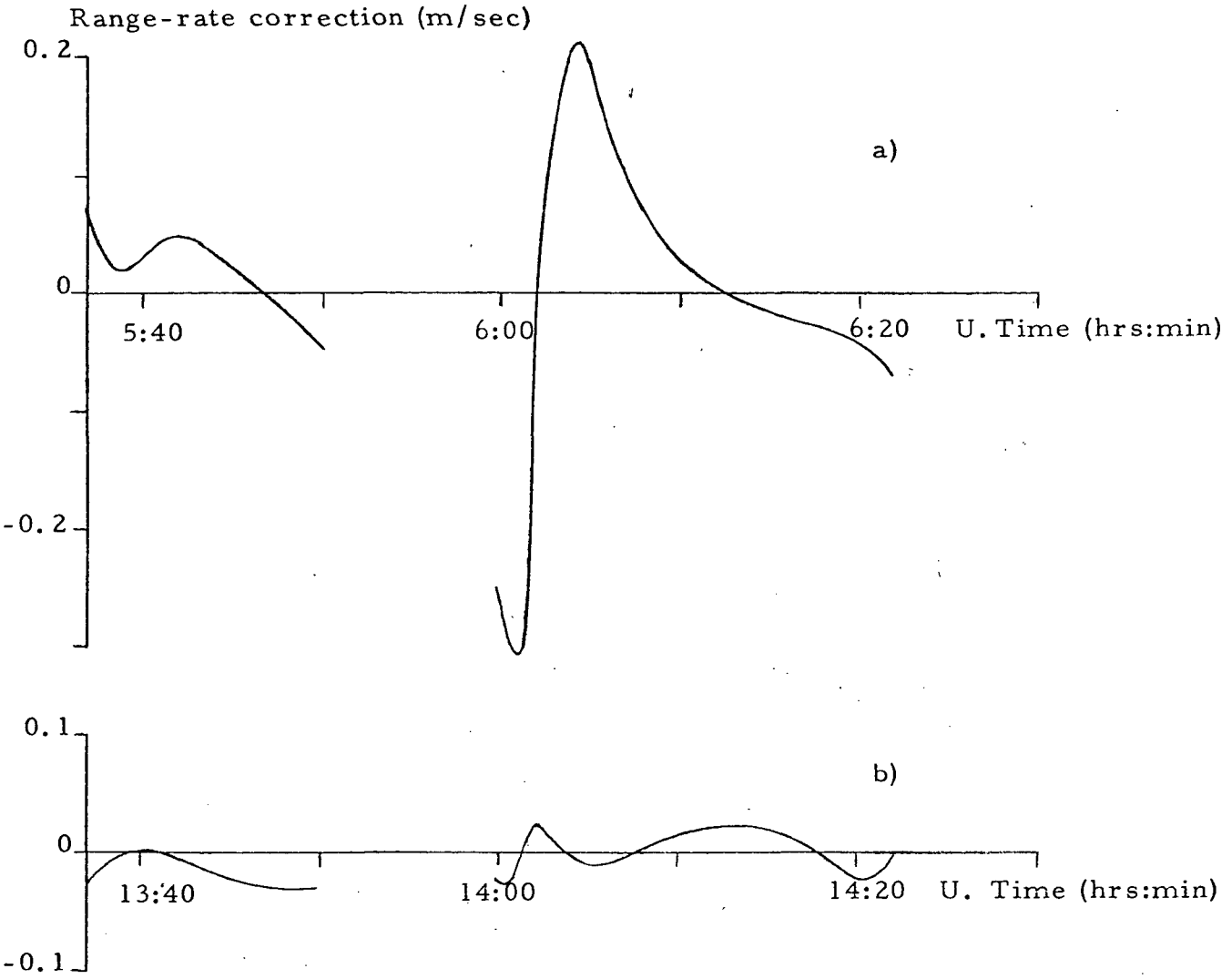

Figure 28. Diurnal effect on range-rate corrections of 300 km orbit in April 1968. In a) at the equator crossing the ionospheric pierce point along the low to high satellite leg occurs at 21 hours local time, when large ionospheric gradients exist along the low satellite orbit.(see Fig. 22b). In b) the pierce point crosses the equator at 5 hours local time, when the ionospheric gradients along the orbit are very small.

In Figure 28b the satellite crosses the equator at 14 hours UT. Here the ionospheric pierce point occurs at 5 hours local time, when the ionospheric gradients along the pierce point curve and hence the corresponding range-rate corrections are about as small as they can get for such an orbit configuration.

3.3.2 Seasonal effects

Range-rate corrections were compared for April 1968 and July 1968 to examine the effect of seasonal variations on range-rate corrections. The solar activity did not influence the result significantly, because the smoothed sunspot numbers were very similar, 107.2 in April and 105.2 in July. The three polar orbits at 300 km altitude shown in Figures 22b, 23 and 24 were examined, all having the equator crossing fixed at 6 hours UT. The corresponding range-rate corrections are presented in Figure 29, and in Figure 30 similar results for the 850 km high orbit of Figure 22a are shown. In each case, maximum ionospheric effects occur in April and minimum effects in July. For other months the effects would be expected to be of intermediate amplitude. Significant changes in peak amplitudes are apparent, as well as time shifts of the peak correction values. In Figures 29b one of the spikes disappears between April and July.

3.3.3 Solar cycle effects

The effect of the solar cycle on range-rate corrections was also considered. Three years were chosen to represent the extremes of solar activity, and in all cases the month of April was selected to eliminate seasonal effects.

Year	Smoothed Sunspot Number
1958	196.8
1968	107.2
1975	18.6

The 1958 solar cycle was the all-time maximum recorded. During 1968 and 1975, the maximum and minimum activity occurred for the last solar cycle. Figure 31 shows the results for two different orbits shown in

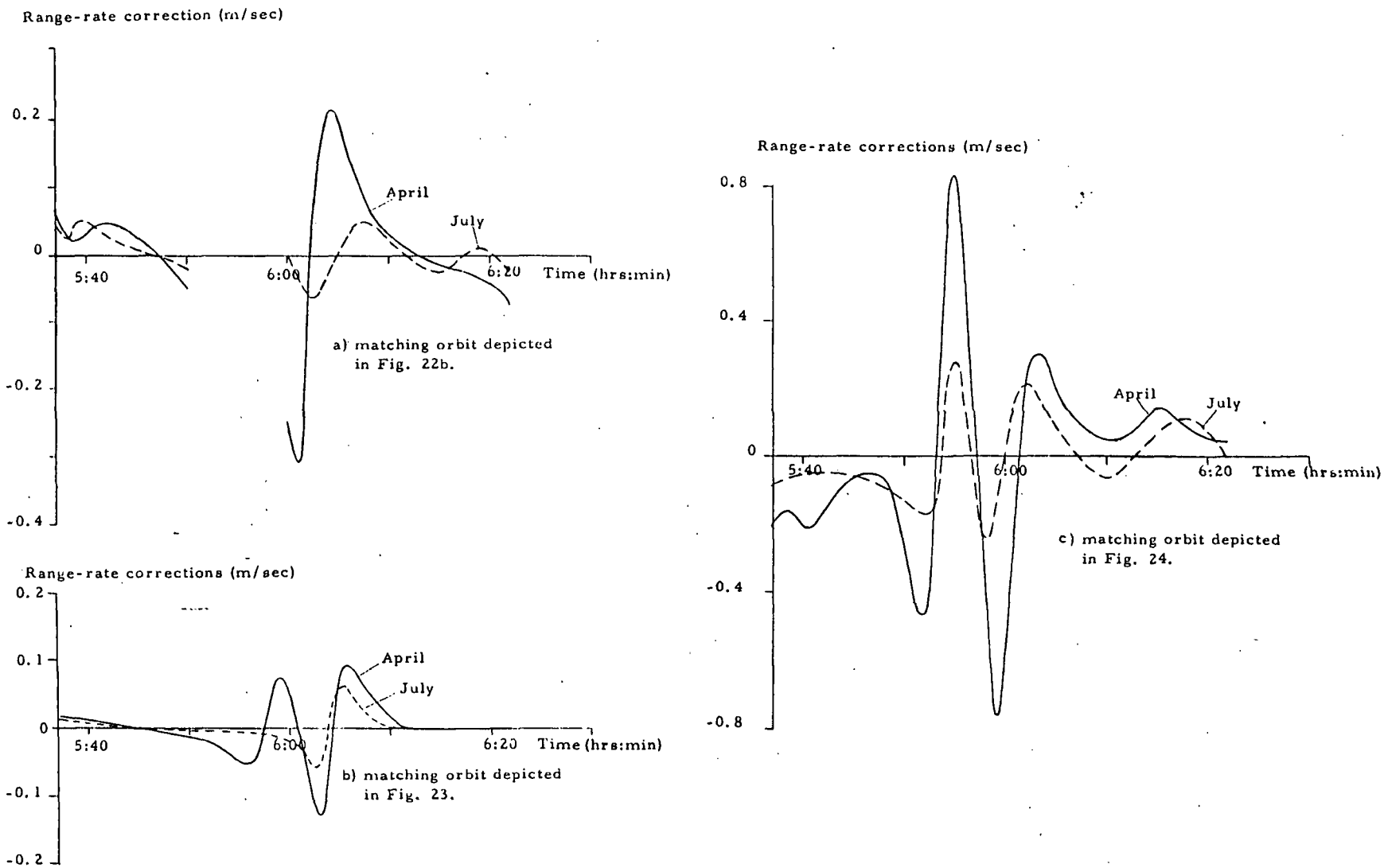

Figure 29. Seasonal effect on range-rate corrections of 300 km orbits in 1968 at about 6 UT. Maximum ionospheric effects are found in April, minimum in July.

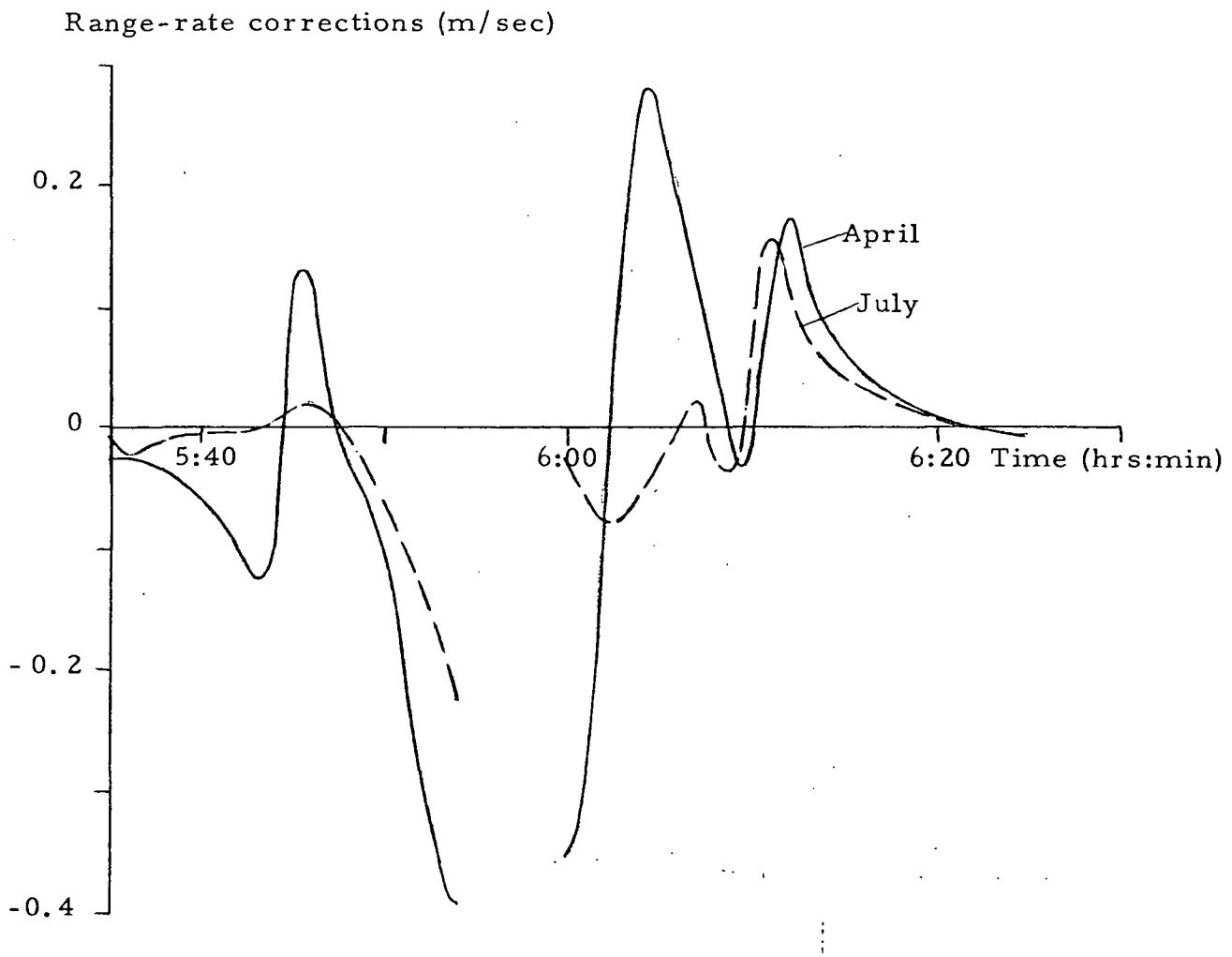

Figure 30. Seasonal effect on range-rate corrections of 850 km orbit in 1968 at about 6 UT. Maximum ionospheric effects are found in April, minimum in July.

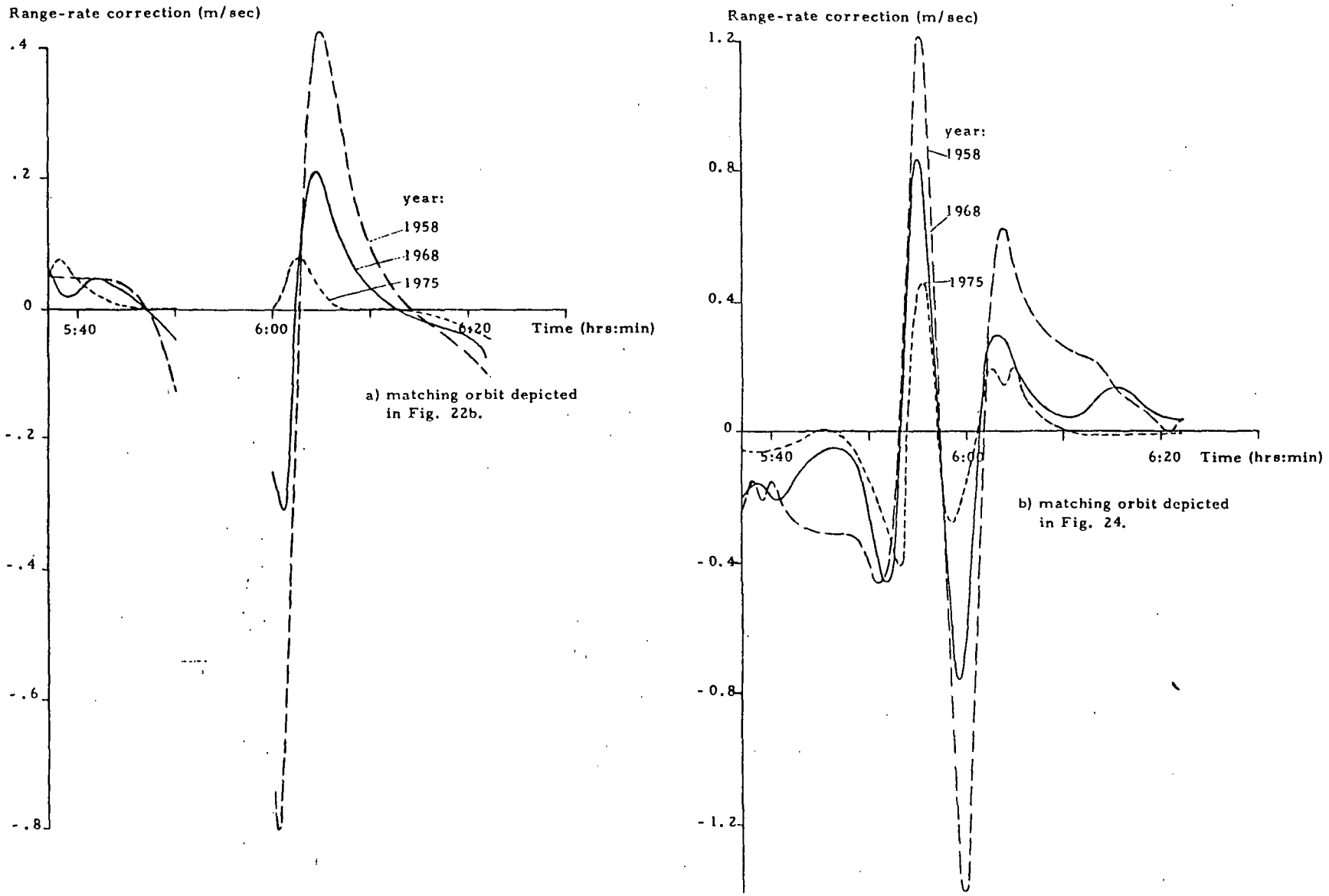

Figure 31. Solar cycle effect on range-rate corrections of 300 km orbits during April at about 6 UT. The 1958 solar cycle was the all-time maximum recorded. The years 1968 and 1975 represent the maximum and minimum region of the last solar cycle.

Figures 22b and 24. The 1958 corrections are in all cases significantly larger than the 1968 results by factors of 1.5 to 2.5. The 1968 results in turn exceed the 1975 results by similar amounts. Shifts in the time of the peak range-rate correction occur for several peaks but without a simple pattern.

3.4 Temporal Gradient Tests with Apollo-Soyuz Orbits

The effect of day-to-day variations in the ionospheric density and height on the range-rate corrections along the satellite link were investigated using an orbit of the Apollo-Soyuz data. Revolution 8 on 16 July 1975, with the tracking frequency of 2.16 GHz was used, and the ionospheric conditions of interest were simulated.

To examine the influence of the deviations in f_0F2 from the monthly mean due to daily variations of solar flux, the month of February 1968 was chosen for the simulations; 1968 was the year of average maximum solar activity. The monthly mean of the solar flux was 173, and corrections were computed for February 1st when solar flux was at a monthly maximum 262, and for February 18th when the flux was at the minimum of 138. As shown in Figure 32, the increased solar flux causes a sharp increase in peak ionospheric range-rate corrections by a factor of 1.1 to 1.8, while the same pattern is maintained for the variations along the arc. This points to the necessity to adjust the monthly mean ionospheric correction model for daily variations as is done in the Bent model.

The height of maximum electron density was computed using the ionospheric model, and then it was raised and lowered by 50 km during the simulations. Such variations represent the possible day-to-day changes in the ionospheric height, and result in changes in the amplitude of the range-rate corrections as well as in a time shift of the peaks, see Figure 33. Lowering the ionosphere by 50 km causes an increase in the amplitude by a factor of 1.4 and a shift of the peak in increasing time along the arc. Raising the ionosphere by 50 km causes a decrease in amplitude and a 40 second shift of the peak in decreasing time along the arc.

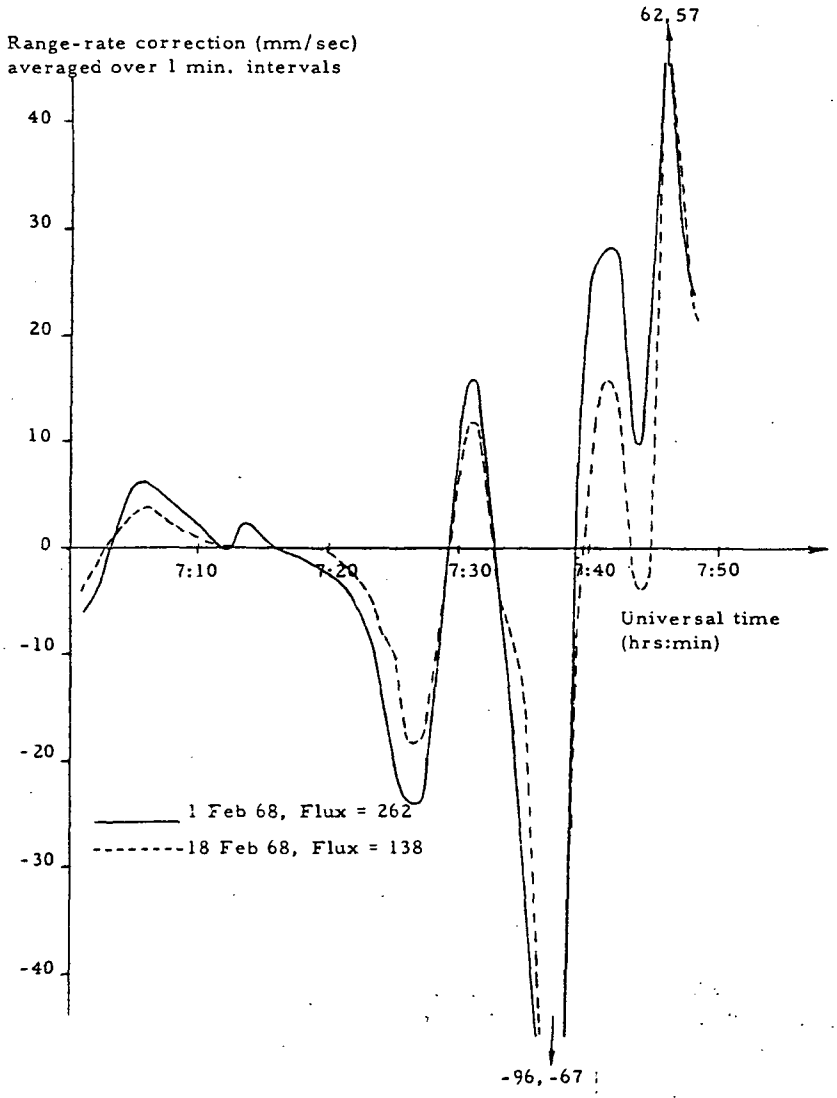

Figure 32. Deviations from monthly mean due to daily variations of solar flux show large effect on the peak values of ionospheric satellite to satellite corrections along arc.

Apollo-Soyuz Orbit

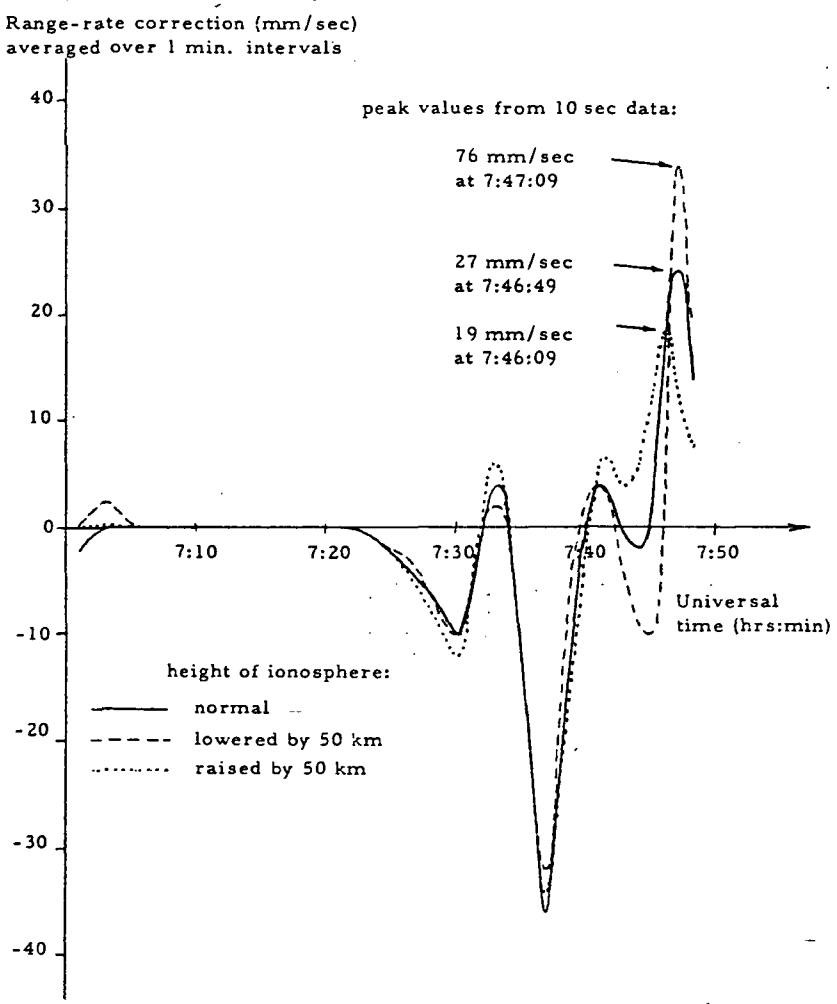

Figure 3.3. Raising and lowering the ionosphere by possible daily variations of 50 km produces amplitude changes and time shifts of the peak corrections along the arc.

Date: 16 July 1975

Apollo-Soyuz Orbit

3.5 Nimbus Simulations

Ionospheric range-rate corrections along the satellite link from Nimbus to ATS-6 were computed using three simulated Nimbus orbits. Retrograde orbits with an inclination of 100° were generated with the satellite at a height of 1100 km. The high satellite was stationary over the equator at longitude 159°. Because the low satellite, at 1100 km, is above the densest part of the ionosphere, range-rate corrections are significant only when the low satellite is near the point of disappearance over the horizon with respect to the high satellite. At this point, the line of sight between the high and low satellites passes through the densest part of the ionosphere at two distinct points.

The orbit shown in Figure 34a was chosen so that the low satellite becomes invisible to the high satellite above the equator and reappears just as it crosses the equator. Corrections are large due to the dominant geometric effect of disappearance which obscures the effect of the steep ionospheric gradients involved (Fig. 35). The equator crossing is at longitude 271°, 5.9 UT (24.0 local time).

In Figure 34b, the low satellite remains just barely visible to the high satellite as it approaches and crosses the equator, hence geometric effects are of minor importance. The matching range-rate corrections in Figure 36 are not as large as in Figure 35, and are due mainly to the steep ionospheric gradients. The equator crossing is at longitude 267°, 6 UT (23.8 local time).

The third orbit (not shown) crosses the equator at longitude 50.9°, 6 UT (9.4 local time). Range-rate corrections for this orbit are shown in Figure 37. The Nimbus orbit is quite similar to the previous case, but it crosses the equatorial anomaly west of the high satellite instead of east. Because of the variations in ionospheric densities, gradients and heights the spikes in the range-rate correction curve along the low satellite arc are of different shape and occur at different times than in Figure 36.

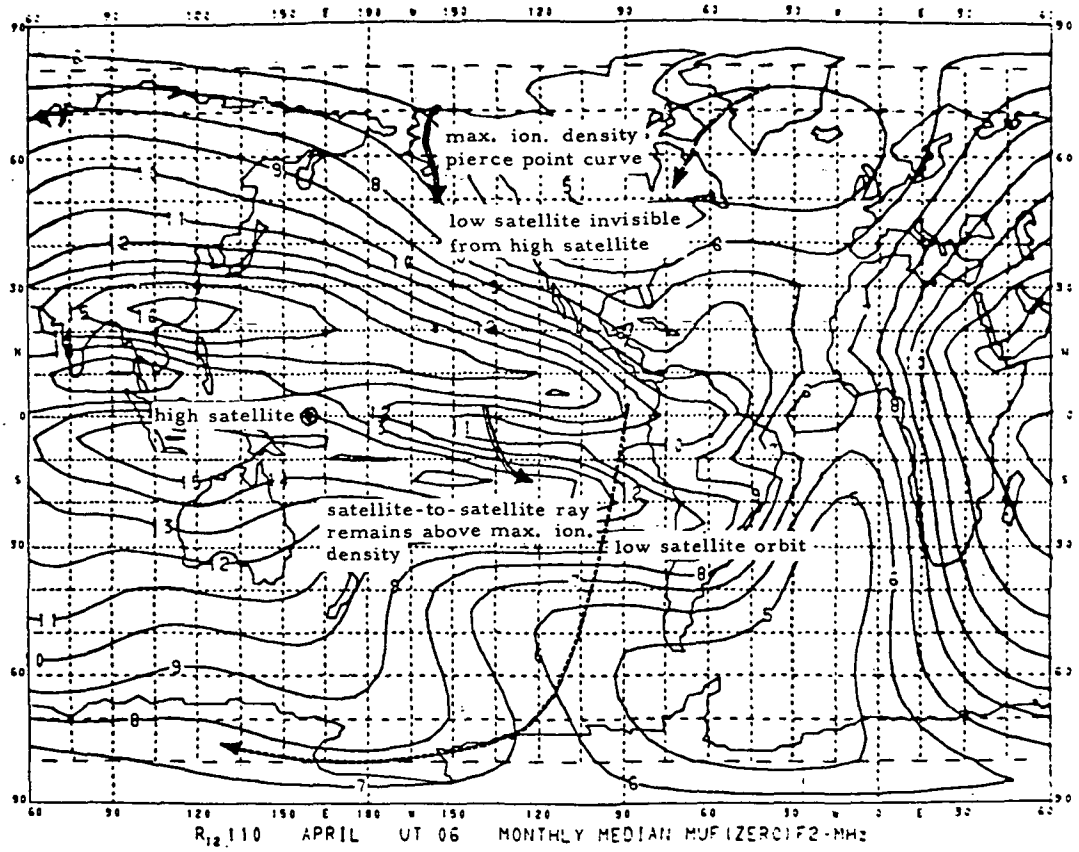

a)

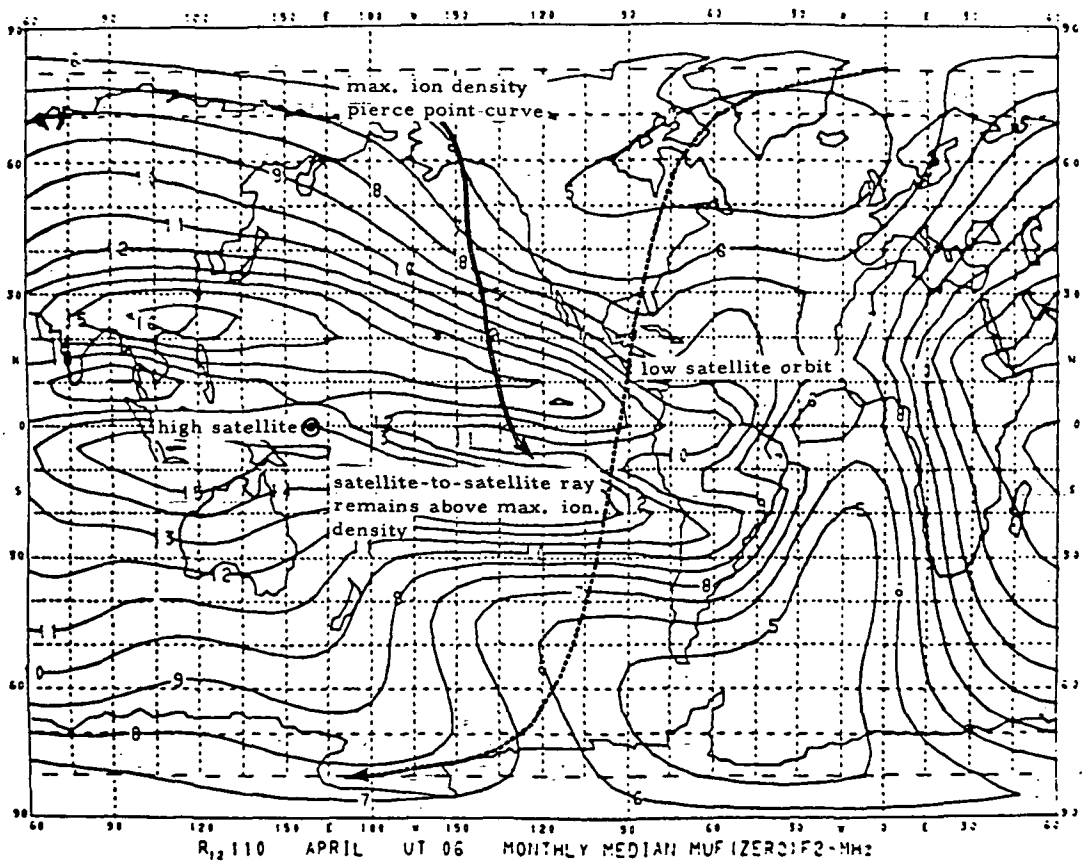

b)

Figure 34. Nimbus orbits superimposed on world map of ionospheric characteristic fxF2.

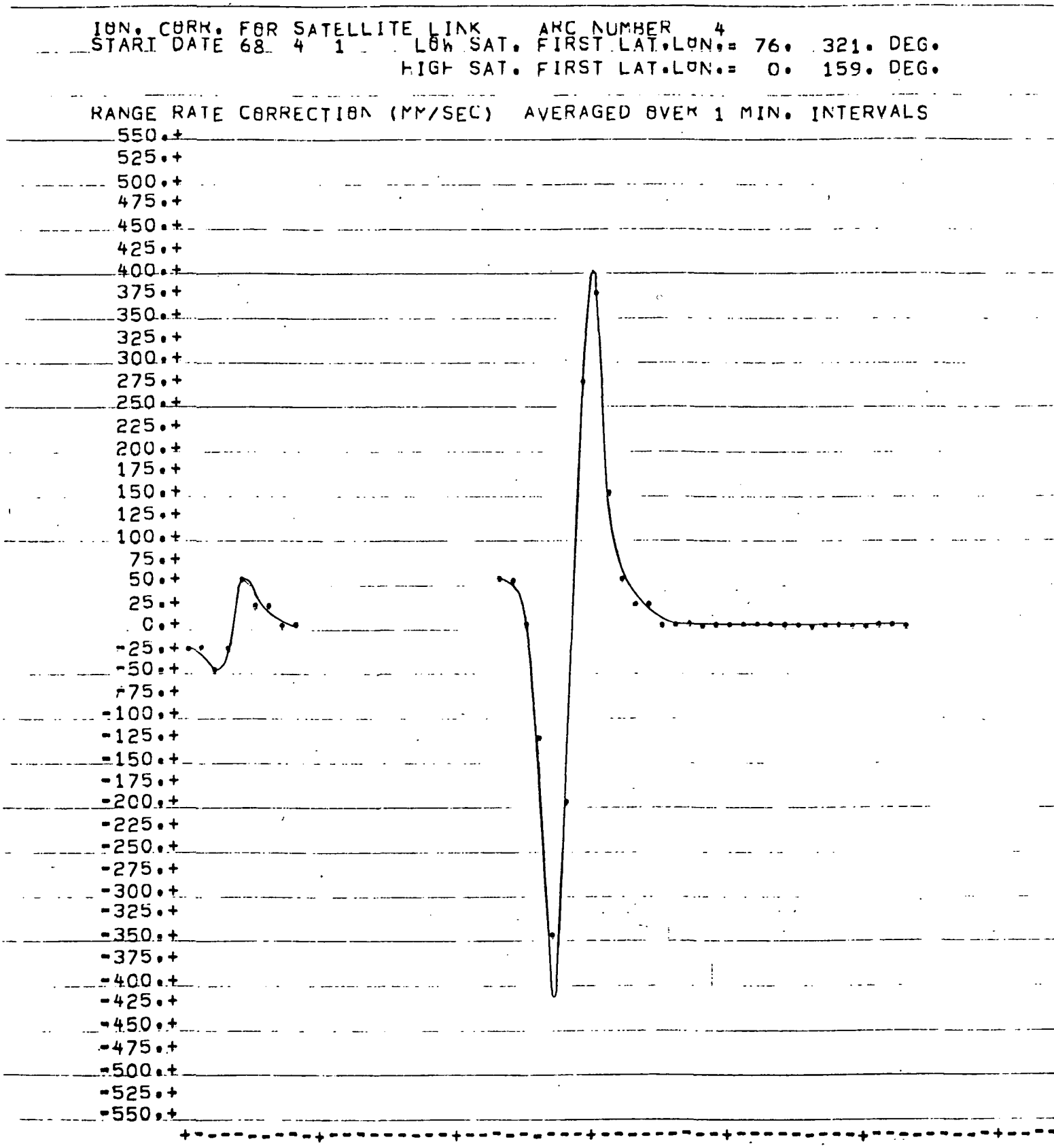

Figure 35. One-way ionospheric range-rate corrections for Nimbus/ATS-6 satellite link. Matching orbit depicted in Figure 34a.

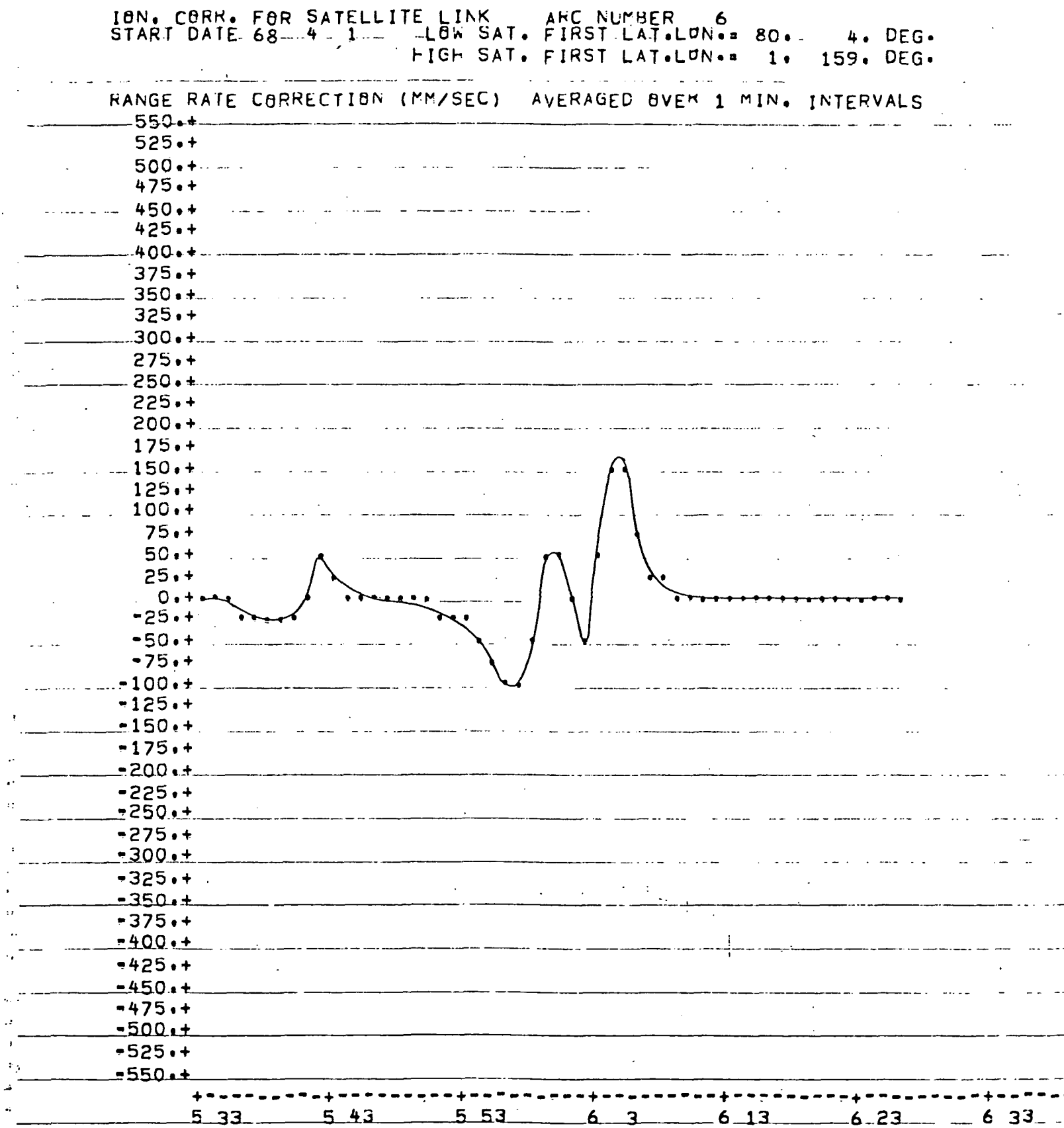

Figure 36. One-way ionospheric range-rate corrections for Nimbus/ATS-6 satellite link. Matching orbit depicted in Figure 34b.

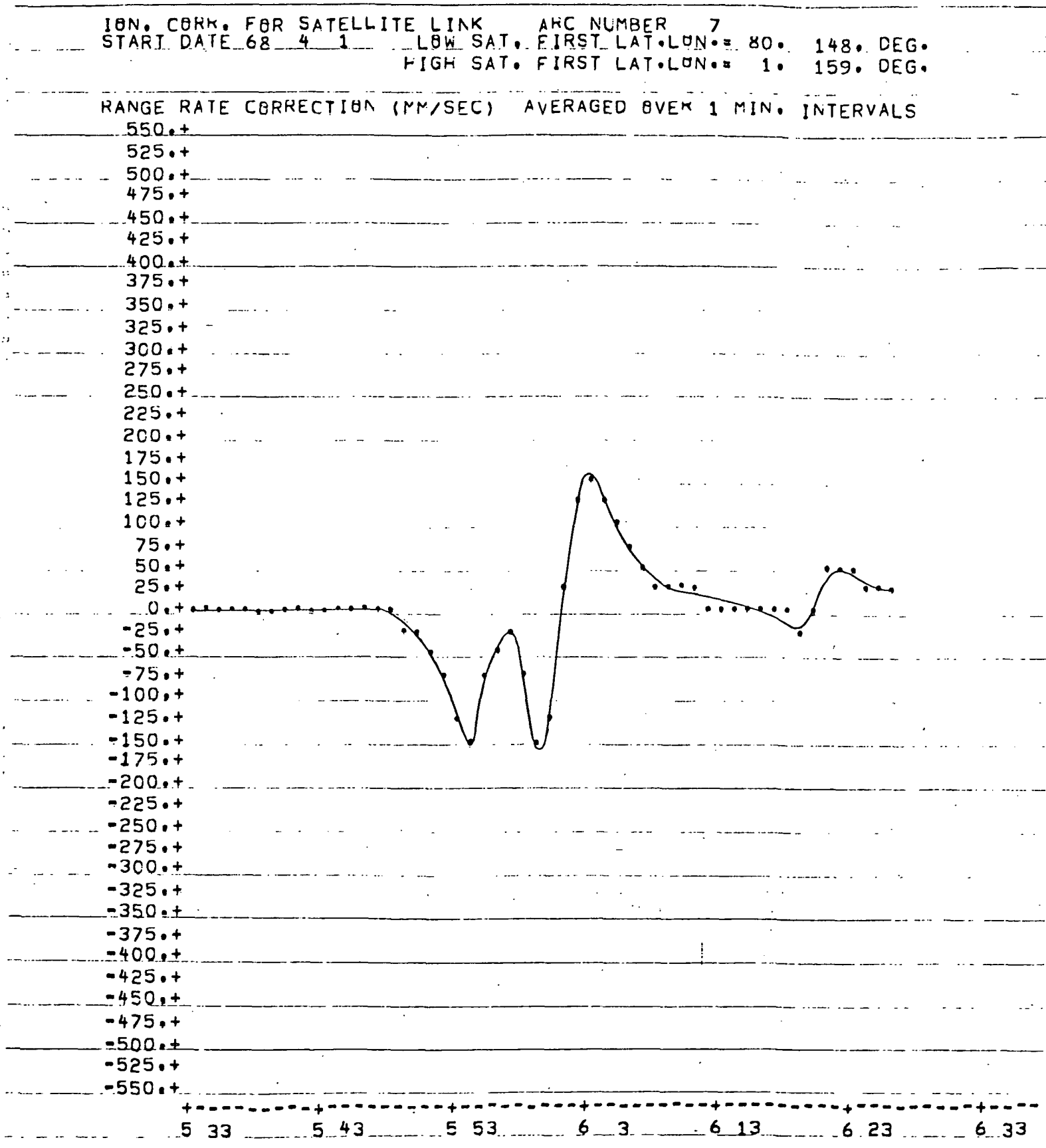

Figure 37. One-way ionospheric range-rate corrections for Nimbus/ATS-6 satellite link.

The connections shown are for a one-way trip between ATS-6 and Nimbus with a transmission frequency of 2.16 GHz.

3.6 Summary of Ionospheric Model Results

The 3-dimensional worldwide Bent ionospheric prediction model was used to show the effects of steep spacial gradients and of short and long term temporal gradients in the ionosphere on satellite-to-satellite range-rate corrections. The satellite orbits were simulated perpendicular to each other, the stationary high satellite over the equator, the low satellites in polar orbits at 200, 300 and 850 km altitude with the tracking raypath sweeping across the equatorial anomaly and the satellite separation in the proximity of the disappearing points. Such a configuration insures significant range-rate corrections along most of the orbit. Tracking frequencies of 1GHz were used to enable easy conversion to a user's frequency and one-way corrections are presented. The impact of the variations in each tested parameter was determined while holding all other conditions constant.

Variations in satellite altitude showed that the higher the satellite, the larger are the range-rate corrections along the arc (Figure 26). This was the case when the refractive effects were mainly due to the gradients in ionospheric density and height, and also when the geometric effect of the satellite raypath disappearing through the curved ionosphere was dominant. The reason for the latter is that the higher the satellite is, the faster it passes from the region where the satellite line pierces the ionosphere to the point of invisibility, and this angular rate is proportional to the ionospheric range-rate values.

The effects of the ionospheric spacial gradients on the range-rate corrections along the satellite-to-satellite line was investigated, while minimizing the geometric effect by holding the angular separation between the satellites fairly constant over the region of the equatorial anomaly, where the largest spacial gradients occur. The range-rate corrections give a very clear picture of the gradients encountered as the satellite connecting beam sweeps across the equatorial anomaly. The spikes in the corrections occur at different times for satellite orbits at different longitudes, because of the

ionospheric variations (Figure 27), and the zero crossings in the refraction corrections very clearly correspond to the maxima and minima in electron density along the tracking beam. This type or range-rate effect is not linked to the beginning or end of a tracking arc, but can occur anywhere in the middle of the orbit. The variation by a factor of 7 in the maximum amplitude of the range-rate corrections between the two selected orbits is mainly due to the satellite configurations. In the first case the low satellite barely remains above the horizon, and the line of sight to the high satellite pierces the ionosphere at a slanted angle. In the second case the satellite separation is less, and the line of sight penetrates the ionosphere at an extremely slanted angle, remaining in the vicinity of the maximum electron density over a very long distance. The maximum one-way correction of 0.8 m/sec is for average solar maximum conditions and could be larger by a factor of 2.5 during a more severe solar cycle.

The effect of both short and long term temporal gradients were investigated, including diurnal variations, day-to-day deviations from the monthly mean seasonal and solar cycle variations.

Range-rate corrections along the satellite orbit can be very large or small depending on the time of the day (Figure 28). At local times, for example 21 hours, when very rapid changes in electron density are encountered as the satellite connecting ray sweeps across the equatorial anomaly while following the low satellite orbit, the resulting range-rate corrections are large. However, at 5 hours local time the ionospheric gradients are about as small as they can get, and the range-rate corrections are at a minimum. If the low satellite has a small inclination, large effects would also occur as the raypath sweeps across the ionospheric sunrise effect.

Data from April and July show how satellite-to-satellite range-rate corrections vary with season (Figures 29, 30). Significant changes in peak amplitude occur as well as time shifts of the peak correction values; the correction curves show no close resemblance in shape. Maximum ionospheric effects occur in April, between 2 to 10 times larger than the minimum effects in July. For other months intermediate amplitudes would be expected.

The solar cycle effects on range-rate corrections were investigated with data from the 1958 solar cycle, the all-time maximum recorded, and with data from 1968 and 1975, the maximum and minimum of the last solar cycle, which represents an anverage cycle. The 1958 corrections, with a maximum value of 1.4 m/sec, are in all cases significantly larger than the 1968 results by factors of 1.5 to 2.5 (Figure 31). The 1968 results in turn exceed the 1975 results by similar amounts. Shifts in the time of the peak range-rate correction also occur.

The effects of the day-to-day variations in ionospheric density and height were investigated using an Apollo-Soyuz orbit at 200 km altitude and a tracking frequency of 2.16 GHz. The daily variations in f_0F2 from the monthly mean are a function of the solar flux, which was 262 on the 1st and 138 on the 18th day of February 1968, which was a period of average maximum solar activity. The increased solar flux causes a sharp increase in peak ionospheric range-rate corrections by a factor of 1.1 to 1.8, while the same pattern is maintained for the variations along the arc (Figure 32).

Possible day-to-day changes in ionospheric height were simulated by raising and lowering the model computed height by 50 km. Lowering the ionosphere caused an increase in amplitude by a factor of 1.4 and a small shift of the peak range-rate correction in increasing time along the arc. Raising the ionosphere caused a similar sized drop in amplitude and a 40 second shift of the peak in decreasing time (Figure 33).

Simulations of a Nimbus satellite retrograde orbit at 100°inclination, 1100 km altitude and at a tracking frequency of 2.16 GHz, illustrated severe range-rate corrections during average solar maximum conditions (Figures 35-37). Maximum one-way corrections of 0.42 m/sec were due to the geometric disappearance effect, and maximum corrections of 0.16 m/sec were due to ionospheric spacial gradients.

4.0 UPDATE WITH ACTUAL IONOSPHERIC OBSERVATIONS FOR THE APOLLO-SOYUZ/ATS-6 TRACKING DATA

The ionospheric range-rate corrections along the satellite link from Apollo-Soyuz to ATS-6 presented an impact on the geodynamic satellite experiments, as the ionospheric effects were of similar order as the gravitational effects to be extracted. In view of these results it was decided to repeat the computation of these corrections to a higher degree of accuracy by updating the predictions with actual measurements of critical frequency taken by the ionospheric sounding stations.

All available hourly f_0F2 data for the time period of the experiment and in the regions of the Apollo-Soyuz arcs were purchased from the World Data Center in Boulder, Colorado. Data from 56 stations were prepared, as shown on the world map in Figure 38 , and 38 of these stations were close enough to the satellite arcs that the data were actually used in the computer reduction. Further f_0F2 data was taken at additional stations, which is not yet available through the World Data Center. These missing stations are primarily from the Indian network, which are the most critical for this work. If additional f_0F2 data was made available, it would be useful to repeat the update for selected arcs.

The model predicted values of f_0F2 are computed for profiles at selected points along the satellite-to-satellite connection line, and from these in turn the ionospheric density distribution between the satellites is determined. An update procedure was used, modifying the predicted f_0F2's by the distance weighted ratio of the measured versus predicted f_0F2 at the nearest update station. The distance weights applied were those from the bell shaped exponential distance function shown in Figure 3. For stations close to the satellite line of sight, the f_0F2 update ratio has nearly full effect, while for distant update stations the weight is so small that there is hardly any difference between the predicted and the updated

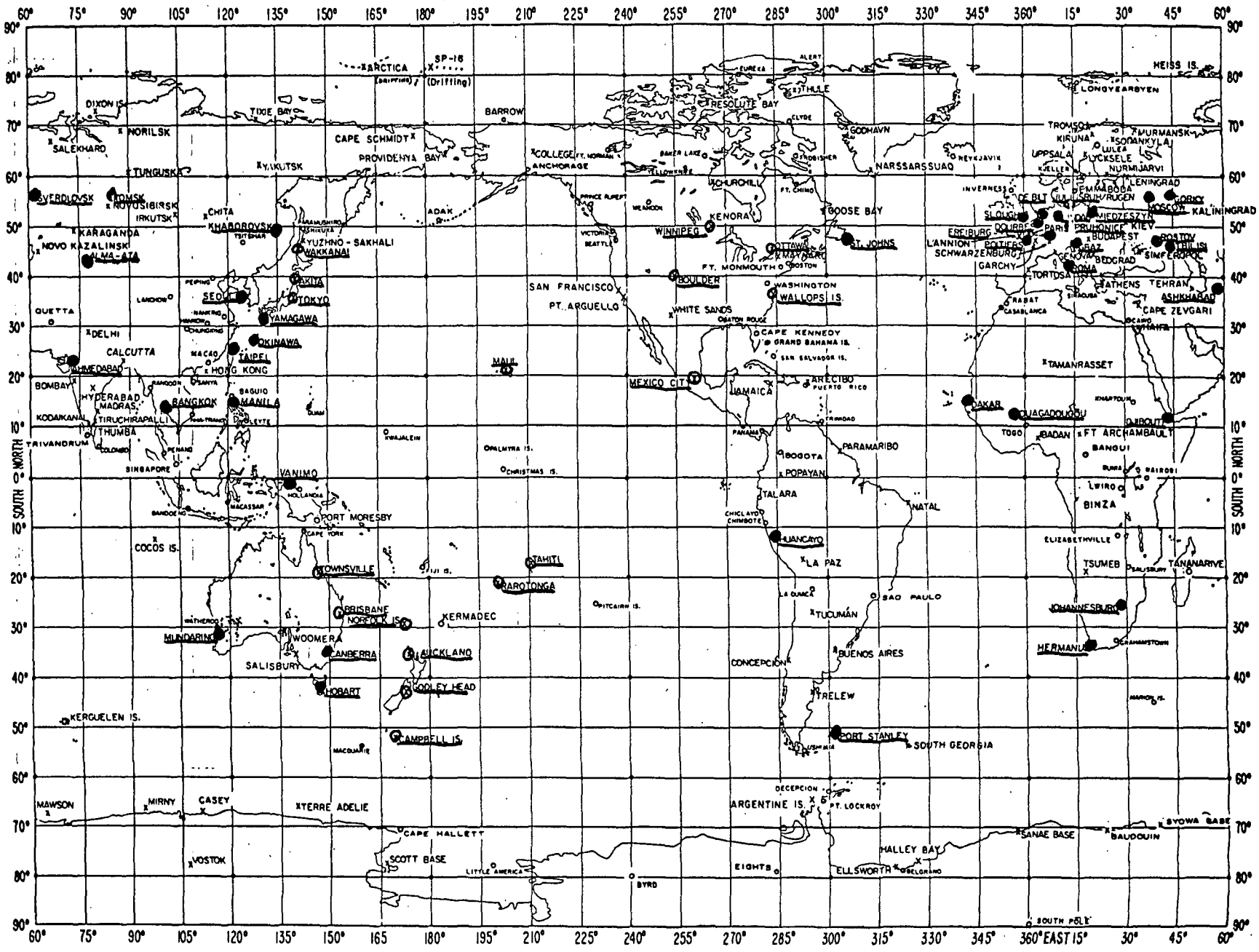

Figure 38 . Ionospheric sounding stations used to update corrections to Apollo-Soyuz tracking data.

ionospheric results. For the update the closest station was always selected, and the hourly f_0F2 ratios were interpolated to the exact times. The update procedure was very carefully incorporated into the satellite-to-satellite correction technique, so as to avoid any inconsistencies and stepfunctions in the electron density calculations which would immediately introduce erroneous variations in the ionospheric range-rate corrections.

Updates were applied over major portions of most of the 30 satellite tracking arcs. Much of the time the update stations were quite distant and hence had only little effect, but at other times update stations were close and significant variations from the predicted range-rate correction curves were achieved. Examples of predicted versus updated range-rate corrections for portions of several satellite arcs are shown in Figures 39 a-e, with particularly large differences apparent along the steep slopes and in a one minute shift of the minimum in Figure 39 b. The corrections are for the one-way trip between ATS-6 and Apollo-Soyuz at the mean round trip frequency of 2.16 GHz, and are to be subtracted from the range-rate tracking observation.

Unfortunately, many of the orbits passed over India for which no update data will be available for several months. This is the main region of interest in analyzing the so-called Indian and Himalayan gravity anomalies, and it is disconcerting that no better analysis with ionospheric update can be achieved at this time.

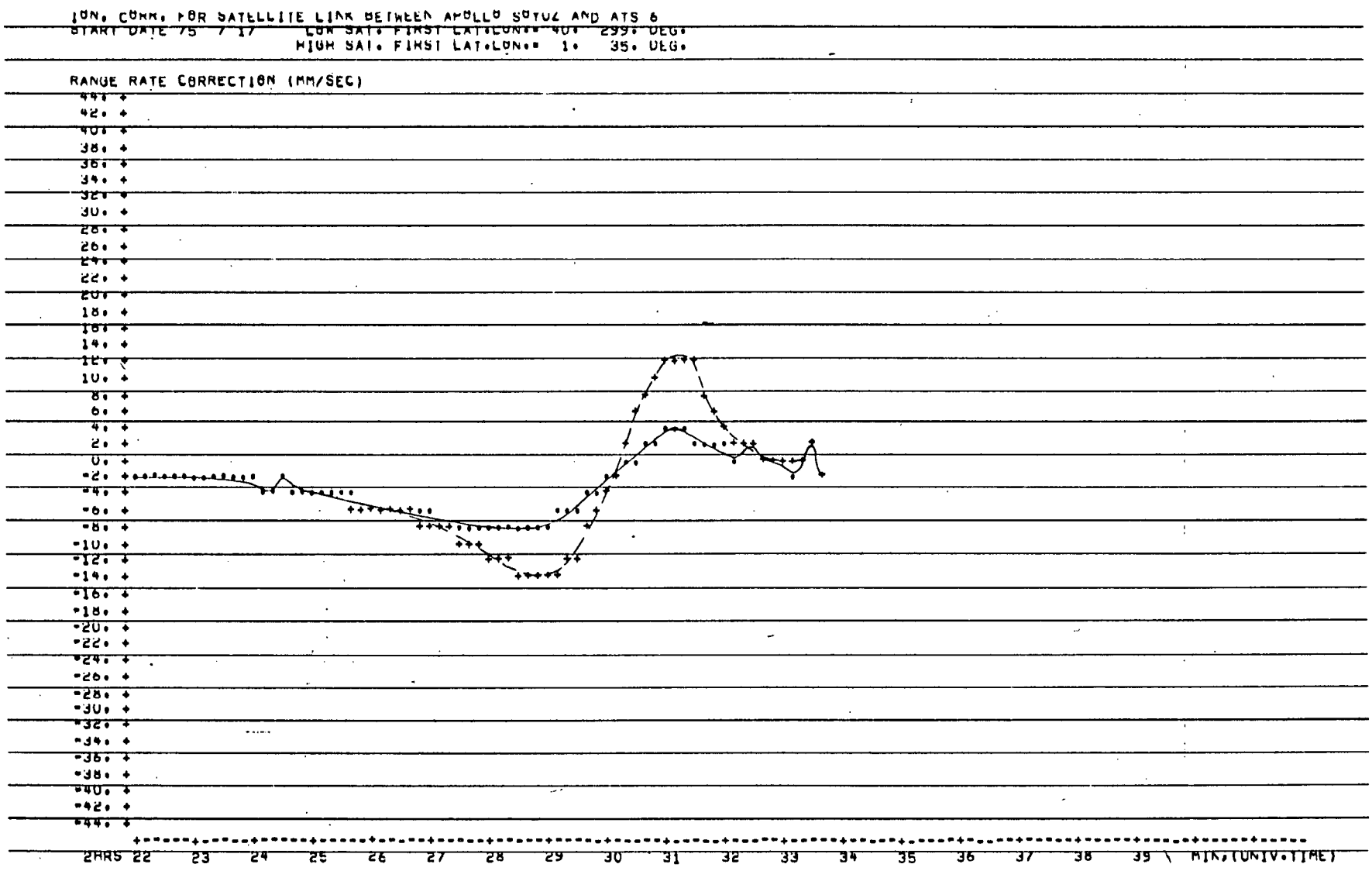

Figure 39 a. Predicted (.) and updated (+) range-rate corrections for part of Apollo-Soyuz arc #5, rev. # 20.

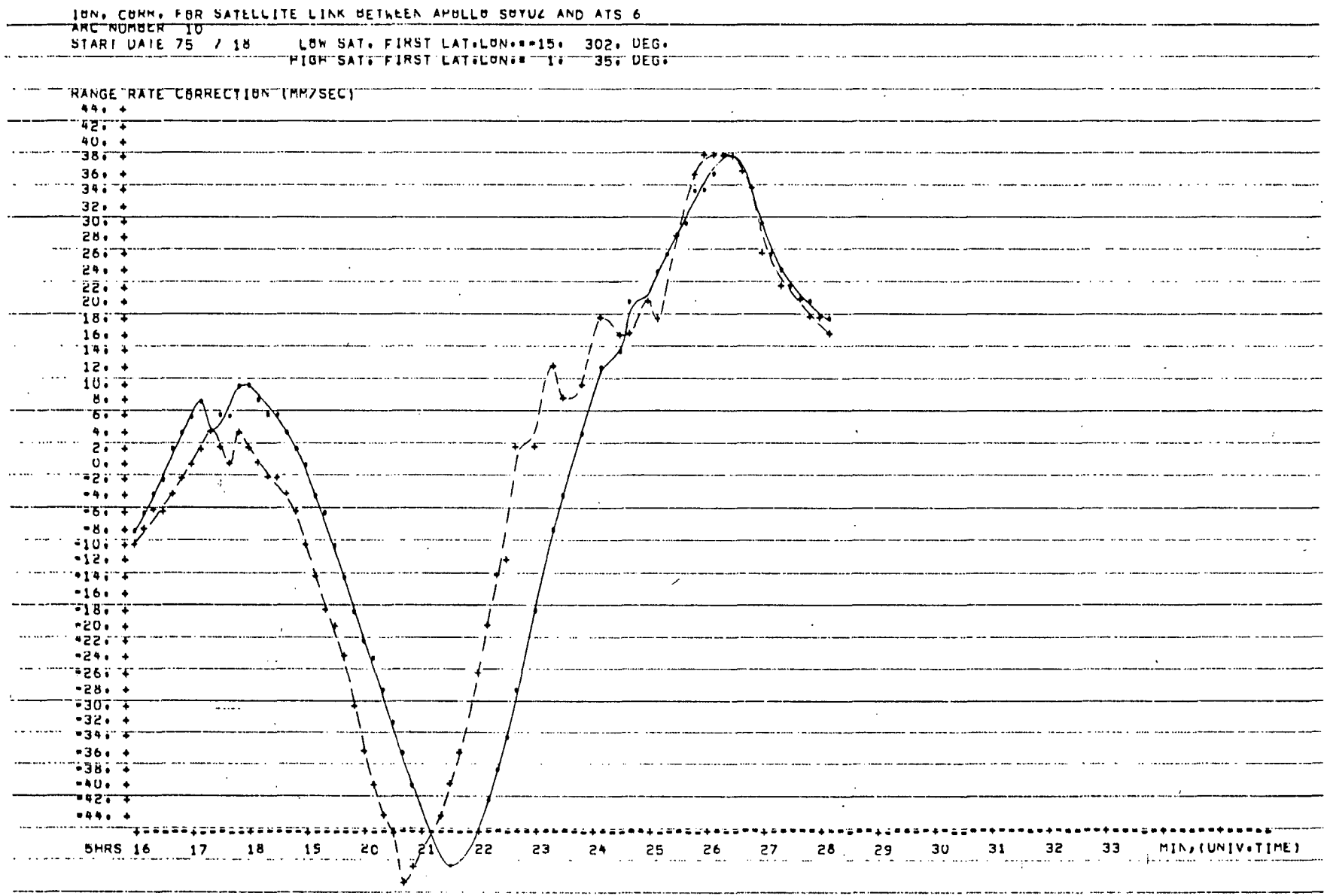

Figure 39b. Predicted (.) and updated (+) range-rate corrections for part of Apollo-Soyuz arc #10, rev. #37.

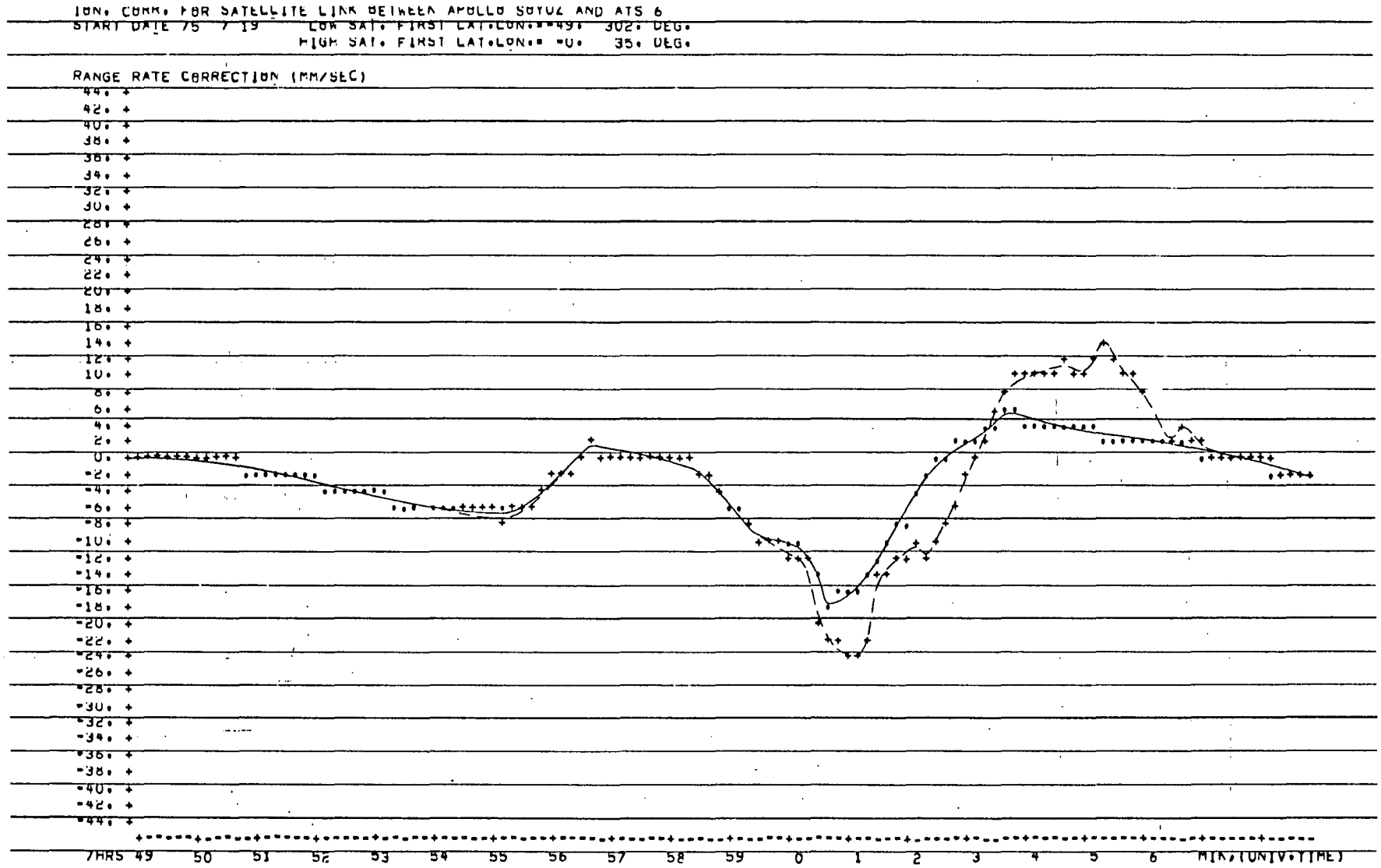

Figure 39 c. Predicted (.) and updated (+) range-rate corrections for part of Apollo-Soyuz arc # 15, rev. # 54.

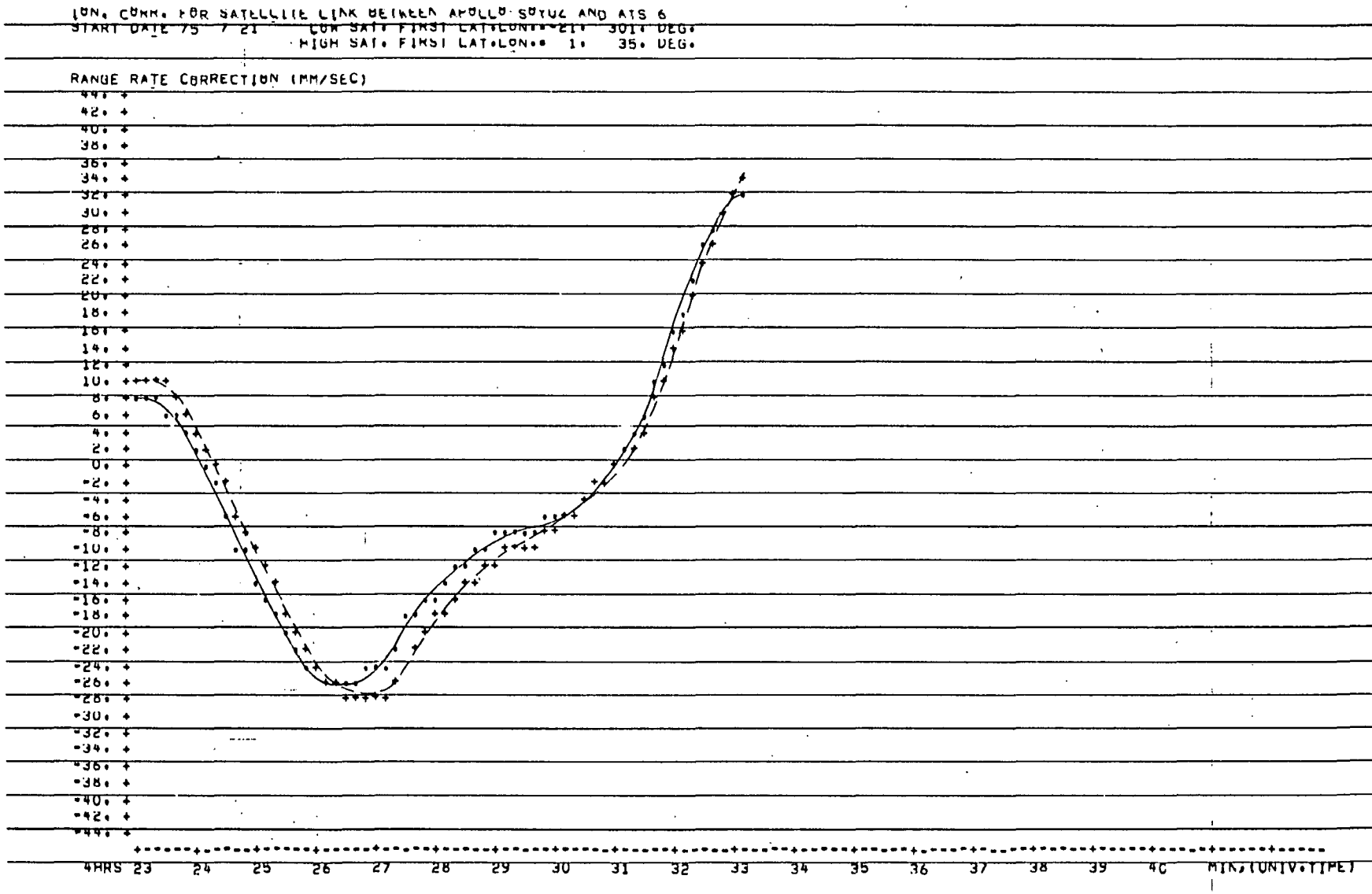

Figure 39d. Predicted (.) and updated (+) range-rate corrections for part of Apollo-Soyuz arc #16, rev. # 82.

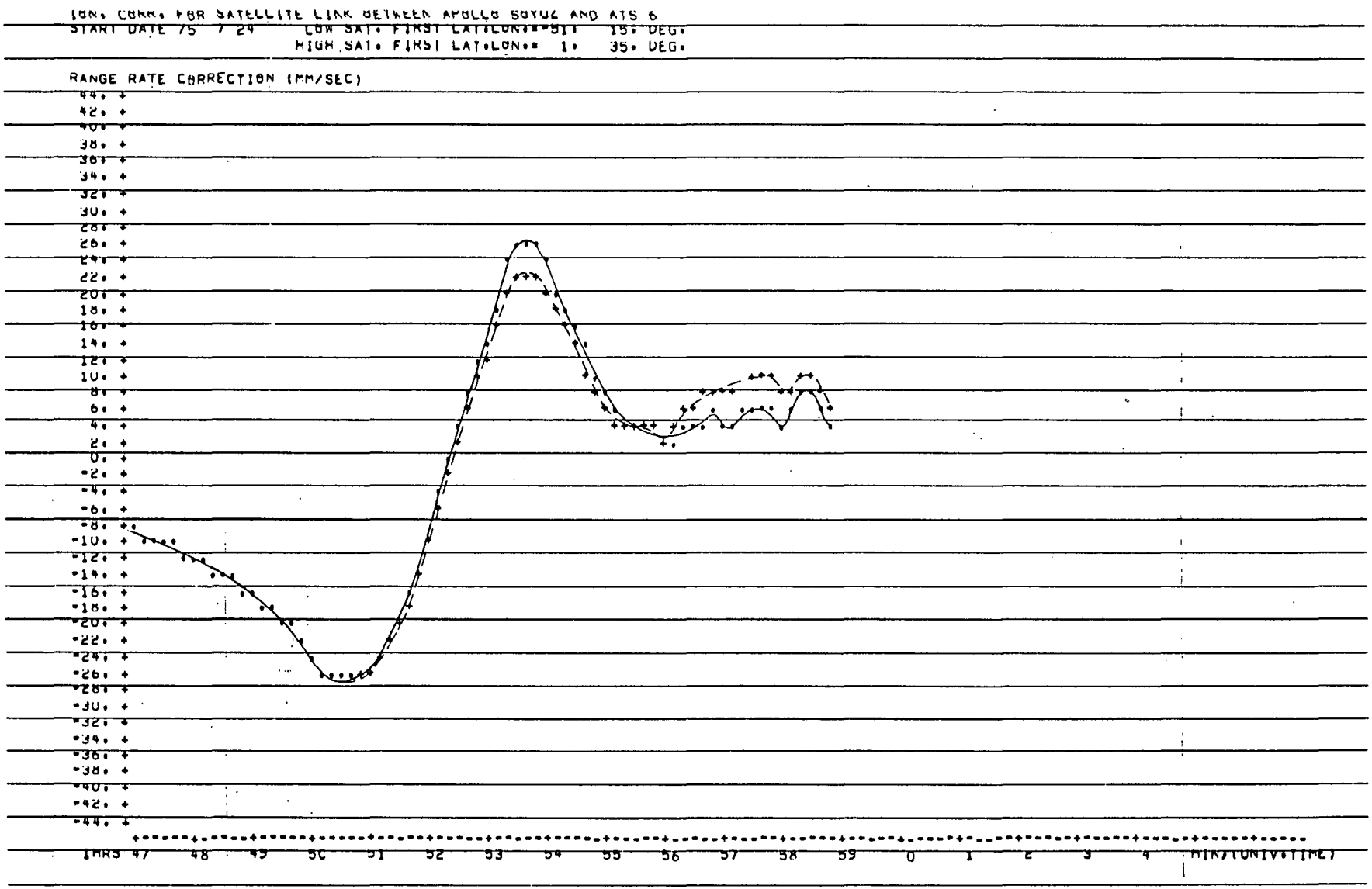

Figure 39 e. Predicted (.) and updated (+) range-rate corrections for part of Apollo-Soyuz arc #26, rev. #126.

5.0 RANGE-RATE CORRECTIONS FOR GEOS

Two actual Geos arcs, revolutions 730 and 254, were provided for ionospheric corrections. Geos was tracked by ATS-6 which in turn was tracked by ground stations. Considering the orbit configurations, it was determined that with the several GHz tracking frequencies involved the ionospheric effects on the range-rate tracking data would be significant only during the first and last seven minutes of visibility of the Geos orbit from ATS-6. Hence only these portions of the data were analyzed.

Table 2 . Frequencies used for tracking Geos-3 via ATS-6 from Rosman, N.C.

ATS-6 to Geos-3 uplink	f_u = 2069.1 MHz
Geos-3 to ATS-6 downlink	f_d = 2247.0 MHz
Computed for satellite link round trip	f = 2152.6 MHz
Rosman to ATS-6 uplink	f_u = 6144.1 MHz
ATS-6 to Rosman downlink	f_d = 3947.0 MHz
Computed for ground link round trip	f = 4696.3 MHz

Table 2 shows the tracking frequencies along the ground and satellite legs, and the computed frequencies used for the one-way ionosphere corrections, which when doubled give the round trip corrections for the particular link. The round trip frequencies are accurately computed using the equation: $\frac{1}{f^2} = \frac{1}{2}\left(\frac{1}{f_u^2} + \frac{1}{f_d^2}\right)$. The only ground tracking station involved was Rosman. The ionospheric corrections for the ground and for the satellite link were computed separately, the one-way corrections for the satellite link are shown in Figure 40 a, b, and ground and satellite link corrections for the end of revolution 730 are listed in Table 3 .

For both revolutions the tracking data did not start immediately when Geos became visible from ATS-6, but about seven minutes later. From the investigations of the geometric effects presented in Section 2, ionospheric

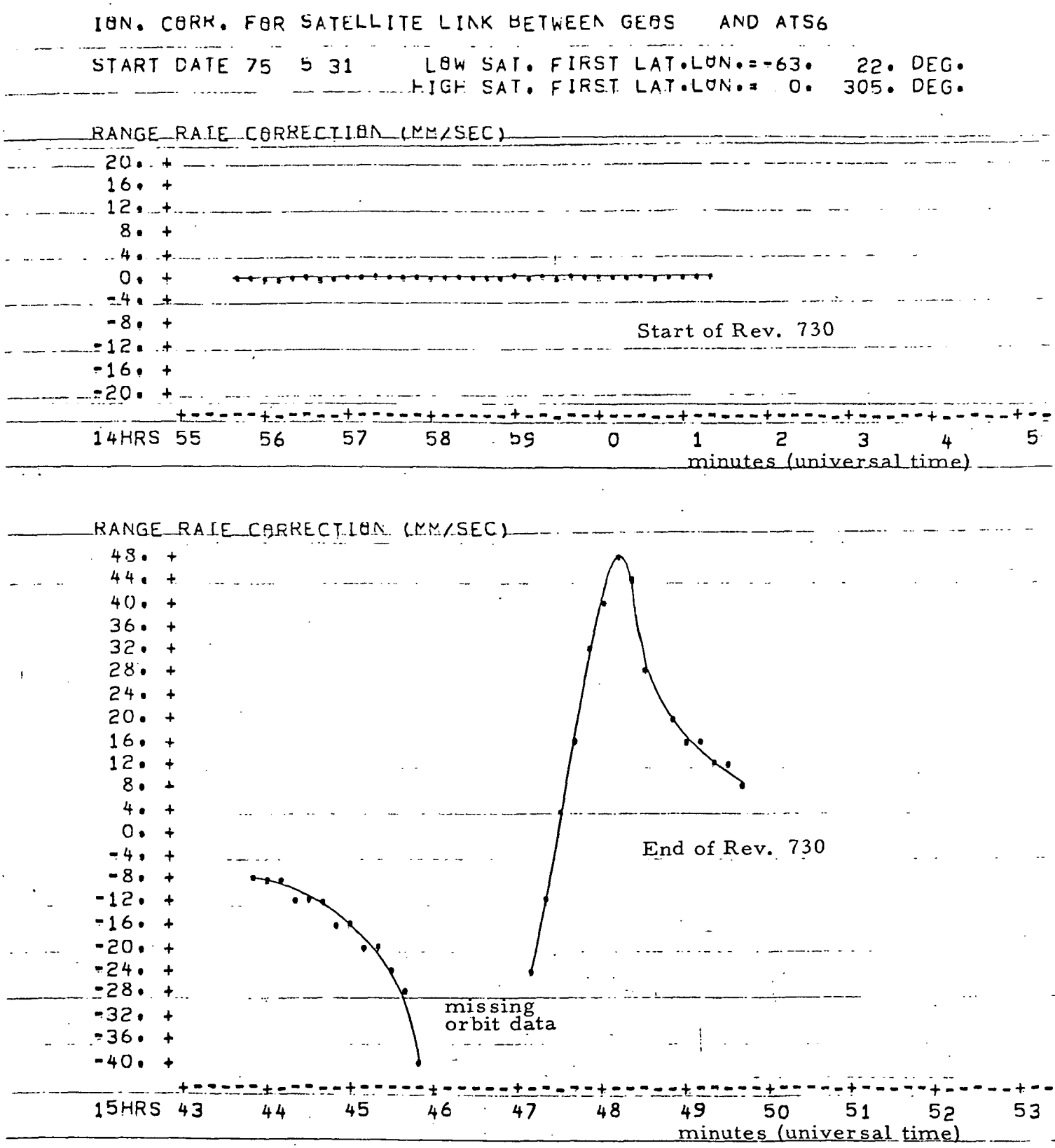

Figure 40 a. One-way ionospheric range-rate corrections for revolution 730 of the Geos/ATS-6 satellite link.

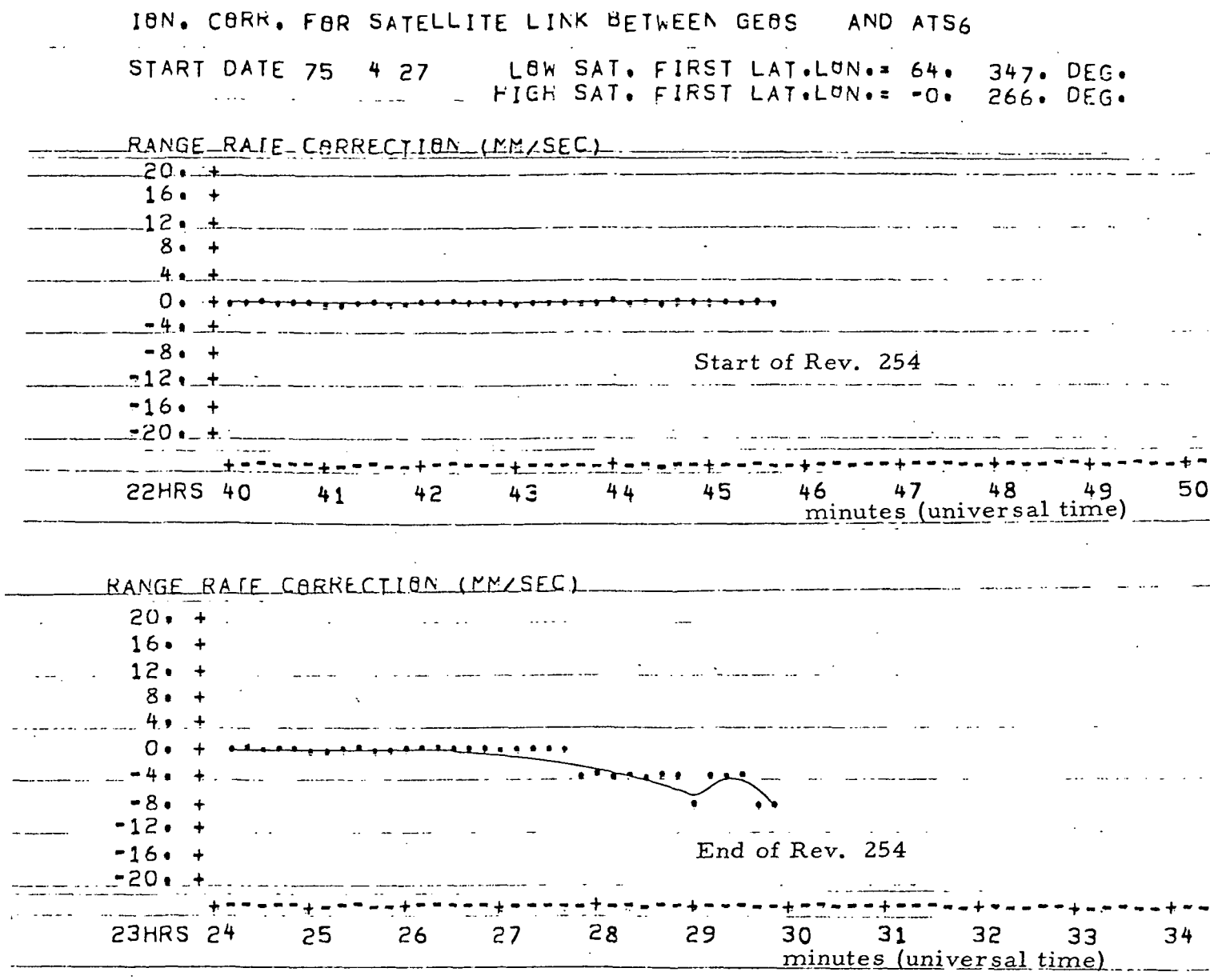

Figure 40 b. One-way ionospheric range-rate corrections for revolution 254 of the Geos/ATS-6 satellite link.

Table 3 .

CORRELATION OF GEOS RANGE-RATE RESIDUALS AND IONOSPHERIC CORRECTIONS
REV730 ENDS 0 MINUTES BEFORE GEOS BECOMES INVISIBLE FROM ATS-6
ONLY FIRST AND LAST 7 MINUTES OF GEOS ARC HAVE LARGE ION. R-R CORR.
YEAR=75, MONTH= 5, DAY=31

	IONOSPHERIC RANGE-RATE CORRECTIONS			RANGE-RATE RESIDUALS (MM/SEC)	
TIME HHMM SS	1) GRND LINK ONE WAY	2) SAT LINK ONE WAY	3) GROUND+SAT ROUND TRIP	4) OBS-COMPUTED ROUND TRIP	5) ADJUSTED (=4)-3)
154345.85	-.7881E-02	-.7429E 01	-.1487E 02	.1760E 01	.1663E 02
154355.85	-.7893E-02	-.8110E 01	-.1624E 02	.4720E 01	.2096E 02
1544 5.84	-.7903E-02	-.9167E 01	-.1835E 02	.4500E 01	.2285E 02
154415.84	-.7914E-02	-.1108E 02	-.2217E 02	.4190E 01	.2636E 02
154425.83	-.7925E-02	-.1244E 02	-.2490E 02	.2930E 01	.2783E 02
154435.83	-.7935E-02	-.1358E 02	-.2719E 02	.1740E 01	.2893E 02
154445.82	-.7946E-02	-.1526E 02	-.3054E 02	.2050E 01	.3259E 02
154455.82	-.7956E-02	-.1713E 02	-.3427E 02	-.1200E 00	.3415E 02
1545 5.81	-.7967E-02	-.1920E 02	-.3841E 02	-.8300E 00	.3758E 02
154515.81	-.7977E-02	-.2152E 02	-.4306E 02	-.1260E 01	.4180E 02
154525.80	-.7989E-02	-.2409E 02	-.4820E 02	-.4020E 01	.4418E 02
154535.80	-.7998E-02	-.2704E 02	-.5409E 02	-.5120E 01	.4897E 02
154545.79	-.8045E-02	-.3857E 02	-.7715E 02	-.4870E 01	.7228E 02
1547 5.74	-.8091E-02	-.2346E 02	-.4694E 02	-.5610E 01	.4133E 02
154715.74	-.8102E-02	-.1070E 02	-.2141E 02	-.2286E 02	-.1447E 01
154725.73	-.8112E-02	.3328E 01	.6640E 01	-.3082E 02	-.3746E 02
154735.72	-.8122E-02	.1780E 02	.3559E 02	-.1716E 02	-.5275E 02
154745.72	-.8132E-02	.3116E 02	.6229E 02	-.3790E 01	-.6608E 02
154755.71	-.8142E-02	.4126E 02	.8251E 02	-.1140E 01	-.8365E 02
1548 5.70	-.8152E-02	.4613E 02	.9224E 02	-.2660E 01	-.9490E 02
154815.70	-.8161E-02	.4338E 02	.8673E 02	-.2660E 01	-.8939E 02
154825.69	-.8177E-02	.2763E 02	.5525E 02	-.1567E 02	-.7092E 02
154845.67	-.8192E-02	.1913E 02	.3824E 02	.3947E 02	.1228E 01
154855.67	-.8201E-02	.1634E 02	.3266E 02	.5547E 02	.2281E 02
1549 5.66	-.8211E-02	.1453E 02	.2904E 02	.1100E 03	.8094E 02
154915.65	-.8221E-02	.1245E 02	.2488E 02	.6545E 02	.4057E 02
154925.65	-.8230E-02	.1106E 02	.2210E 02	.9684E 02	.7474E 02
154935.64	-.8240E-02	.9548E 01	.1908E 02	.9600E 03 edited	.9409E 03 edited
			RMS RESIDUALS:	.6689E 01	.9945E 01

effects should be significantly larger than in gound-to-satellite tracking only during the first and last seven minutes of visibility. Accordingly, no significant range-rate errors are apparent in Figure 40 a, b for the start of the tracking data for revolutions 730 and 254. Data for the end of revolution 730 was available all the way to the time of disappearance, and large ionospheric range-rate corrections due to the geometric effect are visible in Figure 40 a. Data for revolution 254 stopped about four minutes before disappearance, and the range-rate corrections just start showing some deviations in Figure 40 b, the large variations however would occur later.

A listing of the ten second data for the end of revolution 730, for which significant range-rate corrections exist, is given in Table 3 . The one-way corrections for the ground link and the satellite link are given, as well as the ground and satellite link round trip corrections. These last total ionospheric range-rate corrections are correlated with the range-rate residuals computed in the orbit determination program. An adjusted residual is formed by substracting from the observed minus computed residual the ionospheric range-rate correction. RMS values of the residuals and the adjusted residuals are formed excluding the last geometrically visible point, as its large residual might be due to tropospheric refraction effects which should be significant for approximately the last twenty seconds only before invisibility.

One would expect the residuals to be lowered when removing the ionospheric refraction errors from the range-rate measurements, however the RMS residuals do not reflect this, and the adjusted RMS residual is the larger one. Even considering model uncertanties, it is unlikely that the ionospheric range-rate effects would deviate much in overall slope, although the magnitude may be slightly different. Such a magnitude effect would not solve the dilemma, however.

The problem lies in the method of trying to correct an already adjusted orbit, and applying the corrections only to the last six minutes of the arc.

The last few minutes are ordinarily somewhat noisy and include many points that are edited to be excluded from the final orbit adjustment. Residuals are high during the last twenty seconds of the geometric satellite visibility and below the geometric horizon because of tropospheric effects that had not been removed. To correct for the troposphere along the satellite link, a model different from the ground to satellite model would have to be used, because the raypath is near horizontal above the earth's surface. The iterative least square adjustment process used in the orbit determination tries to minimize the range-rate residuals over the whole arc not just over the last few minutes, hence considering just the end of the arc might distort the picture significantly. Also, range-rate corrections should be applied before the iterative process occurs; in this manner the corrected data for the whole arc should, when adjusted for the minimum residual, reflect a lower RMS residual. Hence, the abbreviated test performed on the Geos data in this section is not conclusive.

6.0 REFERENCES

1. Llewellyn, S. K., J. R. Lipofsky, R. B. Bent, G. Nesterczuk, P. E. Schmid, "Gravsat/Geopause Refraction Study", NASA Contractor Report No. NASA CR-2891, 1977.

2. Bent, R. B., S. K. Llewellyn, G. Nesterczuk, P. E. Schmid, "The Development of a Highly-Successful Worldwide Emperical Ionospheric Model and its Use in Certain Aspects of Space Communications and Worldwide Total Electron Content Investigations", IES-Ionospheric Effects Symposium 1975, Sponsored by the Naval Research Laboratory, Arlington, VA, 1975.